

NASA/TM-20210024786/PART1



9- by 15-Foot Low-Speed Wind Tunnel Acoustic Upgrade Part 1: Supporting Studies

*David Bruce Stephens, Martin J. Krupar, and Christopher J. Miller
Glenn Research Center, Cleveland, Ohio*

*Steven J. Sedensky
Jacobs Technology, Brook Park, Ohio*

NASA STI Program . . . in Profile

Since its founding, NASA has been dedicated to the advancement of aeronautics and space science. The NASA Scientific and Technical Information (STI) Program plays a key part in helping NASA maintain this important role.

The NASA STI Program operates under the auspices of the Agency Chief Information Officer. It collects, organizes, provides for archiving, and disseminates NASA's STI. The NASA STI Program provides access to the NASA Technical Report Server—Registered (NTRS Reg) and NASA Technical Report Server—Public (NTRS) thus providing one of the largest collections of aeronautical and space science STI in the world. Results are published in both non-NASA channels and by NASA in the NASA STI Report Series, which includes the following report types:

- TECHNICAL PUBLICATION. Reports of completed research or a major significant phase of research that present the results of NASA programs and include extensive data or theoretical analysis. Includes compilations of significant scientific and technical data and information deemed to be of continuing reference value. NASA counter-part of peer-reviewed formal professional papers, but has less stringent limitations on manuscript length and extent of graphic presentations.
- TECHNICAL MEMORANDUM. Scientific and technical findings that are preliminary or of specialized interest, e.g., “quick-release” reports, working papers, and bibliographies that contain minimal annotation. Does not contain extensive analysis.
- CONTRACTOR REPORT. Scientific and technical findings by NASA-sponsored contractors and grantees.
- CONFERENCE PUBLICATION. Collected papers from scientific and technical conferences, symposia, seminars, or other meetings sponsored or co-sponsored by NASA.
- SPECIAL PUBLICATION. Scientific, technical, or historical information from NASA programs, projects, and missions, often concerned with subjects having substantial public interest.
- TECHNICAL TRANSLATION. English-language translations of foreign scientific and technical material pertinent to NASA's mission.

For more information about the NASA STI program, see the following:

- Access the NASA STI program home page at <http://www.sti.nasa.gov>
- E-mail your question to help@sti.nasa.gov
- Fax your question to the NASA STI Information Desk at 757-864-6500
- Telephone the NASA STI Information Desk at 757-864-9658
- Write to:
NASA STI Program
Mail Stop 148
NASA Langley Research Center
Hampton, VA 23681-2199

NASA/TM-20210024786/PART1



9- by 15-Foot Low-Speed Wind Tunnel Acoustic Upgrade Part 1: Supporting Studies

*David Bruce Stephens, Martin J. Krupar, and Christopher J. Miller
Glenn Research Center, Cleveland, Ohio*

*Steven J. Sedensky
Jacobs Technology, Brook Park, Ohio*

National Aeronautics and
Space Administration

Glenn Research Center
Cleveland, Ohio 44135

July 2022

Acknowledgments

The NASA Environmentally Responsible Aviation Project funded the 9- by 15-Foot Low-Speed Wind Tunnel (9×15 LSWT) background noise measurements conducted in 2012, along with the original study by Jacobs Technology in 2012. The NASA Aeronautics Test Program funded the roughness noise testing at Virginia Polytechnic Institute and State University (Virginia Tech) from 2013 until 2015 when it was superseded by the Aeronautics Evaluation and Test Capabilities Project. The Facility Manager for the 8- by 6-Foot Supersonic Wind Tunnel and 9×15 LSWT complex was David Stark, and the Project Manager for the improvement task was Jeffrey Chambers. Thanks to both for supporting the work described in this report. Thanks to W. Nathan Alexander at Virginia Tech for overseeing the roughness noise testing and discussing the findings. The writing of this report was funded by the NASA Advanced Air Transportation Technologies project. Thanks to Carl H. Gerhold, Brian Howerton, Martha Brown, and Michael Jones from NASA Langley Research Center for supporting the Normal Incidence Tube and Curved-Duct Test Rig experiments. Thanks to Clif Horne from NASA Ames Research Center for providing a sample panel from the National Full-Scale Aerodynamics Complex (NFAC) 40- by 80-Foot Wind Tunnel (40×80 WT) and further discussions. Thanks to Joseph Sacco of NASA Ames NFAC for many conversations about the diffusion bonded panels used in the 40×80 WT.

This work was sponsored by the Advanced Air Vehicle Program
at the NASA Glenn Research Center

Trade names and trademarks are used in this report for identification
only. Their usage does not constitute an official endorsement,
either expressed or implied, by the National Aeronautics and
Space Administration.

Level of Review: This material has been technically reviewed by technical management.

Contents

Summary	1
1.0 Introduction	1
1.1 Very Brief History of 9- by 15-Foot Low-Speed Wind Tunnel	1
1.2 Motivation for Tunnel Renovation	2
1.3 Motivation for Report	2
1.4 Report Structure	2
2.0 Noise in 9- by 15-Foot Low-Speed Wind Tunnel Test Section	3
2.1 9- by 15-Foot Low-Speed Wind Tunnel Flow Surface	4
2.2 Jacobs Engineering Group Assessment	4
3.0 Literature Review	8
4.0 Roughness Noise Testing	9
4.1 2013 Roughness Noise Test	9
4.1.1 Sample Holding Frame for Roughness Noise Testing	10
4.1.2 Experimental Setup	10
4.1.3 Test Matrix	12
4.1.4 Noise Due to Flow Over Perforate	13
4.1.5 Effect of Flow Velocity	15
4.1.6 Noise Due to Flow Over Fiberglass Cloth	15
4.1.7 Noise Due to Flow Over Gaps	15
4.2 2014 Roughness Noise Test	17
4.2.1 Acoustic Box for Roughness Noise Testing	17
4.2.2 Effect of Acoustic Box	19
4.2.3 Test Matrix	19
4.2.4 Data Processing	21
4.2.5 Noise From Fiberglass Cloth	21
4.2.6 Effect of Hole Size	21
4.2.7 Effect of Plate Thickness	21
4.2.8 Other Fabric Types	23
4.2.9 NASA Ames Research Center 40- by 80-Foot Wind Tunnel Sample	23
4.2.10 Micronic Wire Cloth Samples	24
4.2.11 Diffusion Bonded Panels	27
4.2.12 Types of Micronic Wire Cloth	27
4.2.13 Orientation of Micronic Wire Cloth	27
4.2.14 Other Observations	29
4.2.15 Conclusions From 2014 Roughness Noise Test	29
4.3 2016 Roughness Noise Test	29
4.3.1 Test Matrix	30
4.3.2 Boundary Layer Bump	30
4.3.3 New Diffusion Bonded Panels	32
4.3.4 Effect of Bump	32
4.3.5 Fasteners	34
4.4 2016 Velocity Measurements	36
4.4.1 Test Matrix	37
4.4.2 Upstream Unsteady Velocity Measurements	37

4.4.3	Downstream Unsteady Velocity Measurements.....	38
4.4.4	Effect of Wire Cloth on Unsteady Velocity Measurements	41
4.4.5	Velocity Spectra	42
5.0	Absorption Coefficient Testing	43
5.1	Method.....	43
5.1.1	Experimental Setup 2014	43
5.1.2	Data Processing	45
5.2	2014 Absorption Test	45
5.2.1	Observations.....	46
5.2.2	Diffusion Bonded Panel With Fiber Contamination	46
5.2.3	Effect of Oil Contamination and Cleaning	48
5.3	2016 Absorption Testing	49
5.3.1	Experimental Setup	49
5.3.2	Melamine Foam.....	50
5.3.3	As-Built 1986 Acoustic Absorber	51
5.3.4	Thin Acoustic Absorber	51
5.3.5	Layered Bulk Absorbers.....	53
5.3.6	Effect of Perforated Plate Thickness	55
5.4	Effect of Micronic Wire Cloth.....	55
5.5	Final Design.....	57
5.6	Prototype Box Evaluation.....	57
6.0	Testing at NASA Langley Research Center	60
6.1	Normal Incidence Tube	60
6.2	Curved-Duct Test Rig.....	60
6.2.1	Curved-Duct Test Rig Test Sample Design	61
6.2.2	Experimental Results.....	63
7.0	Computational Study	65
7.1	Model Geometry.....	65
7.2	Three-Dimensional Model Details.....	68
7.3	Two-Dimensional Model Details.....	69
7.4	Configuration Options Evaluated	70
7.5	Selected Option: Lengthen Test Section by 5 Ft	71
7.6	Nonreflecting Boundary Condition	72
7.7	Evaluation of Wall Treatment.....	74
7.8	Traverse Corners.....	76
8.0	Analytical Study	77
8.1	Maximum Theoretical Tone Error: One-Dimensional	78
8.2	Maximum Theoretical Tone Error: Two-Dimensional.....	79
8.3	Maximum Theoretical Tone Error: Three-Dimensional.....	80
9.0	Conclusion.....	81
	References.....	81

9- by 15-Foot Low-Speed Wind Tunnel Acoustic Upgrade

Part 1: Supporting Studies

David Bruce Stephens, Martin J. Krupar, and Christopher J. Miller
National Aeronautics and Space Administration
Glenn Research Center
Cleveland, Ohio 44135

Steven J. Sedensky*
Jacobs Technology
Brook Park, Ohio 44142

Summary

The 9- by 15-Foot Low-Speed Wind Tunnel at NASA Glenn Research Center was refurbished in a major construction project starting in June 2017 and ending in March 2019, with some interruptions. Studies supporting this effort started years earlier and continued through the end of construction. The focus of the refurbishment project was to reduce the background noise in the test section during operation. The major focus of the supporting studies was the wind tunnel flow surface. These studies included roughness noise testing of samples, impedance measurements, computational simulations, and analysis. NASA Langley and Ames Research Centers both contributed, as did Virginia Polytechnic Institute and State University. This report describes the major efforts and findings of the supporting studies.

1.0 Introduction

This report describes research performed in support of an upgrade to the NASA Glenn Research Center 9- by 15-Foot Low-Speed Wind Tunnel (9×15 LSWT). The work described here took place between 2012 and 2019. The most significant noise reduction aspect of the effort was the use of a low “roughness noise” flow surface to replace the perforated sheet metal flow surface. The noise due to flow over these panels (roughness noise) was evaluated at Virginia Polytechnic Institute and State University (Virginia Tech). Those tests and results are discussed. The acoustic quality of the low-noise panels was studied at a number of facilities, including NASA Langley Research Center and NASA Glenn. The acoustic absorber to be placed behind the flow surface was also tested, with comparisons made between fibrous and foam bulk absorbers at NASA Glenn Acoustical Testing Laboratory (ATL).

1.1 Very Brief History of 9- by 15-Foot Low-Speed Wind Tunnel

The 9×15 LSWT was built in the return leg of the 8- by 6-Foot Supersonic Wind Tunnel (8×6 SWT) in 1969 (Ref. 1). The 9×15 LSWT was designed for performance testing of vertical and short takeoff and landing (V/STOL) aircraft models. By 1975, “softwall” acoustic treatment for the test section was added, consisting of 2 in. of fiberglass with a protective screen installed over the hard-wall surface of the tunnel (Refs. 2 and 3). A second-generation “deep” acoustic treatment was installed in 1986, using boxes filled with an unwoven Kevlar® (DuPont™) bulk absorber and fit between the tunnel structure (Refs. 4 and 5). The deep treatment was sought specifically in support of noise measurements of model turboprop

*Currently employed by NASA Glenn Research Center.

systems, featuring loud noise levels but low frequencies where the original shallow treatment would not be effective. The 1986 treatment was used for more than 30 years, as the 9×15 LSWT was very frequently used for acoustic and performance testing of aircraft propulsion systems. The acoustic quality of the test section has been considered by a number of authors (Refs. 6 and 7).

1.2 Motivation for Tunnel Renovation

As interest in high-speed turboprop systems waned, focus shifted towards turbofan models of increasing bypass ratios and decreasing fan pressure ratios. Noise has correspondingly been reduced over the decades. Since the mid-1990s, most turbofan models tested for noise in the 9×15 LSWT have been operated with a tunnel speed of Mach 0.10, in order to lower the tunnel background noise level and ensure good signal-to-noise ratio for microphone measurements. A tunnel speed of Mach 0.10 was determined to be fast enough to provide the desired aerodynamically clean inflow condition at the fan face for engine models where the nacelle inlet was sufficiently long. By the mid-2000s, fan models had become quiet enough that the signal-to-noise ratio of the tunnel was a concern, even when operating at Mach 0.10. Future turbofan engines are expected to feature shorter inlets to reduce weight and drag. A side effect is that the inlet provides less flow conditioning than the longer inlets previously in use. To achieve the desired inflow at the fan face, the tunnel must be operated at a higher free-stream velocity that more closely matches the intended flight speed. This raises the background noise level in the facility, making acoustic measurements of advanced turbofans increasingly challenging.

1.3 Motivation for Report

The purpose of this report is to document the preconstruction testing and analysis that guided the requirements for the construction project. A set of reports (Refs. 8 and 9) describing the mid-1990s upgrades to the National Full-Scale Aerodynamics Complex (NFAC) 40- by 80-Foot Wind Tunnel (40×80 WT) at NASA Ames Research Center were extremely valuable to the 9×15 LSWT improvement effort and the present authors hope this report will provide similar benefit to future wind tunnel engineers. Studies that are decidedly specific to the 9×15 LSWT such as test section background noise measurements and system-level benefits will be provided in a separate report.

1.4 Report Structure

This report focuses on supporting studies investigating the flow-induced noise of potential materials for the wind tunnel flow surface, along with the impact of these materials on the anechoic quality of the test section. The central motivation for the tunnel upgrade project was to lower the background noise in the facility, as previously mentioned. Section 2.0 discusses the concept of roughness noise as it affects inflow noise measurements in the 9×15 LSWT. Section 3.0 provides a brief literature review. Section 4.0 describes a series of roughness noise tests conducted at Virginia Tech. Section 5.0 will describe the testing done at the ATL to investigate the acoustic quality of panels being considered. Section 6.0 describes testing done at NASA Langley where the established facilities for acoustic liners for aircraft engines were pressed to investigate the liners to be considered for the 9×15 LSWT. Section 7.0 describes a set of finite-element acoustic simulations done in support of the upgrade process. Section 8.0 includes some supporting analysis and Section 9.0 is a summary. All of the results that were found to be useful are included, along with a number of things that were found to not be successful. The report is intended to be thorough, but not exhaustive.

2.0 Noise in 9- by 15-Foot Low-Speed Wind Tunnel Test Section

During February and March of 2012, there was a schedule opening and a funding opportunity to take a set of background noise measurements in the facility. The Environmentally Responsible Aviation (ERA) project was going to be performing noise testing of aircraft engine fan models in the 9×15 LSWT over the next several years and there was interest in understanding potential improvements to the facility. Microphones were placed around the entire loop of the 8×6 SWT and 9×15 LSWT complex (8×6/9×15), with the 9×15 LSWT leg and test section particularly well instrumented. A portion of these results were reported in Reference 7, while additional findings will be documented in an upcoming companion report to the present report. The microphone instrumentation used in the 9×15 LSWT test section is shown in Figure 1. There are three fixed microphones and one traversing probe with three microphones.

A typical result showing measured pressure spectral density through the 9×15 LSWT leg is given in Figure 2. Channels 7 and 8 are upstream of the test section while channel 9 is the wall microphone in the test section, as pictured in Figure 1. Below about 1,500 Hz, the levels of the three curves are similar, although the noise propagating through the inlet contraction may be smoothing the spectral levels some. In the test section, however, considerable additional noise is observed above about 2,000 Hz.

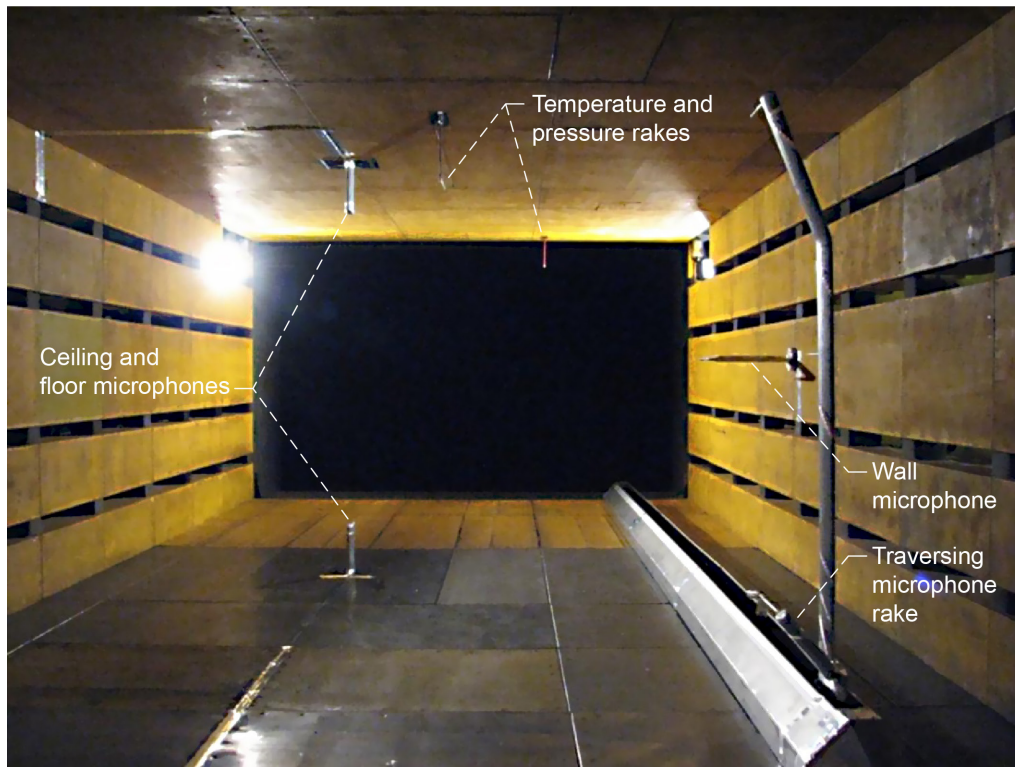


Figure 1.—Microphone installation used in 2012 empty tunnel survey. Downstream looking upstream.

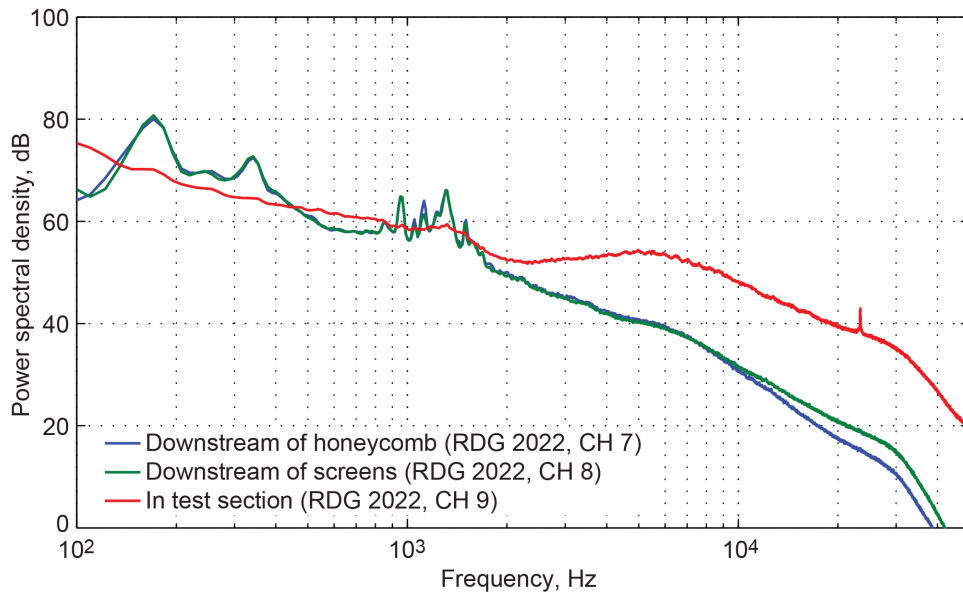


Figure 2.—Measured sound spectra in 9- by 15-Foot Low-Speed Wind Tunnel leg at Mach 0.20. Channel (CH). Reading (RDG).

2.1 9- by 15-Foot Low-Speed Wind Tunnel Flow Surface

The walls of the 9×15 LSWT were formed by dozens of individual boxes built of perforated steel plate over a 33-cm- (13-in.-) deep bulk Kevlar® sound-absorbing material. This steel plate is 0.16 cm thick (16 ga) and perforated with 0.32-cm-diameter (1/8-in.) holes creating an open area of 40 percent, backed by a 20-wires-per-inch mesh screen that serves to keep the fill from egressing. There are four slots in each of the two sidewalls and many seams and gaps between acoustic boxes that contribute to the rough surface. Additionally, the original 1986-era acoustic boxes were painted with yellow nonskid paint, further adding to the rough surface. Replacement floor boxes made of stainless steel were not painted. A closeup photograph of the flow surface is shown in Figure 3.

The construction of an individual acoustic box is principally folded sheet steel, as shown in Figure 4. The 33-cm- (13-in.-) deep portion of the box is visible, as is the 2-in.- (5-cm-) deep flange that is fastened to the structural beams using the visible through holes. The perforated flow surface is apparent.

2.2 Jacobs Engineering Group Assessment

The ERA project also funded Jacobs Engineering Group, Inc., to perform an external assessment of the background noise in the facility. This company has extensive experience with acoustic wind tunnels, principally for the automotive industry, and the lead engineers for the NASA project have authored a paper surveying a number of the large acoustic wind tunnels around the world (Ref. 10). The noise data taken through the 9×15 LSWT loop and associated aerodynamic data were used by Jacobs to create a one-dimensional (1D) model of the noise sources and loss mechanisms in the tunnel. In this way, the noise measurements could be expressed as a sum of different noise sources and targets for reduction can be identified. The 9×15 LSWT is a very peculiar wind tunnel for a number of reasons, such as the location of the cooler within the loop, the slotted walls, and the use of a seven-stage compressor to provide the airflow. All of these have significant potential effect on the background noise measured in the test section. A major conclusion from their study was that the additional noise observed in the test section above 2 kHz is due to the tunnel airflow over the rough walls of the test section. Jacobs had recently considered

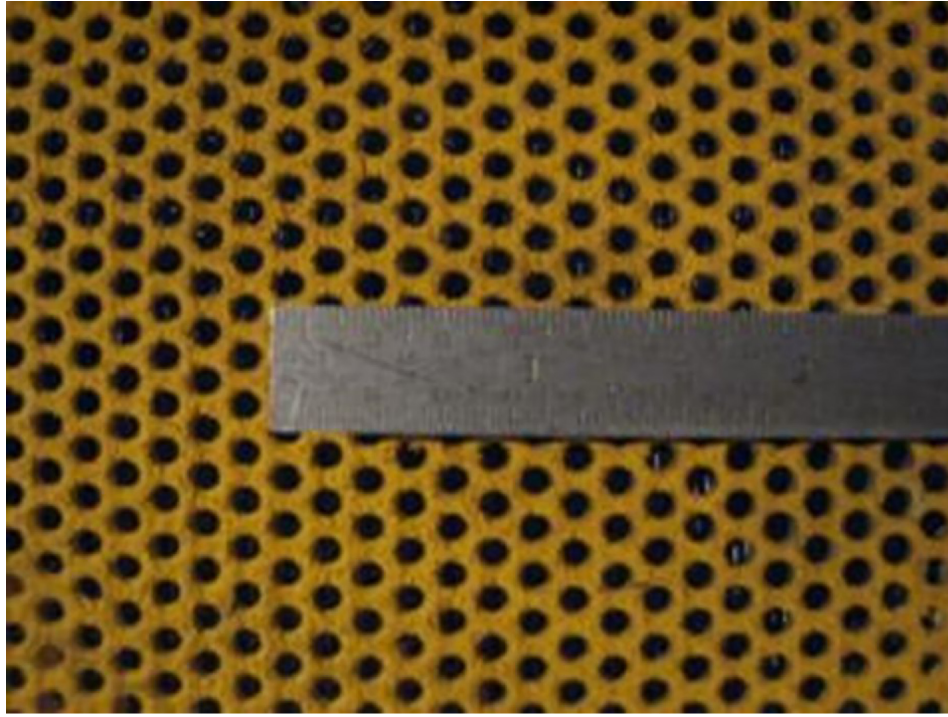


Figure 3.—Test section perforate from 1986- to 2016-era 9- by 15-Foot Low-Speed Wind Tunnel.

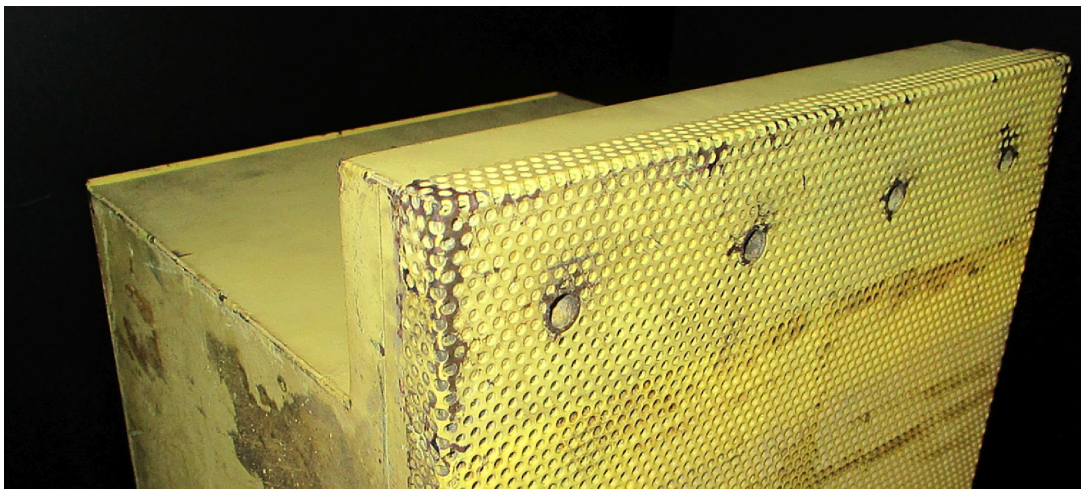


Figure 4.—Acoustic box from 1986- to 2016-era 9- by 15-Foot Low-Speed Wind Tunnel.

the noise due to airflow over rough surfaces in wind tunnels (Ref. 11), based on the experience of two large automotive acoustic tunnels in the Detroit, Michigan, area. They developed a version of Howe's boundary layer noise model to predict the noise inside a wind tunnel test section with noise contributions from various rough surfaces located around an observer. The model was adjusted to fit the measurements from the test section, using a roughness height of 1.5 mm (1/16 in.), based on the thickness of the 16-ga perforated steel sheet making up the facility flow surfaces. The resulting prediction is shown in Figure 5, where the close agreement in spectral shape and scaling with tunnel speed provide compelling evidence that roughness noise is a major problem in the facility.

The Jacobs team proposed covering the acoustic boxes with a smoother flow surface to lower the roughness noise. Specifically, they proposed using a woven fiberglass cloth bonded to the perforate, which is an approved construction material they had previously used in acoustic wind tunnels, although not for test section walls. It is a 30- by 24-threads-per-inch weave. A photograph of the proposed fiberglass cloth is shown in Figure 6.

The fiberglass cloth had a wide weave of 0.94-mm width crossed by a narrower weave with a 0.46-mm width. A closeup photograph is shown in Figure 7.

The model predicted that by reducing the roughness height from 1.5 to 0.1 mm, a 7-dB reduction in the self-noise from the tunnel walls could be achieved. The prediction is shown in Figure 8.

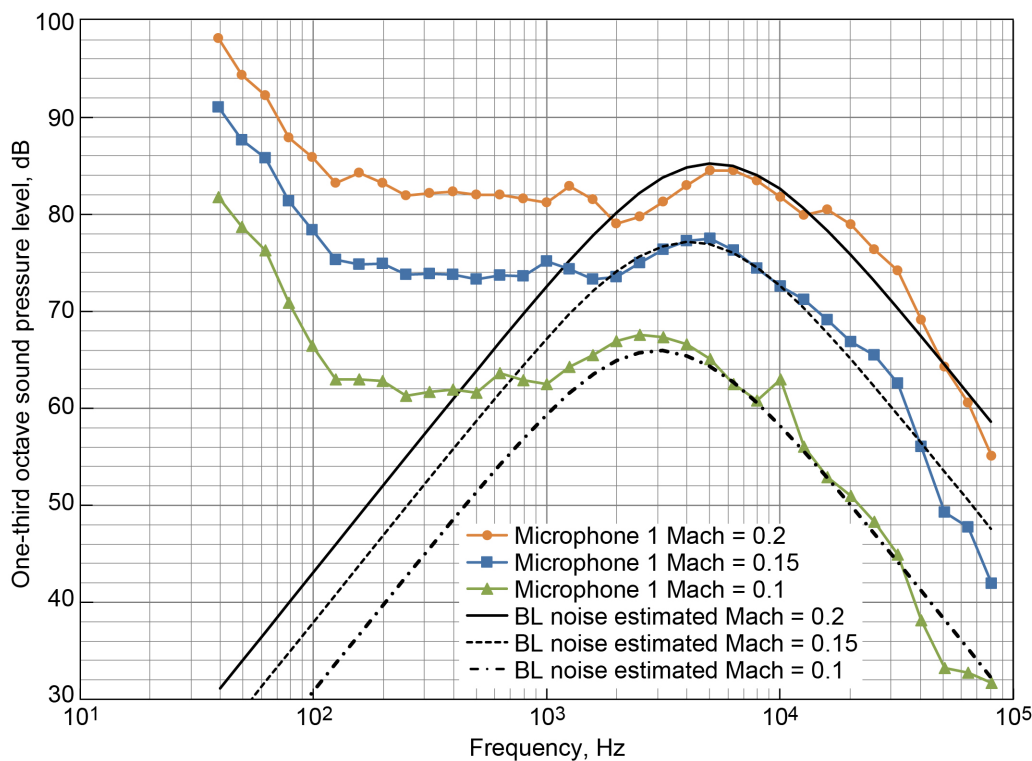


Figure 5.—Boundary layer (BL) noise prediction results at various tunnel speeds compared to actual measured data in 9- by 15-Foot Low-Speed Wind Tunnel. Sound levels are on one-third octave bands, model roughness height was 1.5 mm.

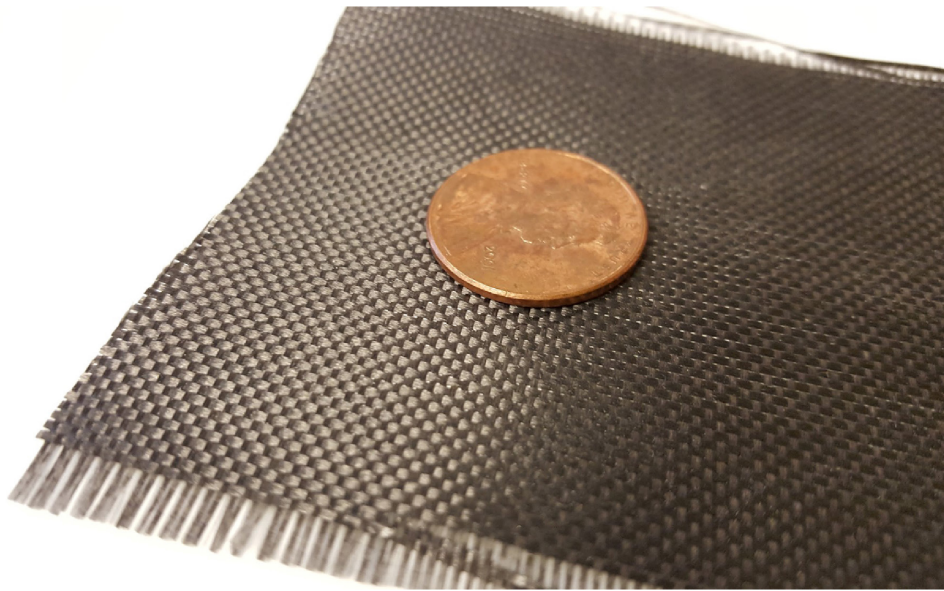


Figure 6.—Fiberglass cloth proposed as smoother flow surface.

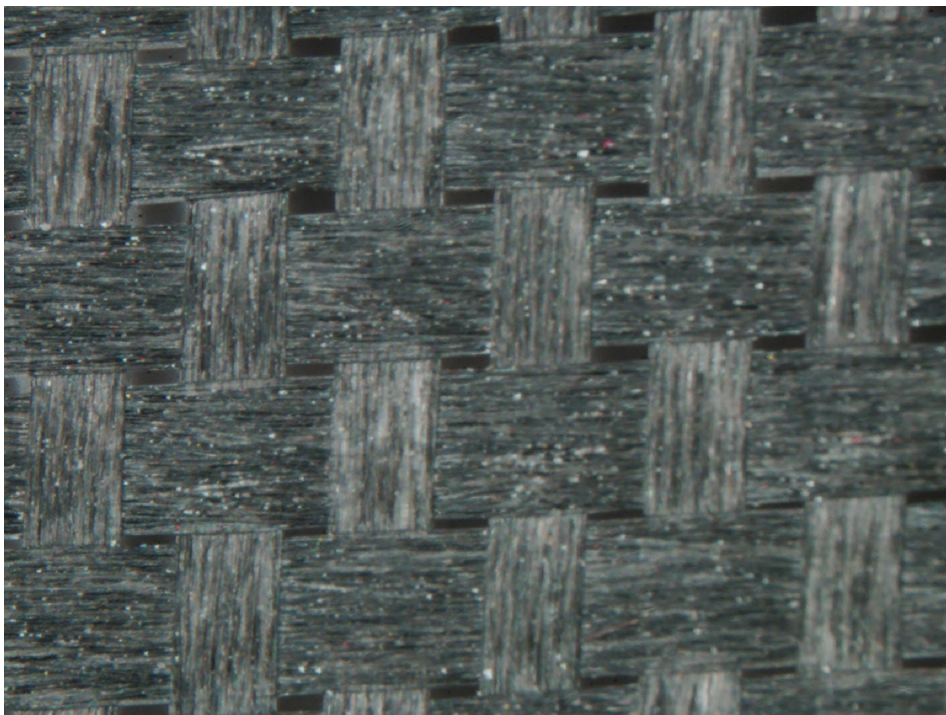


Figure 7.—Closeup of fiberglass cloth showing weave pattern.

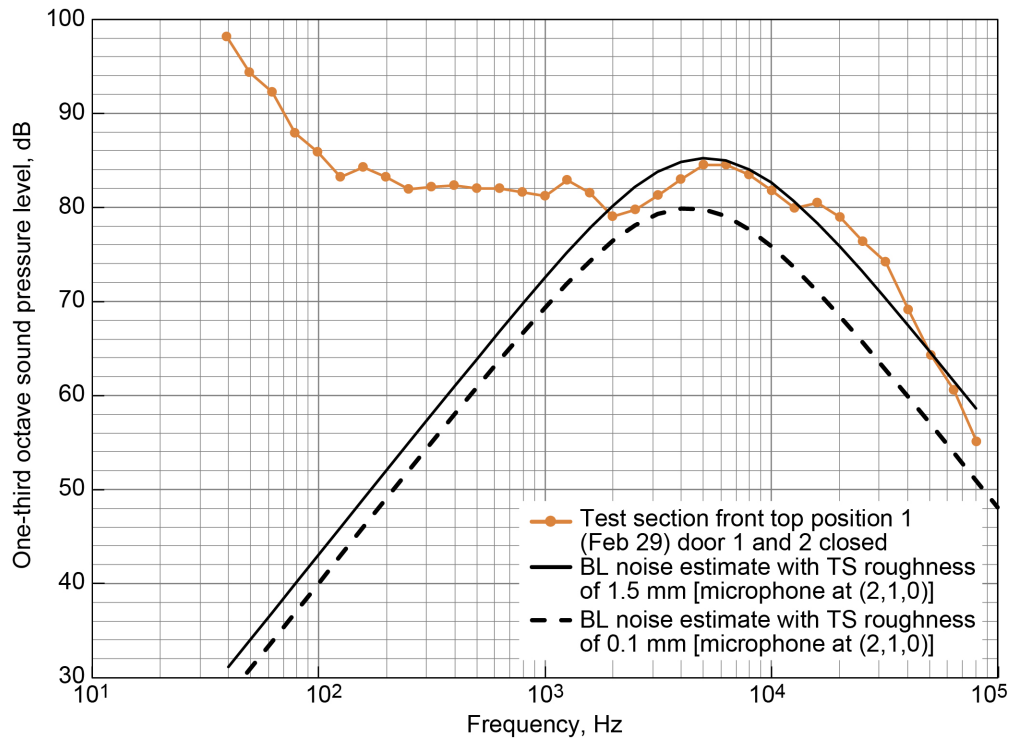


Figure 8.—Predicted attenuation to boundary layer (BL) noise with reduced test section (TS) wall roughness.

3.0 Literature Review

A brief discussion of roughness noise is included, along with some references that may be of interest to the reader.

A considerable portion of the previous research on roughness noise considers, essentially, sandpaper. A study by Hersh (Ref. 12) is an oft-cited example, where a pipe flow exhausts into an anechoic room and the interior surface of the pipe is covered with sandpaper. This type of noise is dipole in nature, scaling with flow velocity to the sixth power. Howe developed a theoretical model for boundary layer noise (Ref. 13) and used Hersh’s measurements to fix parameters for the spectral shape.

Liu and Dowling (Ref. 14) studied the contribution of roughness noise to airframe noise for a large commercial aircraft. Their paper also serves to review existing literature, summarize equations, and illustrate how poorly typical noise models capture roughness noise experiments. Their experiment is typical of many roughness noise studies, with a plate containing the rough surface mounted to the exit of an open jet wind tunnel. In addition to the roughness noise of interest and the preexisting facility noise, this method adds noise due to the impingement of the jet onto the plate, plus the extension of the plate through the jet shear layer.

A significant advancement in the experimental study of noise due to flow over rough surfaces began in 2007, when Devenport built a dedicated roughness noise test facility at Virginia Tech. The initial report on the facility (Ref. 15) discusses design, construction, and instrumentation. Compared to other roughness noise experiments, the key concept is the use of a rectangular wall “slot” jet exhausting onto a large aluminum plate in an anechoic room. This arrangement avoids the need to pass any supports or samples through a shear layer, which is a common parasitic noise source in aeroacoustic experiments. The use of a 121-cm- (3.95-ft-) wide jet allows a sample of up to 61-cm (2-ft) width to be placed in the potential core of the slot jet, with only a small axial velocity variation. The jet supply is a blower mechanically

decoupled from the test chamber, with an acoustically treated plenum ahead of a specially shaped nozzle. Microphones are placed in the still air above the sample, so there is very little self-noise on the microphones. The roughness noise facility has been used for a variety of tests, including studies of regularly spaced elements (Ref. 16) and boundary layer flows over gaps and steps (Ref. 17). These are relevant primarily because they eliminate the random nature of sandpaper-type roughness and also lend themselves to computational simulation.

4.0 Roughness Noise Testing

In order to improve confidence in the magnitude of potential noise reduction modifications, NASA contracted with Virginia Tech to conduct a series of noise tests on the various surfaces of interest. These tests ended up spanning 4 years under several test campaigns, as listed below.

- 2013 campaign: This was a preliminary test to investigate whether the facility was going to produce useful data to compare against the 9×15 LSWT measurements and to see if we could measure a noise reduction with the fiberglass cloth. A set of samples with gaps in the flow surface was also tested. The samples were mounted in a frame on top of the existing aluminum plate of the roughness noise facility. Virginia Tech prepared a conference paper based on this study (Ref. 18).
- 2014 campaign: Based on the results of the 2013 test, a set of 30 samples was developed. These samples were designed to investigate different combinations of perforates and cloth, different types of cloth, and a few specific concepts. The test facility was modified to include an acoustic absorber behind the perforate, to better mimic the wall boundary condition in the 9×15 LSWT. Virginia Tech prepared a conference paper based on this study also (Ref. 19).
- 2016 campaign: A set of prototype diffusion bonded panels made of wire cloth over perforated plate were tested, with varying manufacturing quality. A number of custom perforate shapes with wire cloth were also tested. A modified boundary layer was also tested, utilizing a “bump” to increase the thickness of the velocity deficit.
- 2017 campaign: The addition of mechanical fasteners into the samples was investigated. These included two sizes of rivets and a press-fit stud fastener. The boundary layer profile downstream of a number of the samples was measured using hot wire anemometry.

The following subsections will describe the testing in more detail and give a summary of the most important findings.

4.1 2013 Roughness Noise Test

It had previously been established that the Virginia Tech roughness noise facility could measure the noise due to airflow over a single 3-mm cube (Ref. 15), so there was little reason to doubt the capability to measure the noise due to airflow over a 30- by 60-cm (1- by 2-ft) sample of perforated plate. This series of tests was intended to evaluate the ability of the facility to measure similar noise characteristics to those observed in the 9×15 LSWT and verify the predicted noise reduction when the fiberglass cloth (pictured in Figure 6) was applied on top of the perforate. At the time, it was not considered that a series of test campaigns would be conducted.

4.1.1 Sample Holding Frame for Roughness Noise Testing

There was also interest in testing the noise over the gaps between the perforated plates. The existing 9×15 LSWT acoustic boxes were made by folding the perforate plate to form the flow surface as a lid, as seen in Figure 4, so samples with bent edges were built. It was necessary to build a frame to smoothly adapt the height from the existing aluminum plate of the roughness noise facility to the height for the samples to be tested. The frame was sized to hold a 30- by 60-cm (1- by 2-ft) sample and had a 7.62-cm (3-in.) border. The border adapted the 6.35-mm (0.25-in.) height of the frame down to within 1 mm of the test surface using a fourth-order curve designed to be tangent at both ends. The equation for the curve is given as

$$y = 0.0412x^4 - 0.2175x^3 + 0.3228x^2 + 0.03937 \quad (1)$$

where units are in inches. The frame had a cutout in a cross shape so that the samples with bent edges could be accommodated in both streamwise and spanwise directions. The frame was designed and machined from aluminum at NASA Glenn.

A rendering of the frame showing the installation of a sample for testing a gap is given in Figure 9. The radius was intended to be small, to mimic the existing acoustic boxes. The gap between the two sample panels could be varied. During testing, the backs of the perforated samples were covered with aluminum tape, to prevent airflow through the corners of the folded perforate. This was done because the rest of the perforated sample was flush with the aluminum frame, so no airflow was expected through the other portion of the perforate. Similarly, for one-piece test panels without gaps, aluminum tape was placed across the back to seal the section that would otherwise have been over the gap.

4.1.2 Experimental Setup

The frame on the surface of the wall jet at Virginia Tech is pictured in Figure 10. The installation of a sample in the frame as tested is given in Figure 11. The microphones are indicated by the numbers 1 to 9. A tenth microphone was installed (pictured below microphone 6) but the data from it was found to be contaminated. Airflow is toward the camera. The frame was held to the aluminum surface by double-sided indoor carpet tape. Aluminum tape was used to smooth the 1-mm (0.039-in.) step around the perimeter of the frame. “Professional strength” adhesive remover was used to clean the metal surfaces as needed.

The locations of the nine microphones are given in Table 1. Measurement angles θ and ϕ are measured from upstream.

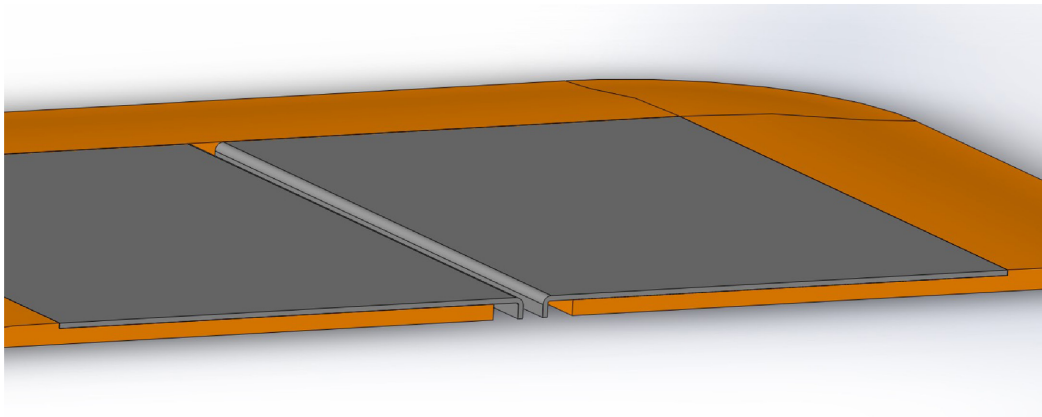


Figure 9.—Rendered cross section of frame and test samples for streamwise gap test.



Figure 10.—Frame used for Virginia Polytechnic Institute and State University testing, without sample installed.

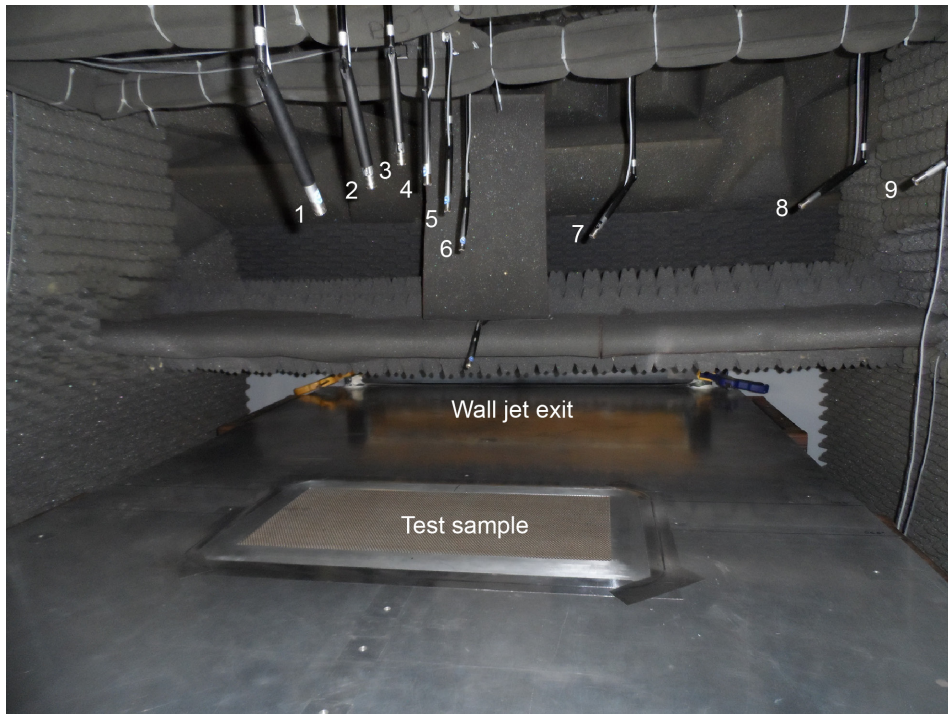


Figure 11.—Wall jet roughness noise facility at Virginia Polytechnic Institute and State University pictured during 2013 testing. Baffle above jet exit is outside of shear layer.

TABLE 1.—LOCATIONS OF MICROPHONES USED IN VIRGINIA POLYTECHNIC INSTITUTE AND STATE UNIVERSITY ROUGHNESS NOISE TESTING

[Distances and angles are from center of sample. Streamwise distance is x , vertical direction normal to surface is y , and cross-stream direction is z . R is radius. Angle θ is measured from downstream, and angle ϕ is measured from vertical.]

Microphone	x , mm	y , mm	z , mm	R , mm	θ , deg	ϕ , deg
1	-489	514	5	710	134	----
2	-313	556	6	638	119	----
3	-164	602	3	623	105	----
4	0	589	2	589	90	----
5	157	556	0	577	74	----
6	275	483	3	555	60	1
7	252	503	271	625	----	47
8	265	549	668	904	----	68
9	8	564	765	950	----	89

TABLE 2.—JET EXIT VELOCITY (U_0), BOUNDARY LAYER THICKNESS AT TEST SAMPLE CENTER AXIAL LOCATION (δ), AND JET LOCAL MAXIMUM VELOCITY AT TEST SAMPLE CENTER AXIAL LOCATION ($U_{1.41}$)

U_0 , m/s	δ , mm	$U_{1.41}$, m/s
20	17.8	6.7
30	17.8	10.3
40	17.7	13.9
50	17.6	17.5
60	17.6	21.2

The facility airflow velocity is set by controlling the slot jet exit velocity, U_0 . The peak velocity in the wall jet decays axially and over the center of the sample (1.41 m downstream of the jet nozzle exit) $U_{1.41}$ is approximately one third of U_0 . The boundary layer thickness δ is defined as 99 percent of the maximum velocity at that axial location. Table 2 contains these data.

4.1.3 Test Matrix

The configurations tested at Virginia Tech in 2013 are given in Table 3. This was essentially a preliminary test, so the scope was limited to a few parameters. The principal objective was to compare the fiberglass cloth over perforate to bare perforate. It was also necessary to verify that the frame was not a parasitic noise source, so a smooth insert was built for the frame. The not-quite-square weave of the fiberglass cloth motivated us to test at both orientations with respect to the flow. We were also interested in testing the noise due to gaps in the surfaces, so both cross-stream and streamwise samples with gaps were built from both solid and perforated plates for a total of 11 configurations. Samples of fabric over perforate were made by using spray adhesive, applied to the perforated plate before the fabric was placed on top. The quality and fit of all parts were quite good, as the perforated and solid plates were cut on a water knife.

TABLE 3.—CONFIGURATIONS TESTED AT VIRGINIA POLYTECHNIC
INSTITUTE AND STATE UNIVERSITY IN 2013

[For configurations 3 and 4, difference is direction of cloth weave.
Orientation 1 is with wider fiber in cross-stream direction,
while for orientation 2, wider fiber is
in streamwise direction.]

Configuration	Description
1	Frame with smooth insert
2	Frame with open perforate
3	Frame with perforate and fiberglass cloth at orientation 1
4	Frame with perforate and fiberglass cloth at orientation 2
5	No frame, smooth wall
6	Frame, perforate with cross-stream gap, 6.2 mm
7	Frame, perforate with cross-stream gap, 0 mm
8	Frame, perforate with streamwise gap, 6.2 mm
9	Frame, smooth plate with cross-stream gap, 6.2 mm
10	Frame, smooth plate with cross-stream gap, 0 mm
11	Frame, smooth plate with streamwise gap, 6.2 mm

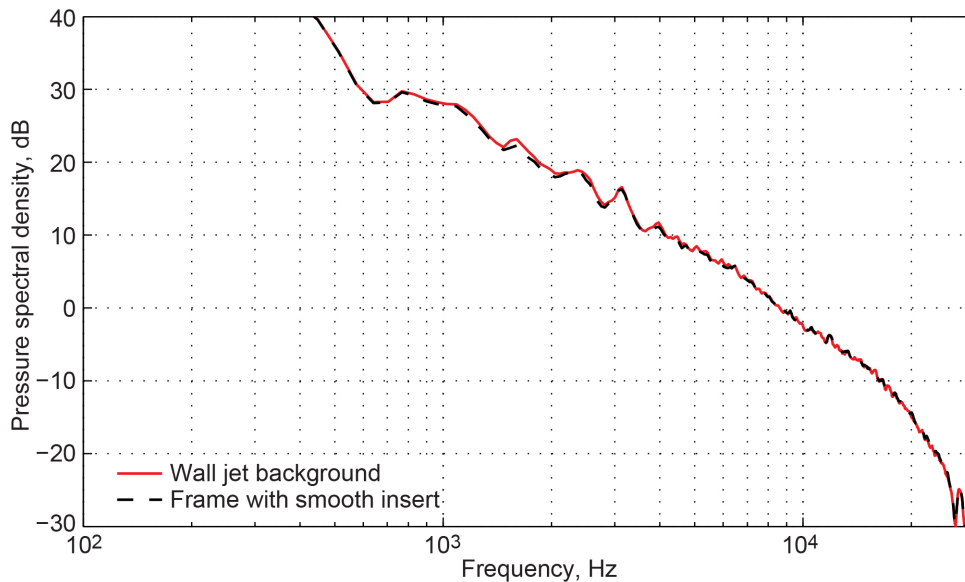


Figure 12.—Effect of frame usage compared with wall jet background noise in 2013 testing.
Microphone 6, 60 m/s jet exit velocity.

4.1.4 Noise Due to Flow Over Perforate

The effect of the frame was evaluated by comparing the bare wall jet flow noise to that when the frame was added with the smooth insert. This measurement is shown in Figure 12, using microphone 6 as an example. At this condition and angle, the results agree to within 1 dB at all frequencies, giving confidence that the impact of the frame is minimal.

Upon replacing the smooth insert with the perforate (configuration 2, see Figure 11) in the wall jet facility, it was immediately apparent that the airflow over perforate produced considerable noise. The facility is low speed and safe for a person to stand in during a test. Just by walking around the test

chamber and listening, it was easy to isolate the noise generated by the perforated plate sample. The present author would liken it to the noise caused by a shallow stream flowing over gravel. The noise recorded by microphone 6 with the perforate plate installed compared with the smooth insert in the frame is given in Figure 13.

The two spectra shown in Figure 13 can be subtracted to give only the additional noise due to the airflow over the perforate sample. The result is given in Figure 14. It is clear that the perforate produces a considerable amount of broadband noise with a relatively simple spectral shape featuring a single maximum near 2,500 Hz at 60 m/s jet exit velocity.

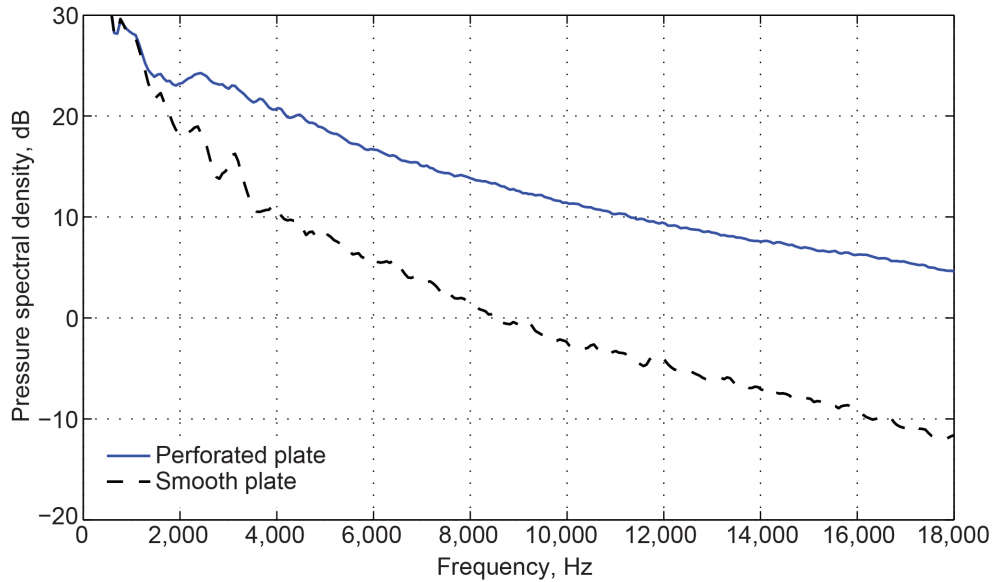


Figure 13.—Measurements of perforated and smooth samples in frame during 2013 test campaign. Microphone 6, 60 m/s jet exit velocity.

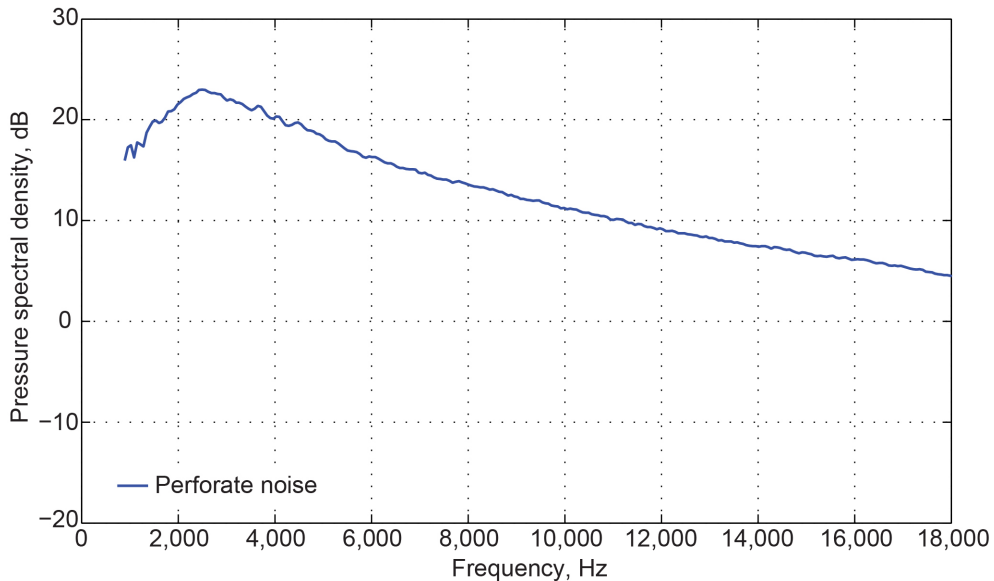


Figure 14.—Measurements of perforated samples after subtracting background noise during 2013 test campaign. Microphone 6, 60 m/s jet exit velocity.

4.1.5 Effect of Flow Velocity

The measured results for all five jet velocities are given in Figure 15. It is seen that the peak noise frequency scales linearly with flow speed.

4.1.6 Noise Due to Flow Over Fiberglass Cloth

The addition of fabric over the perforate changed the nature of the sound audibly. As shown in Figure 16, the peak noise was reduced by more than 10 dB at 2,500 Hz, but additional noise peaking at about 18 kHz was generated. This finding caused immediate concern and motivated follow-on studies. For full-scale testing, noise at 18 kHz is nearly ultrasonic, but the models tested in the 9×15 LSWT are often subscale, with scale factors of around 2 to 5. This means that additional noise at high frequencies would not be acceptable. Since the fiberglass cloth had two different fiber sizes, it was tested in each orientation. Orientation 1 is with the wider fiber in the cross-stream direction while, for orientation 2, the wider fiber is in the streamwise direction.

4.1.7 Noise Due to Flow Over Gaps

Finally, there was the investigation of noise due to gaps in the perforate. It turned out that this was a relatively small additional penalty compared with the flat perforate. The largest gap that could be arranged was 6.2 mm (0.25 in.). The noise for this gap is shown in Figure 17.

The background subtraction to isolate noise due to the gap is shown in Figure 18. When the difference is less than 1 dB, no data is plotted. The maximum cross-stream gap is quieter than the minimum gap-closed configuration. The streamwise gap is very quiet, barely above the background noise. Based on these findings, it was decided to focus further studies on the covering for the perforate and simply work to minimize the number of gaps in the design of the new 9×15 LSWT flow surface.

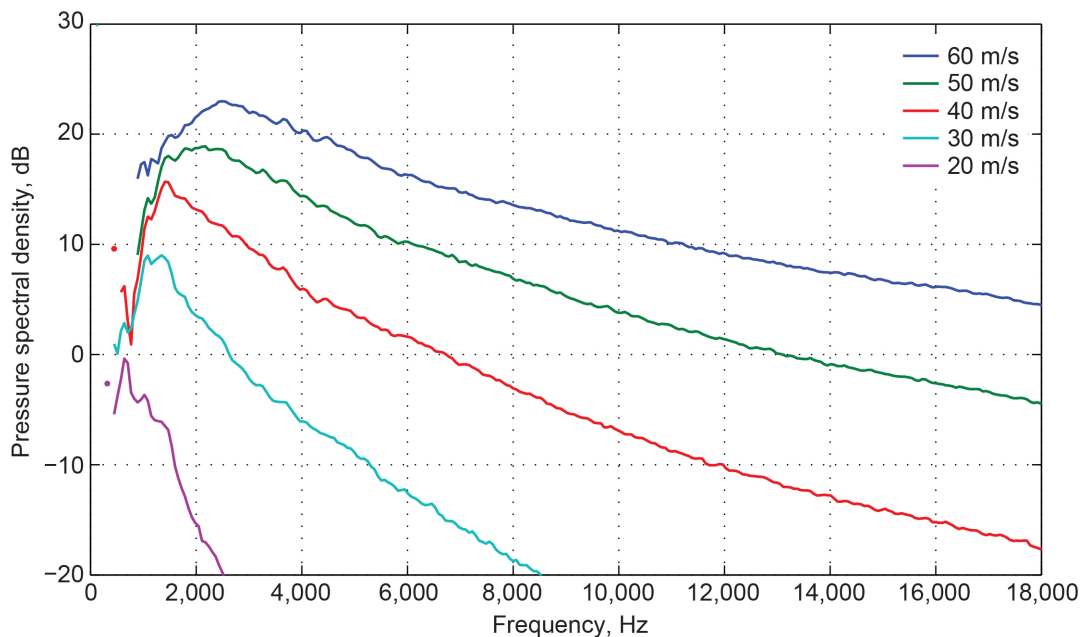


Figure 15.—Measurement between perforated and smooth samples in frame. Microphone 6, 60 m/s jet exit velocity.

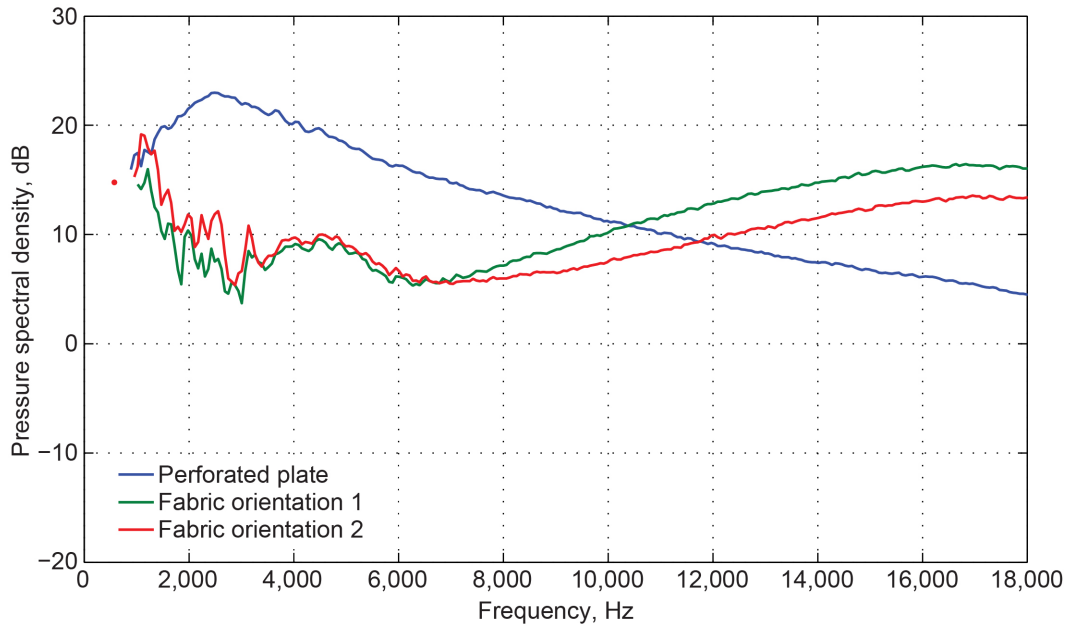


Figure 16.—Summary chart showing effect of fabric over perforate compared with bare perforate. Virginia Polytechnic Institute and State University 2013 test. Microphone 6, 60 m/s jet exit velocity.

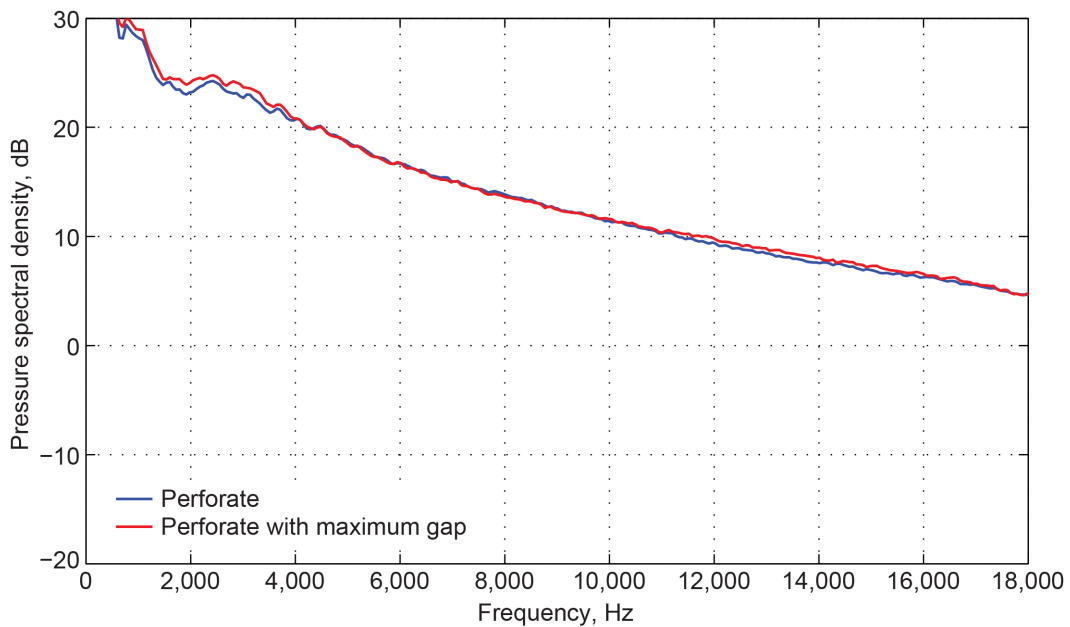


Figure 17.—Effect of gap in perforate. Virginia Polytechnic Institute and State University 2013 test. Microphone 6, 60 m/s jet exit velocity.

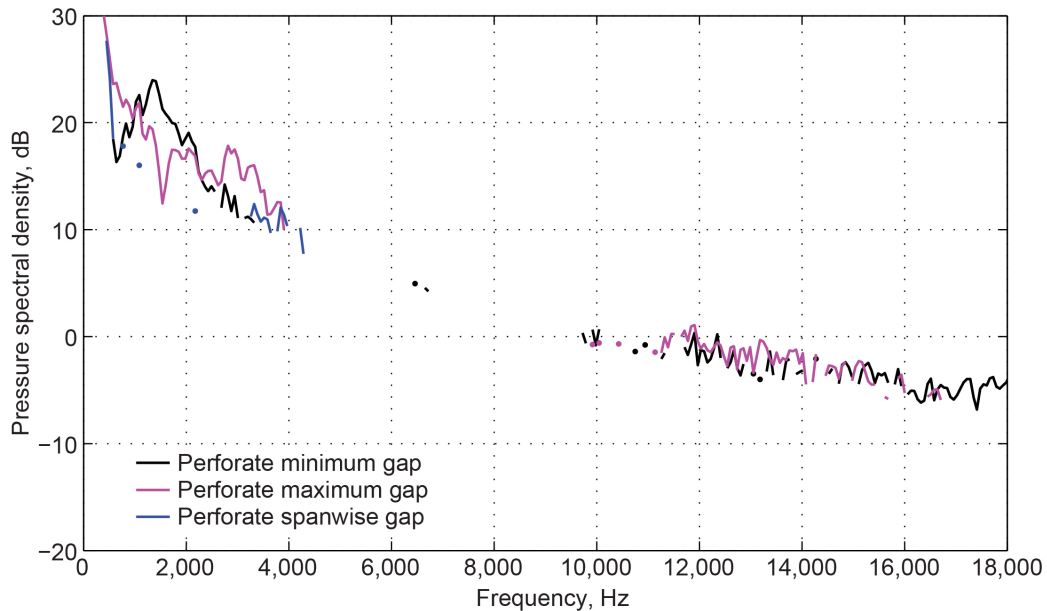


Figure 18.—Summary slide showing additional noise caused by gaps compared with noise from flat bare perforate. Virginia Polytechnic Institute and State University 2013 test. Microphone 6, 60 m/s jet exit velocity.

4.2 2014 Roughness Noise Test

The main findings from the 2013 test were that (1) flow over bare perforate made a lot of noise and was likely a major source of noise in the test section, and (2) fiberglass cloth was not the ideal replacement flow surface. It was confirmed that the Roughness Noise Wall Jet Facility at Virginia Tech is a very suitable place to make the noise measurements. Gaps were found to be a much smaller contribution to the noise than bare perforated plate. Virginia Tech independently performed one additional test that was originally neglected, testing a solid plate covered with woven fabric (Kevlar[®], in their case). Remarkably, they found it produced only barely more noise than the smooth metal panel. Clearly the combination of cloth and perforate was interacting in a nonlinear manner. This encouraged us to refine our test setup to better represent the 9×15 LSWT acoustic treatment.

4.2.1 Acoustic Box for Roughness Noise Testing

The flow surfaces of the 9×15 LSWT test section are made of perforated plate over a 34-cm- (13.5-in.-) deep bulk acoustic absorber. In order to duplicate this boundary condition in the wall jet facility, it was necessary to cut the aluminum plate flow surface of the wall jet and mount a box of bulk absorber below. Fortunately, the Virginia Tech team was committed to the project and agreed to make the necessary modifications. A 30- by 60- by 34-cm (12- by 24- by 13.5-in.) box was built of plywood and filled with the unwoven Kevlar[®] batting that is used in the 9×15 LSWT. A sheet metal bottom was used, and the box was sealed to be airtight. As described in the report by Dahl and Woodward (Ref. 5), the 9×15 LSWT acoustic treatment is made of two layers of Kevlar[®] of different densities. The lower layer (further away from the flow surface) is 17.7 kg/m³ (1.1 lbm/ft³) or 18 sheets of the Kevlar[®] material compressed to 17.2 cm (6.8 in.) thick. The upper layer is the same thickness but only 6.4 kg/m³ (0.4 lbm/ft³) or around seven sheets. A 20-wires-per-inch mesh screen is placed above the upper layer and then the perforated plate was placed on top to form the flow surface. All of these details were replicated in the acoustic box to be used at Virginia Tech. Figure 19 shows the acoustic box installed in the Virginia Tech test facility, as seen from below. Figure 20 shows the top view of the acoustic absorber box in the wall jet facility.



Figure 19.—View of acoustic absorber box installed below wall jet facility at Virginia Polytechnic Institute and State University. Photograph taken June 2, 2014.



Figure 20.—Top view of Kevlar® (DuPont™) treatment inside acoustic box, mesh (20 wires per inch) screen on top. Perforate plate flow surface and tape for edges yet to be applied.

The flush-mount sample installation at the wall jet facility is shown in Figure 21. The initial idea was to use magnet tape to hold the perforated plate to the box, and this worked well for carbon steel test samples. Several samples were subsequently produced that were built of stainless steel, so all samples were taped around the edges to the wall jet plate and this was found to be satisfactory.

4.2.2 Effect of Acoustic Box

The first question was whether the acoustic box made any difference to the measurement. This was quickly answered in the affirmative, as can be seen in Figure 22. For frequencies below 17 kHz for the bare perforate and below 11.6 kHz for the fabric-covered perforate, the addition of the acoustic box made the self-noise louder, by 2 to 4 dB. At frequencies above this crossover frequency, the noise was lower. In the case of the fabric-covered perforate, the noise was as much as 10 dB lower. Possibly, this is due to some kind of resonance in the individual cavities that is present with a solid back plate but absent when the perforate holes are open to a large cavity filled with bulk absorber.

4.2.3 Test Matrix

Lacking a predictive method linking the perforate with cloth cover to flow-induced noise, a larger sample set was devised that might provide insight into noise trends. The samples provided to Virginia Tech are listed in Table 4. Samples A to P were provided in an initial set. These were selected with a focus on answering a specific set of questions, given in Table 5. Subsequent samples Q to W were provided in a second round of testing during 2014 under an addendum to the research contract. Sample G represents the 1986 9×15 LSWT construction, with bare perforate as the flow surface. The 10-mesh (10 wires per inch) screen was found to have no impact on the noise and was not necessarily present in subsequent tests. The 10-mesh screen was installed to reduce fiber migration, as the Kevlar® bulk absorber tended to be pulled through the holes of the perforate out into the tunnel flow. All the top layers we were considering were determined to serve this benefit as a side effect, so it was not used in any other testing.



Figure 21.—Flush mount installation showing panel size. Facility can also accept panels up to 61 by 61 cm (2 by 2 ft), as this figure illustrates. Fasteners visible are covered with clear piece of thin packing tape. Test sample edges are treated with aluminum tape.

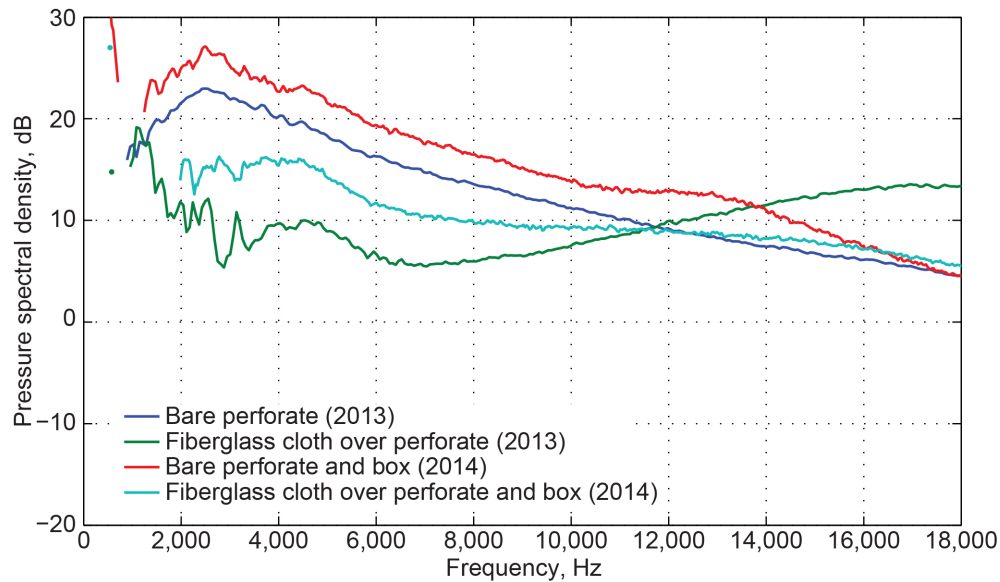


Figure 22.—Comparison of 2013 versus 2014 measurement showing effect of acoustic box under sample. Perforate was 40 percent open with 3-mm (1/8-in.) holes for all four samples shown. Microphone 6, 60 m/s jet exit velocity.

TABLE 4.—SAMPLES FOR 2014 VIRGINIA POLYTECHNIC INSTITUTE AND STATE UNIVERSITY ROUGHNESS NOISE TEST

Test sample	Top layer	Perforate
A	None	Solid
B	Fiberglass cloth	Baseline (40 percent open, 1/8-in. holes, 16 ga)
C	Fiberglass cloth	Solid
D	Fiberglass cloth	2× bigger holes (40 percent open, 1/4-in. holes, 16 ga)
E	Fiberglass cloth	1/2 thickness (40 percent open, 1/8-in. holes, 22 ga)
F	Fiberglass cloth	Greater percent open area (58 percent open, 1/4-in. holes, 16 ga)
G	None	Baseline with 10-mesh (10-wires-per-inch) screen below
H	Fiberglass cloth	Small holes (30 percent open, 1/16-in. holes, 16 ga)
I	Fiberglass cloth at 45° angle	Baseline
J	Felt	Baseline
K	Fiberglass Style 120	Baseline
L	325 by 325 wire cloth	Baseline
M	200 by 600 wire cloth	68 percent open, 0.189-in. holes, 16 ga
N	Coarse wire cloth	Unspecified large holes
O	None	Unspecified small holes
P	None	Unspecified small holes, painted
Q	2,300 by 325 wire cloth	Baseline
R	600 by 200 wire cloth	Baseline
S	200 by 600 wire cloth	Baseline
T	200 by 600 wire cloth	63 percent open, 5/16-in. holes, 16 ga
U	165 by 600 wire cloth	63 percent open, 5/16-in. holes, 16 ga
V	200 by 600 wire cloth	63 percent open, 5/32-in. holes, 16 ga
W	200 by 600 wire cloth	Baseline perforate, diffusion bonded

TABLE 5.—PARAMETRIC TEST POINTS FOR 2014 ROUGHNESS NOISE TEST

Comparison	Purpose
B versus C	Compare noise of fabric over solid versus perforated panel
B versus D	Evaluate effect of hole size for fiberglass cloth over perforate
B versus E	Evaluate effect of plate thickness for fiberglass cloth over perforate
D versus F	Evaluate effect of percent open area for fiberglass cloth over perforate
B versus H	Combined hole size and percent open area effect
B versus I... P	Effect of other fabric types over baseline perforate

4.2.4 Data Processing

As an improvement to examining individual spectra, some postprocessing of the data was introduced. The best data was determined to be from microphones 2 to 6, as these consistently had good signal-to-noise ratio and represented the directivity of most interest. These channels were used for the following results. First, background noise was subtracted from the spectra of interest to give a spectra due to the sample only. Next, the amplitude was corrected for distance to a line parallel to the surface, as this would account for the geometry seen by a single observer in the tunnel, in the case of a sufficiently large sample. The pressure spectra were averaged before conversion to decibels. These spatially averaged spectral density curves will be denoted PSD_{avg} in the remainder of this section. Data processing was carried out using MATLAB® (The MathWorks, Inc.) (Ref. 20).

4.2.5 Noise From Fiberglass Cloth

After confirming the effect of the acoustic box, the next question was whether the flow over fiberglass cloth on a solid panel showed the same low noise level as reported by Virginia Tech for Kevlar® 120. As shown in Figure 23, it was confirmed. The flow over fiberglass cloth adhered to a solid panel is extremely quiet, and unmeasurable except at frequencies above about 12.5 kHz. It was clear that a perforate layer under the fabric has a huge impact on the flow-induced noise.

4.2.6 Effect of Hole Size

The effect of perforate hole size was investigated using a perforated plate covered with fiberglass cloth. The results are shown in Figure 24. It can be seen that hole size affects the lower frequency peak, moving from 2,400 Hz with 1/4-in. holes to 4,300 Hz with 1/8-in. holes and 5,600 Hz with 1/16-in. holes. The spectral shape of the high-frequency end of the measurement is essentially the same, and the amplitude is apparently controlled by the percent open area, where 30 percent open is the quietest and 58 percent is the loudest, with both 40 percent area samples being in the middle and very similar in level and shape. This set of experiments was only conducted with fiberglass cloth over perforate, so it is an assumption that similar trends would be observed with bare perforate or perforate with wire cloth covering.

4.2.7 Effect of Plate Thickness

The effect of thickness was considered, and the results are shown in Figure 25. The baseline 16-ga plate was compared with a 24-ga plate. The height of the acoustic box was adjusted so that the sample was still flush with the facility flow surface. Thickness of the plate had a small effect on the roughness noise, with the thinner plate being louder by about 0.5 dB at 18 kHz. It is not known if the plate acoustic transparency matters, or if this effect is due to flow noise only. This difference could also be within experimental uncertainty, or there could be other differences between the handmade samples that were

not spotted at the time of testing. As seen in Section 5.3.6, the plate thickness has a meaningful effect on the acoustic transparency of the fabric and plate combination, so thinner perforate is preferred for anechoic quality of the facility.

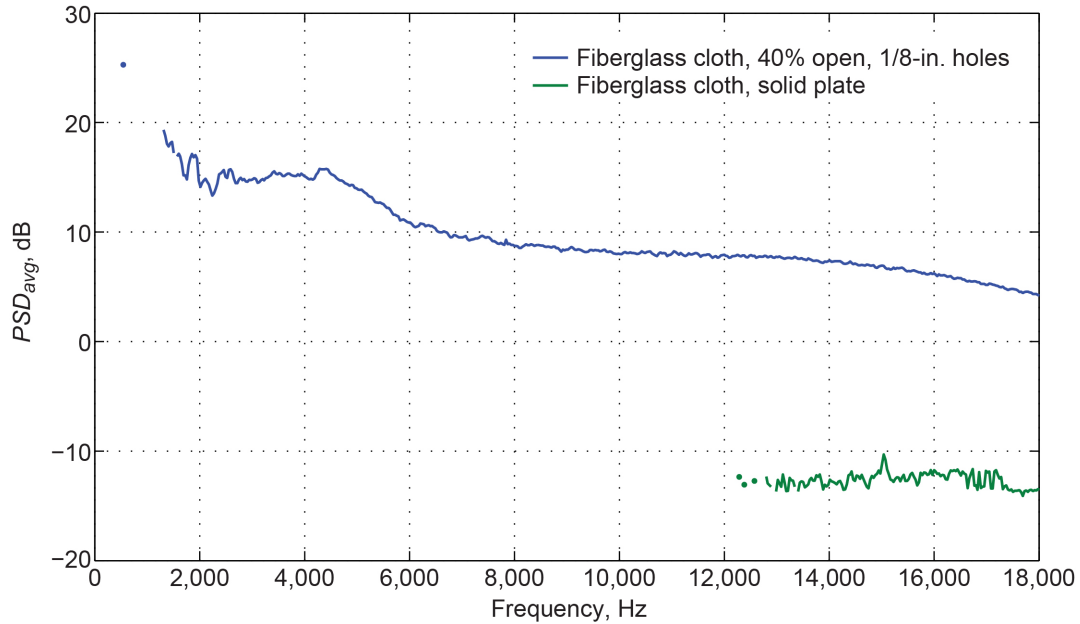


Figure 23.—Fiberglass cloth over baseline perforate compared with fiberglass cloth over solid panel. Samples B and C from Table 4. Jet exit velocity of 60 m/s. Spatially averaged pressure spectra density (PSD_{avg}).

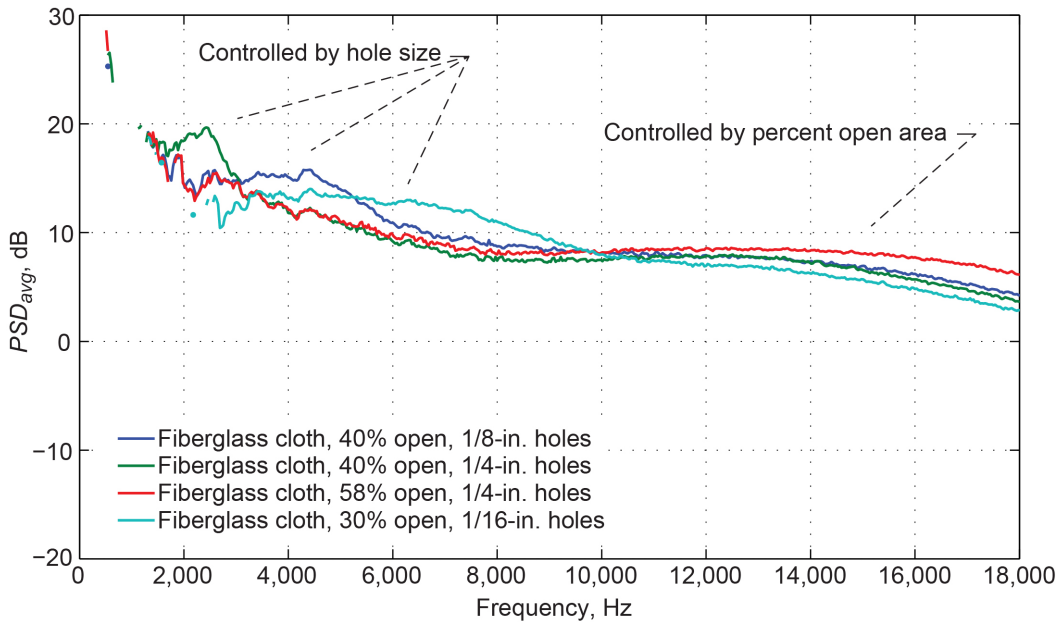


Figure 24.—Effect of hole size on noise due to flow over fiberglass cloth bonded with spray adhesive to perforated steel plate. Samples B, D, F, and H from Table 4. Jet exit velocity of 60 m/s. Spatially averaged pressure spectra density (PSD_{avg}).

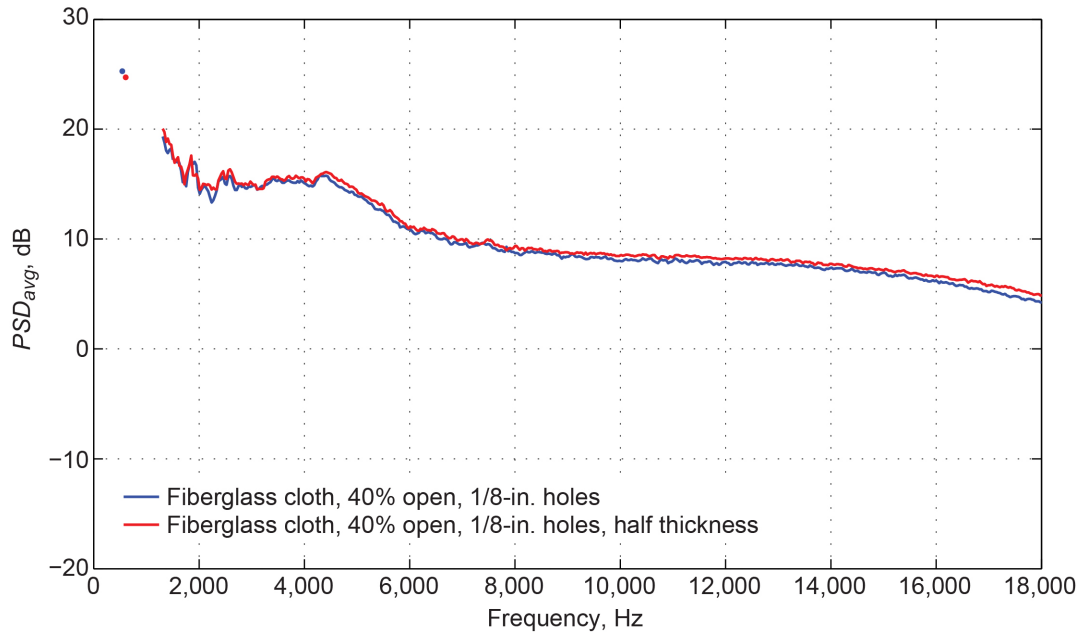


Figure 25.—Effect of plate thickness on flow-induced noise. Samples B and E from Table 4. Jet exit velocity of 60 m/s. Spatially averaged pressure spectra density (PSD_{avg}).

4.2.8 Other Fabric Types

The effect of other fabrics and materials was more complicated to investigate. Figure 26 shows several different fabrics over the baseline (40-percent open, 1/8-in. hole, 16 ga) perforate sheet. This test was not intended to be parametric, but to survey a wide range of fabric types.

The basic fiberglass cloth over perforate is shown in blue. By comparison, turning the fabric to 45° is considerably louder. Perhaps this is due to increased turbulence created due to the flow hitting angled threads. Fiberglass 120 is a “4-harness” weave, where the threads go over three fibers, then under one. This is typically intended for composite fabrication where nonflat shapes are required. When used as a flow surface, it was found to be quieter than the baseline at frequencies above around 7,000 Hz. The noise reduction is around 6 dB at frequencies higher than 14 kHz. This is perhaps due to the somewhat irregular weave. The square weave micronic wire cloth (sample L) is much louder at low frequencies and quieter at high frequencies. This material has extremely low flow resistance (2 to 3 MKS Rayl) and is visibly porous due to the square weave. It seems reasonable that in the limit of flow resistance going to zero, the noise might approach that of a bare perforate sample. Finally, it can be seen that the felt sample is extremely quiet. This unwoven material perhaps does not cause any periodic flow disturbance. The durability of this material and suitability for a building material was questionable, but it is clearly very quiet.

4.2.9 NASA Ames Research Center 40- by 80-Foot Wind Tunnel Sample

The most remarkable result was found when testing the portion of the NASA Ames 40×80 WT diffusion bonded panel (40×80 sample). As shown in Figure 27, the woven fiberglass does reduce roughness noise quite a lot, with a peak reduction of around 10 dB, but the samples from the NASA Ames 40×80 WT facility reduced the self-noise another 7 dB and the high-frequency noise by 10 to 15 dB. No other sample reduced noise across all frequencies except for the felt, which we did not feel was a viable choice due to durability concerns. This noise reduction potential is captured in Figure 28, which is the decibel difference between the baseline perforate panel representing the existing flow surface from the

9×15 LSWT and the diffusion bonded micronic wire cloth panel from the 40×80 WT. This finding focused our attention on micronic wire cloths.

Compared to sample L, the 40×80 sample uses a different micronic wire cloth. The cloth on sample L was a 325- by 325-mesh-per-inch square weave with 0.036-mm wire diameter, with a published flow resistance of 2 to 3 MKS Rayl. The 40×80 sample M has a 200- by 600-mesh-per-inch twill Dutch weave cloth, with wire sizes of 0.061 mm for the coarser weave and 0.046 mm for the fine weave, with a flow resistivity of 8 to 10 MKS Rayl. The perforate plates were also somewhat different, as listed in Table 4. The percent open area was significantly higher for the 40×80 sample (68 versus 40 percent) and had larger hole size (0.189 versus 0.125 in.).

Additionally, the sample from the 40×80 WT was tested upside down, with the wire cloth between the perforate and the bulk absorber. As a practical matter, the floor of the 40×80 WT is built with the wire cloth behind the perforate for durability. Figure 29 shows the result, with the implication that a substantial self-noise penalty results from this installation, ranging from 5 to 10 dB. It is much quieter to have the wire cloth as the flow surface, even though the net flow resistance of the combination is the same.

4.2.10 Micronic Wire Cloth Samples

Our first effort to mimic the NASA Ames 40×80 WT panel was to use spray adhesive to affix wire cloth to an off-the-shelf perforated steel panel having slightly different percent open area and hole size than the Ames 40×80 sample. The same 200 by 600 acoustic wire cloth could be commercially procured. Figure 30 shows the result, and it can be seen that we are immediately in the ballpark. The 40×80 sample had some imperfections and handling damage, likely due in part to being around 20 years old.

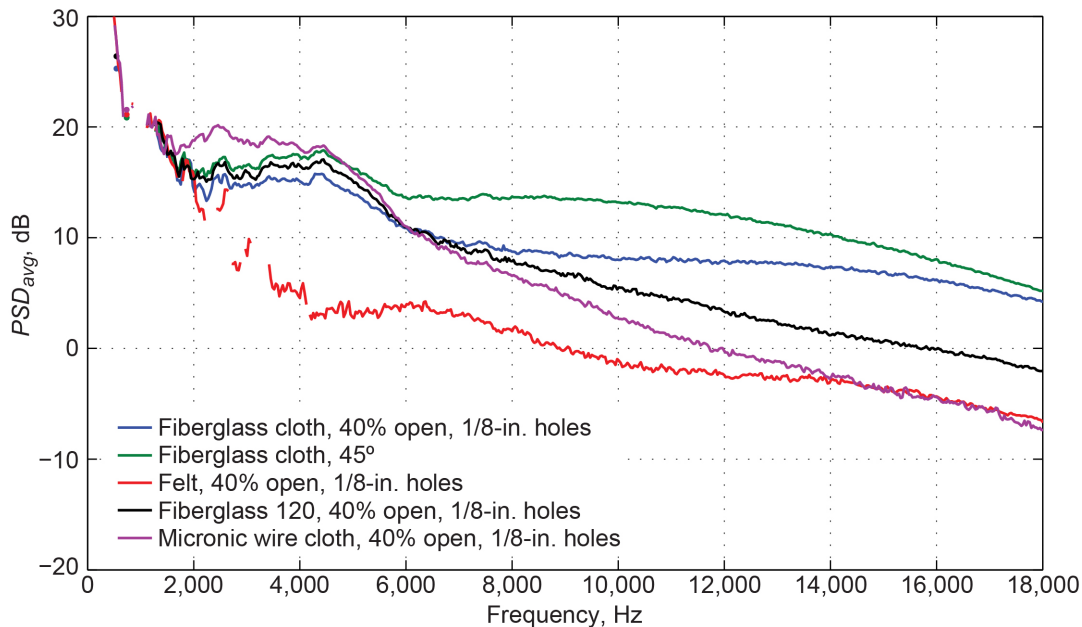


Figure 26.—Various cloths over baseline perforate. Samples B, I, J, K, and L from Table 4. Jet exit velocity of 60 m/s. Spatially averaged pressure spectra density (PSD_{avg}).

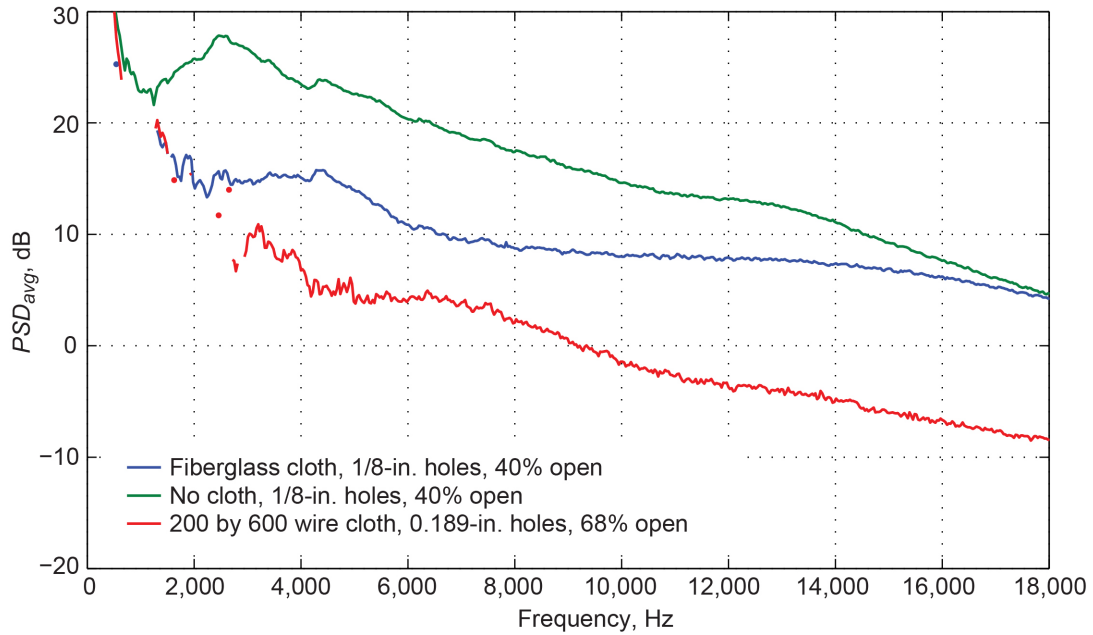


Figure 27.—Most important result, comparing existing 9- by 15-Foot Low-Speed Wind Tunnel flow surface to fiberglass cloth option and 40- by 80-Foot Wind Tunnel National Full-Scale Aerodynamics Complex flow surface. Samples B, G, and M from Table 4. Jet exit velocity of 60 m/s. Spatially averaged pressure spectra density (PSD_{avg}).

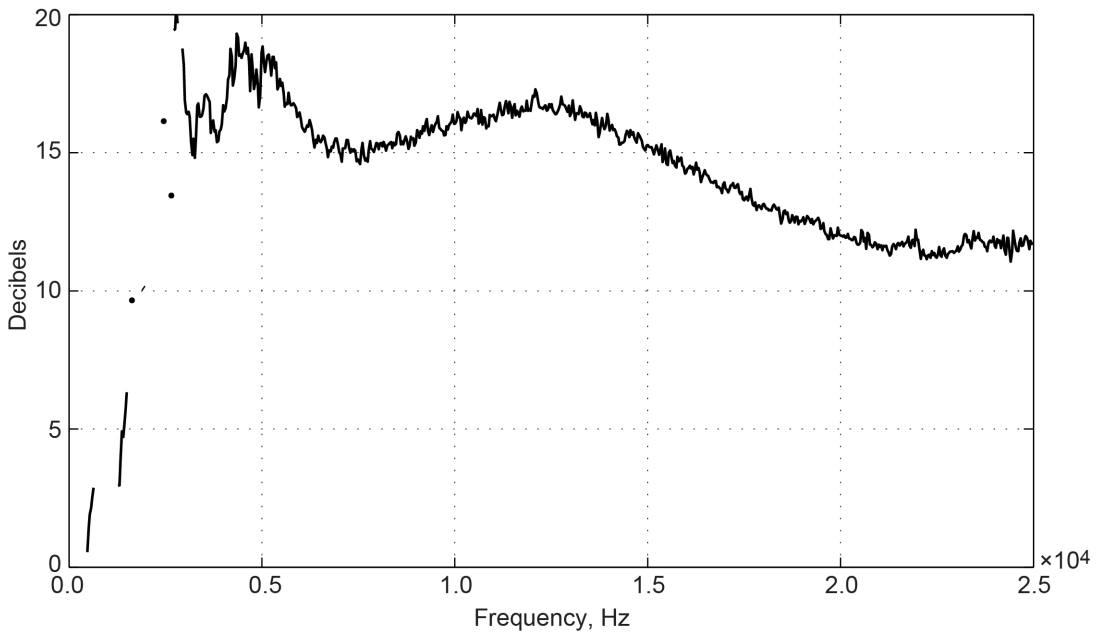


Figure 28.—Decibel difference between samples from 9- by 15-Foot Low-Speed Wind Tunnel (bare perforate, sample G) and 40- by 80-Foot Wind Tunnel (200 by 600 wire cloth over perforate, sample M). Spectra as shown in Figure 27. Jet exit velocity of 60 m/s.

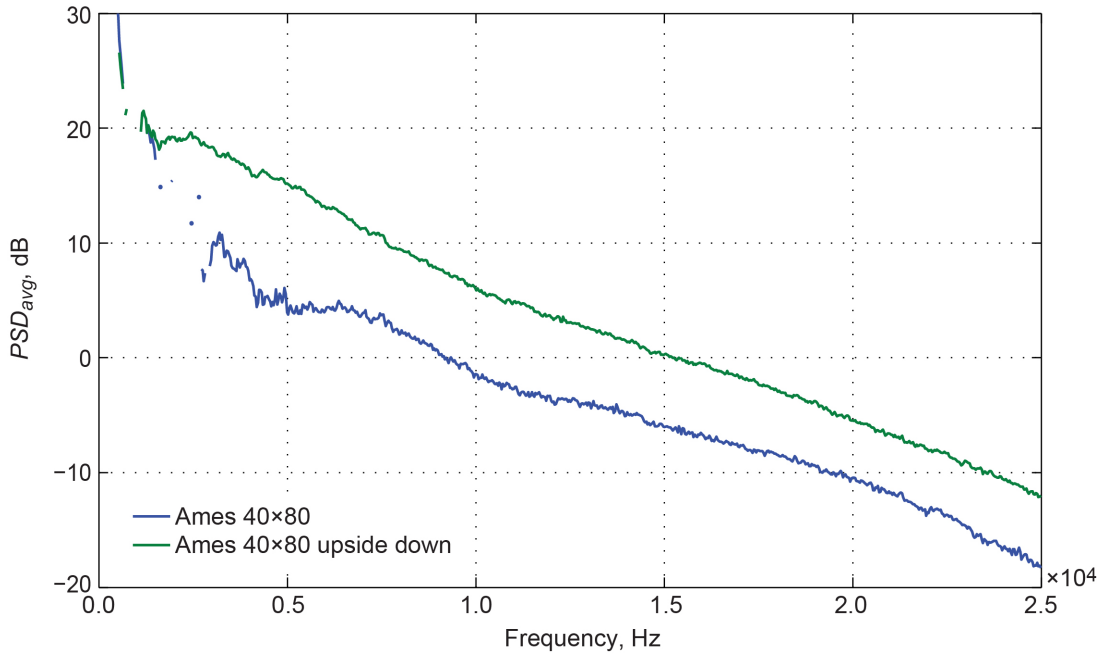


Figure 29.—Effect of normal (wire cloth on flow surface side) versus upside down (wire cloth between perforate and bulk absorber) for NASA Ames Research Center 40- by 80-Foot Wind Tunnel panel (Ames 40×80), representing wall and ceiling versus floor installation, respectively. Sample M from Table 4. Jet exit velocity of 60 m/s. Spatially averaged pressure spectra density (PSD_{avg}).

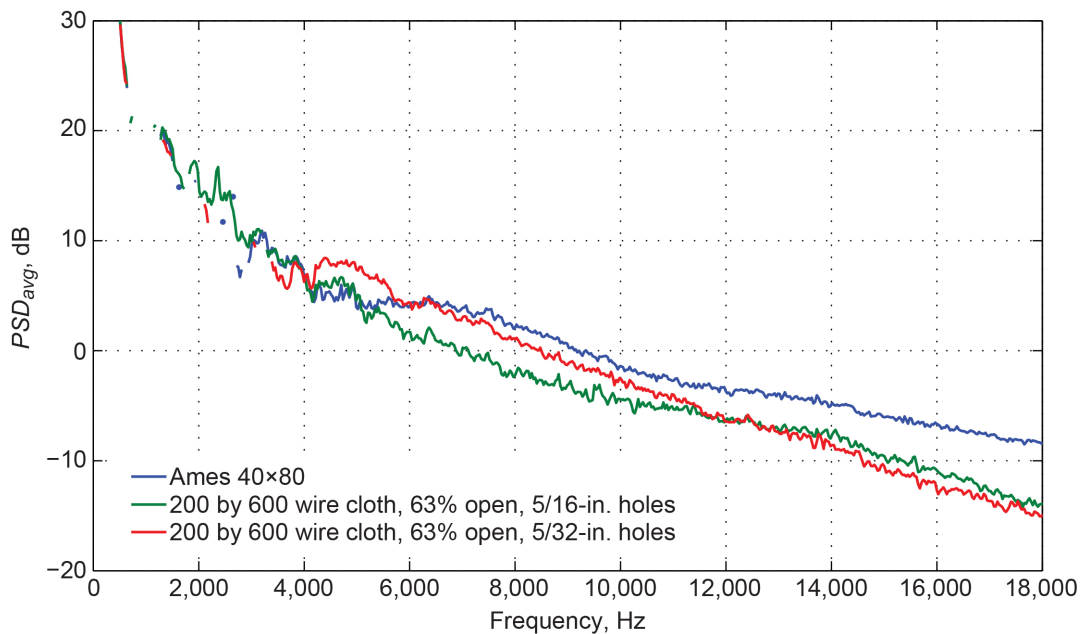


Figure 30.—Spray-adhesive versions of 200 by 600 wire cloth on perforate compared with the sample from NASA Ames Research Center 40- by 80-Foot Wind Tunnel (Ames 40×80). Samples M, T, and V from Table 4. Jet exit velocity of 60 m/s. Spatially averaged pressure spectra density (PSD_{avg}).

4.2.11 Diffusion Bonded Panels

Our first attempt at working with a vendor to make a diffusion bonded panel was only somewhat successful. The resulting panel was significantly rough to the touch, with fibers embedded in the wire cloth. These fibers come from the material used to separate layers in the diffusion bonding process. This was apparent in the roughness noise measurement, as Figure 31 shows that there was a substantial broadband noise increase. This contamination is described throughout the 40×80 WT report (Ref. 9) and an extensive set of cleaning procedures were used to remove the majority of the unwanted material. Wishing to avoid this, other vendors were pursued as will be discussed in Section 4.3.

4.2.12 Types of Micronic Wire Cloth

The 200 by 600 wire cloth was obviously a reasonable candidate, but other materials were also pursued. The 325 by 325 wire on sample L had not performed well, presumably due to having too little flow resistance, as shown in Figure 26. A cloth with slightly tighter wire weave of 165 by 800 was also tested, and indeed did have lower roughness noise, as shown in Figure 32.

4.2.13 Orientation of Micronic Wire Cloth

The 200 by 600 cloth is a twilled Dutch weave, with fewer (200) thicker straight fibers in one direction and more (600) thinner fibers passing over and under them. This presented two possible directions to orient the cloth with respect to the flow. A closeup view of the wire cloth examined from the NASA Ames 40×80 sample is shown in Figure 33.

It was found that the quieter configuration was with the higher number of wires parallel to the flow. With the wire cloth as pictured in Figure 33, the flow should thus be in the left to right direction rather than top to bottom. The noise measurement is shown in Figure 34. A jeweler’s loupe or similar magnifying device is required to identify the orientation of the fabric. This requirement had some impact on the maximum size of panel that could be produced as the wire cloth is manufactured in a preferred orientation.

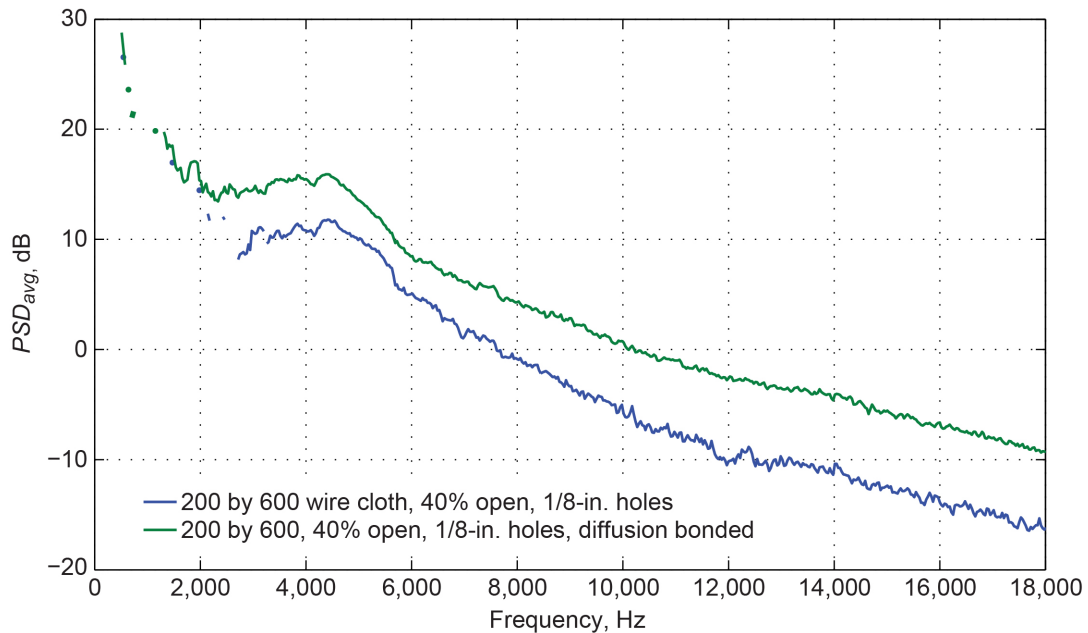


Figure 31.—Spray-adhesive versions of 200 by 600 wire cloth on perforate compared with diffusion bonded prototype. Samples S and W from Table 4. Jet exit velocity of 60 m/s. Spatially averaged pressure spectra density (PSD_{avg}).

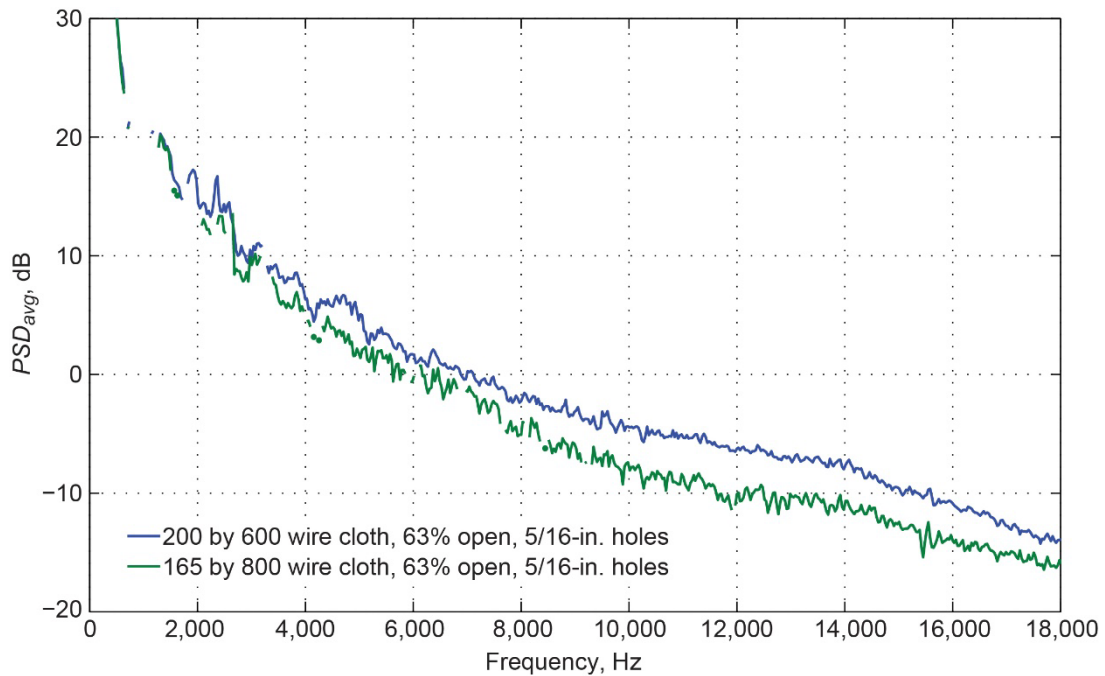


Figure 32.—Spray-adhesive versions of 200 by 600 wire cloth on perforate compared with 165 by 800 wire cloth on perforate. Samples T and U from Table 4. Jet exit velocity of 60 m/s. Spatially averaged pressure spectra density (PSD_{avg}).

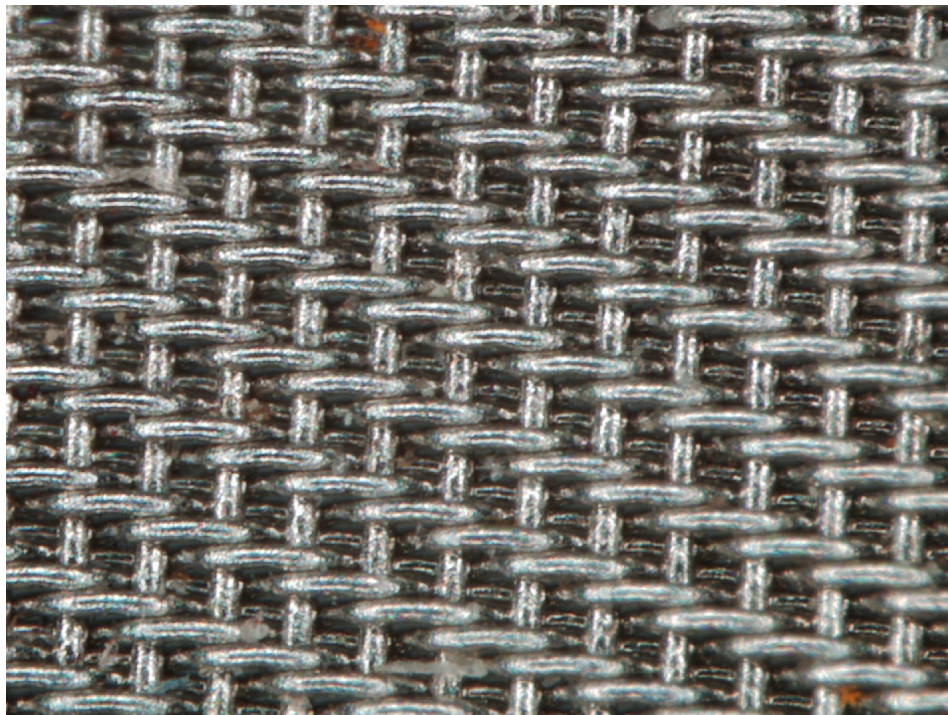


Figure 33.—Microscope inspection of NASA Ames Research Center 40- by 80-Foot Wind Tunnel (40×80 WT) sample to get close look at 200 by 600 micron wire cloth. From NASA Ames 40×80 WT design report (Ref. 8), the wire cloth has 200 warp by 600 shute wires per inch, 0.0024- and 0.0018-in. diameter, respectively.

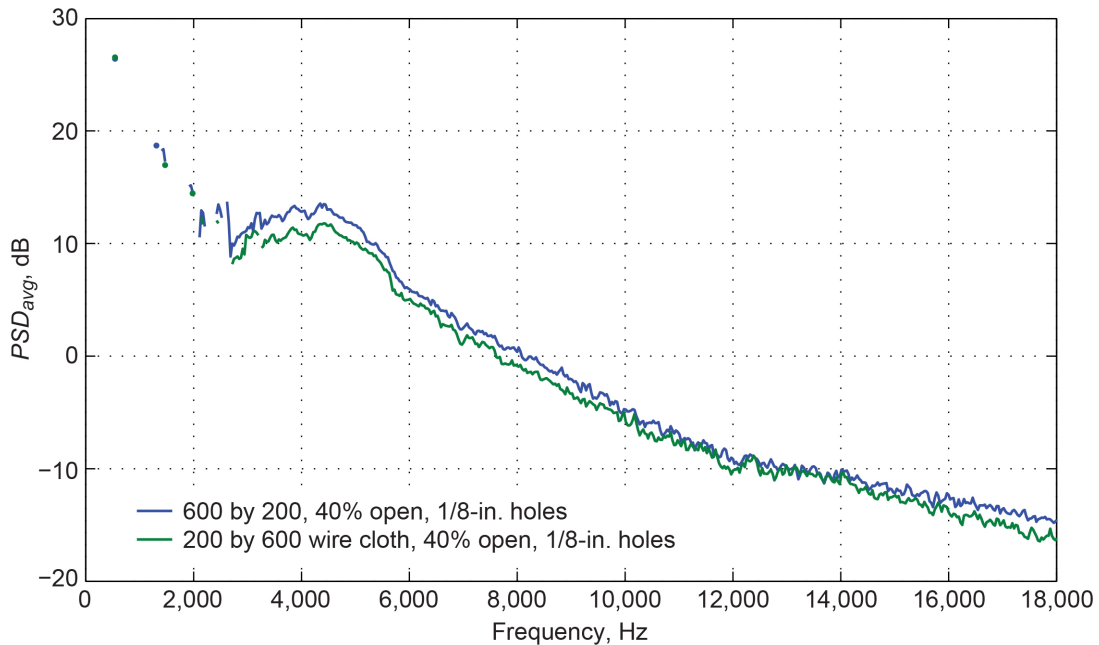


Figure 34.—Spray-adhesive versions of 200 by 600 wire cloth and same cloth rotated 90°. First number is cross-stream wire count and second number is streamwise wire count. Samples R and S from Table 4. Jet exit velocity of 60 m/s. Spatially averaged pressure spectra density (PSD_{avg}).

4.2.14 Other Observations

The 2,300 by 325 wire cloth over baseline perforate was as quiet as a solid steel panel to within our measurement capability, so no results are shown for this combination. This confirmed that a very smooth and very high flow resistance surface would have very low self-noise. Samples N, O, and P were provided by Jacobs Engineering from their various suppliers. They were not competitive for self-noise, and the construction details may be proprietary, so their results are not included here.

4.2.15 Conclusions From 2014 Roughness Noise Test

The testing in 2014 concluded successfully, as we found a suitable and proven solution for a quiet flow surface for the 9×15 LSWT. The diffusion bonded micronic wire cloth on perforate, as installed in the 40×80 WT since the mid-1990s was quieter than anything else we tested. It also had proven durability, given it had already been used in a wind tunnel for 20+ years at flow speed up to Mach 0.4. The report on the 40×80 WT upgrade (Ref. 8) explains that the team at NASA Ames was pursuing a “low-drag” lining, but clearly the low roughness noise was a happy side effect. The wire cloth should be on the flow side for lowest noise, which was our goal. We pursued vendors for diffusion bonded panels.

4.3 2016 Roughness Noise Test

The diffusion bonding manufacturing process turned out to be more of a challenge than we expected. Several of the examples produced by vendors were contaminated with fibrous materials that are used to separate the layers in the oven. A similar experience was noted in the 40×80 WT report (Ref. 8), and they reported extensive care and cleaning were required to produce acceptable samples. Some samples had no contamination, and the vendor explained a proprietary method was used to separate layers. Some samples

that we procured had the wire cloth dimpled down into the perforate like a golf ball. Clearly, more roughness noise testing was in our future.

4.3.1 Test Matrix

A third research contract was arranged with Virginia Tech to test the best of the diffusion bonded panels we were able to procure. Also, we had become interested in the acoustic properties of panels thinner than 16 ga, so two thinner wire cloth samples built with spray adhesive were tested. Finally, we wanted to investigate the effect of boundary layer thickness on the radiated noise and make measurements of the velocity field above the perforate. These tests were intended to help understand how the noise changes between the low-speed wall jet facility and the 9×15 LSWT. The bare perforate sample was tested again for repeatability confirmation and so boundary layer measurements could be acquired. Table 6 shows the test matrix for all the samples.

Three reasonably good diffusion bonded panels were identified. All three panels were built with 63 percent open perforate, 4-mm (5/32-in.) holes, and 165 by 800 wire cloth. Panel 5 had dimples 0.15 to 0.18 mm (0.006 to 0.007 in.) deep, seen in Figure 35. Panel 12 had dimples 0.10 to 0.13 mm (0.004 to 0.005 in.) deep. Panel 13 was initially the same as panel 12, but was pressure washed from the back side to try to smooth out the dimples. Visually it was clear that this made a difference, but the dimple depth was not recharacterized.

4.3.2 Boundary Layer Bump

Among the many differences between the wall jet facility and the 9×15 LSWT, boundary layer thickness was to be investigated. To increase the thickness of the wall jet, we built a 0.5-in.-high geometrically scaled version of the two-dimensional (2D) NASA Wall-Mounted Hump (Ref. 21) that would span the entire width of the wall jet facility. The intent was to cause a near-wall velocity deficit that would thicken the boundary layer without producing additional noise. The bump feature, as shown in Figure 36, was built-in pieces with a thermoplastic printer.

The installation of the bump in the Virginia Tech roughness noise facility is shown in Figure 37. The pieces were held together with aluminum tape, which was also used to secure the bump to the plate. The downstream edge of the bump was 6 in. upstream of the sample test leading edge.

TABLE 6.—TEST MATRIX FOR THIRD CAMPAIGN (2016) AT VIRGINIA TECH

Sample or panel	Surface characteristics			Measurements			
	Percent open area	Hole size, mm	Wire mesh	Acoustics	Boundary layer	Acoustics with bump	Boundary layer with bump
Diffusion bonded panel 5	63	4	165 by 800	x	x	x	x
Diffusion bonded panel 12	63	4	165 by 800	x	--	--	--
Diffusion bonded panel 13	63	4	165 by 800	x	--	x	--
20-ga perforate	63	4	200 by 600	x	--	x	--
22-ga perforate	63	4	200 by 600	x	--	x	--
Sample L	40	3.2	325 by 325	x	x	x	x
Sample G	40	3.2	-----	x	x	x	--
Sample A	---	----	-----	x	x	x	x



Figure 35.—Diffusion bonded panel 5 showing dimpling of approximately 0.18-mm (0.007-in.) depth.



Figure 36.—Segment of two-dimensional linear hump geometry used to create modified boundary layer on wall of roughness noise facility at Virginia Polytechnic Institute and State University.



Figure 37.—Virginia Polytechnic Institute and State University roughness noise facility with cross-stream linear bump installed upstream of test sample.

4.3.3 New Diffusion Bonded Panels

The results for the diffusion bonded panels are shown in Figure 38. These three panels did not have fibrous contamination in the wire cloth, unlike sample W from 2014. As hoped, correspondingly lower roughness noise levels were found. It should be noted that the 2014 sample W used 200 by 600 wire cloth, while the 2016 samples were all made with 165 by 800 wire cloth. This may contribute to some of the noise difference in the 8- to 20-kHz range, as noted in Figure 32. The effect of dimpling was determined to be small by comparison, although diffusion bonded panel 5 was measurably the loudest of the three 2016 panels. It was recommended that dimpling be limited to the range tested, a maximum of 0.18 mm (0.007 in.).

4.3.4 Effect of Bump

The noise impact of the bump was measured by comparing a solid panel with and without the bump. The effect was found to be negligible below about 17 kHz, with the bump being slightly louder by about 1.5 dB at 20 kHz. Figure 39 shows the measured spectra from microphone 2 with the smooth plate and the bump. A slight 1.5-dB decrease around 7 kHz was also observed, but this is close to the measurement uncertainty and may only reflect repeatability.

Figure 40 shows sample G, the “9×15 baseline,” measured in 2014 and 2016, with and without the upstream bump. The 2014 and 2016 samples were found to have some differences in the 12- to 14-kHz range. This is possibly due to sample variation, as a new sample was made for 2016. Oxidation, flatness, imperfections, etc., could all contribute to the observed differences. When the bump was added upstream of the 2016 test sample, the noise was found to decrease at most frequencies. This is likely because the boundary layer is thicker, so the near-wall flow is slower. The effect of the bump on the flow velocity will be shown in Section 4.4.

The trend that the bump lowered the noise continued with the diffusion bonded panel samples. This leads to some slightly strange results in the processed data as presented, since the most downstream

microphone used (microphone 2) sometimes now was as quiet as the smooth plate. Also, the noise floor for the 2016 testing was slightly higher than in 2014. The processing, therefore, is sometimes including it in the average and sometimes excluding it, leading to a messier spectra. Figure 41 is the main takeaway from the testing with the bump, showing there is not a substantial difference in noise reduction, and the diffusion bonded panel is still a quiet solution.

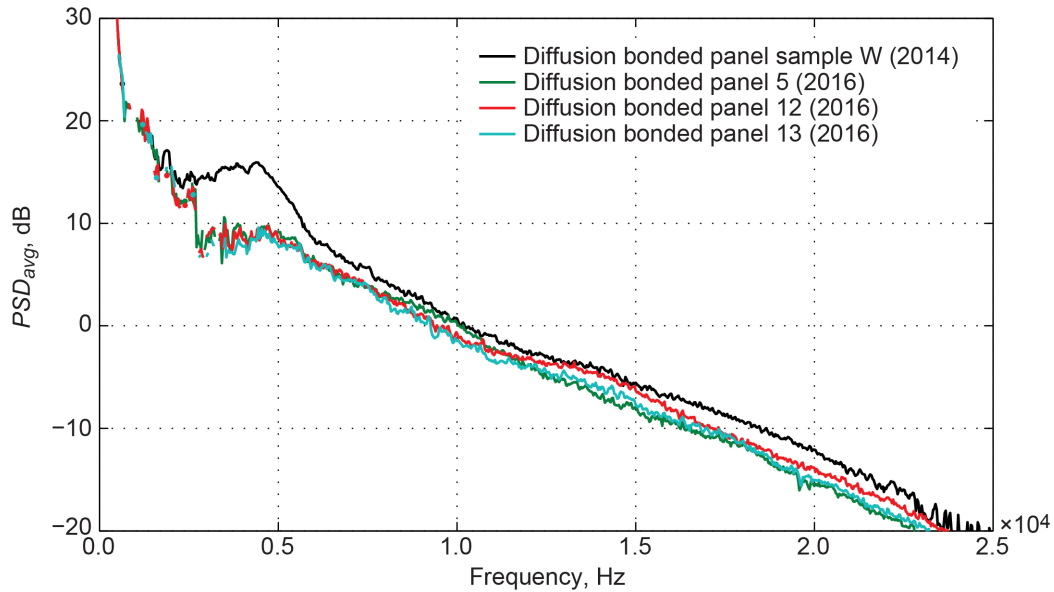


Figure 38.—Comparison of four diffusion bonded panels. Jet exit velocity of 60 m/s. Spatially averaged pressure spectra density (PSD_{avg}).

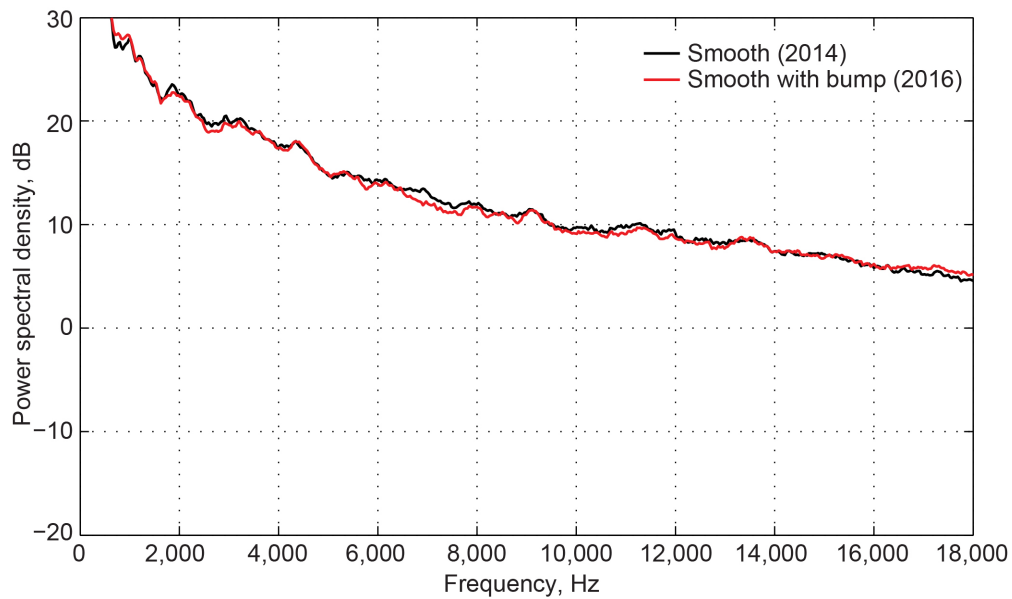


Figure 39.—Smooth wall (sample A) with and without bump, microphone 2, measured in 2016. Jet exit velocity of 60 m/s.

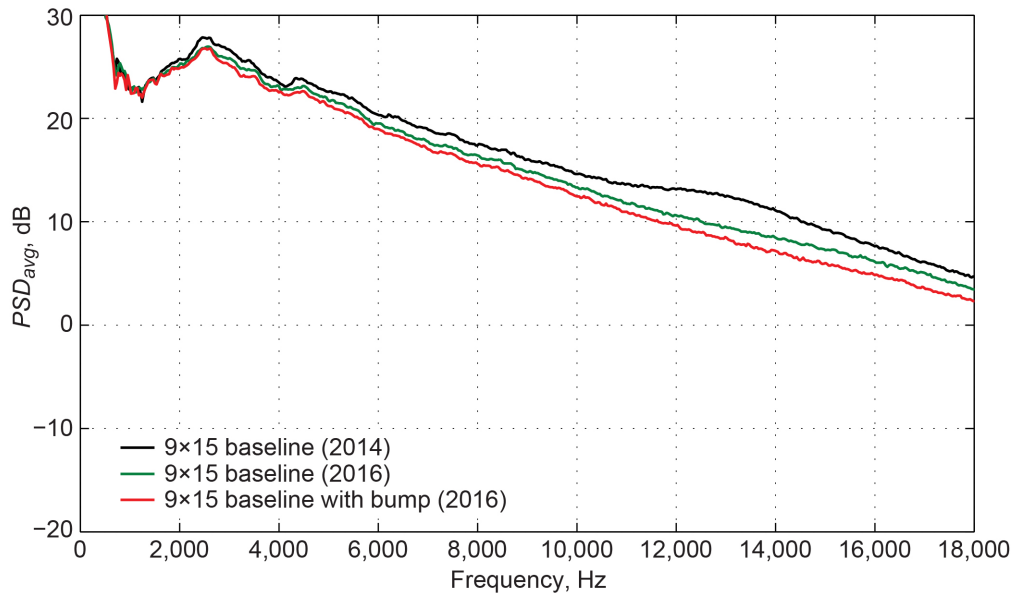


Figure 40.—Surface averaged noise measurement showing repeatability of baseline perforate plate “9×15 baseline” (sample G) and effect of upstream linear bump. Jet exit velocity of 60 m/s. Spatially averaged pressure spectra density (PSD_{avg}).

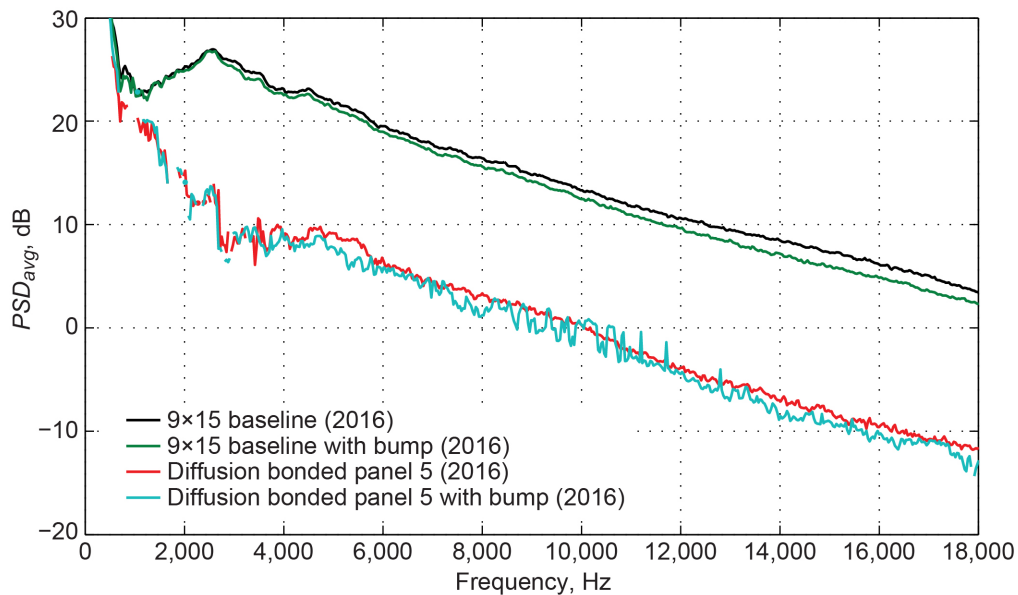


Figure 41.—Surface averaged noise measurement for bare perforate “9×15 baseline” (sample G) and diffusion bonded panel 5 configurations, with and without upstream linear bump. Jet exit velocity of 60 m/s. Spatially averaged pressure spectra density (PSD_{avg}).

4.3.5 Fasteners

The original design for the implementation of the diffusion bonded panels in the 9×15 LSWT was to weld them into box assemblies. There was some difficulty welding the diffusion bonded panels without damaging the wire cloth. Mechanical fasteners are an alternative, but flow over rivets was suspected to be a noise source. A set of panels was built and shipped to Virginia Tech for testing, featuring a grid of eight fasteners roughly approximating the density expected in the final construction. Solid panels were built

and tested along with diffusion bonded panels. A last minute addition to the fastener lineup was a press-fit stud that grabbed the perforate in the existing holes and provided a threaded rod below. Figure 42 shows the noise measurement of the three options. The threaded stud was the quietest, and essentially indistinguishable from the unmodified diffusion bonded panel. This fastener was chosen for use in the construction project. Photographs of the rivets in the test panels are shown in Figure 43 and Figure 44 while the press-fit stud is shown in Figure 45.

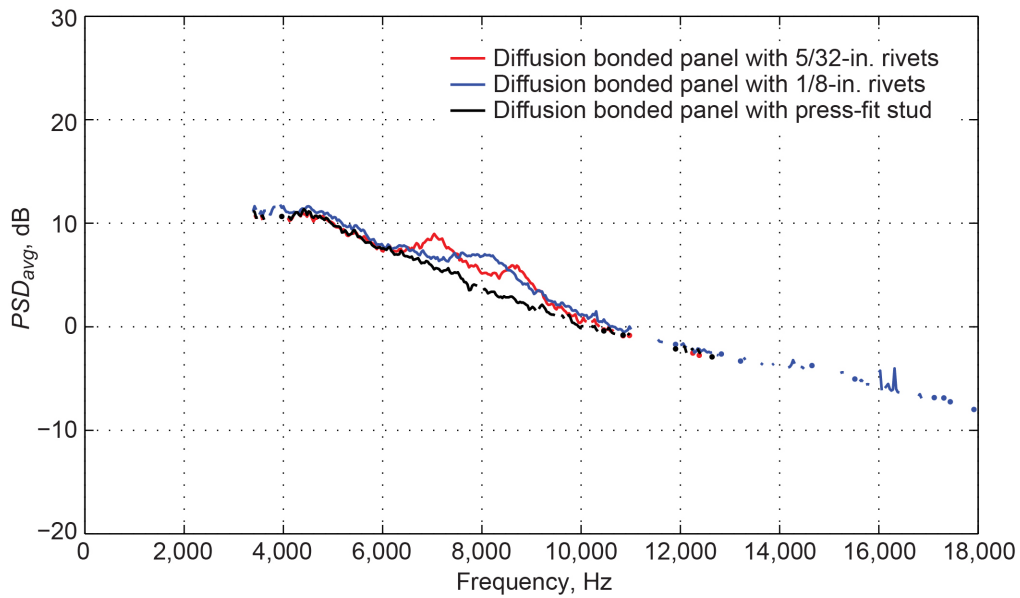


Figure 42.—Comparison of three different fastener types in similar diffusion bonded panels. Jet exit velocity of 60 m/s. Spatially averaged pressure spectra density (PSD_{avg}).

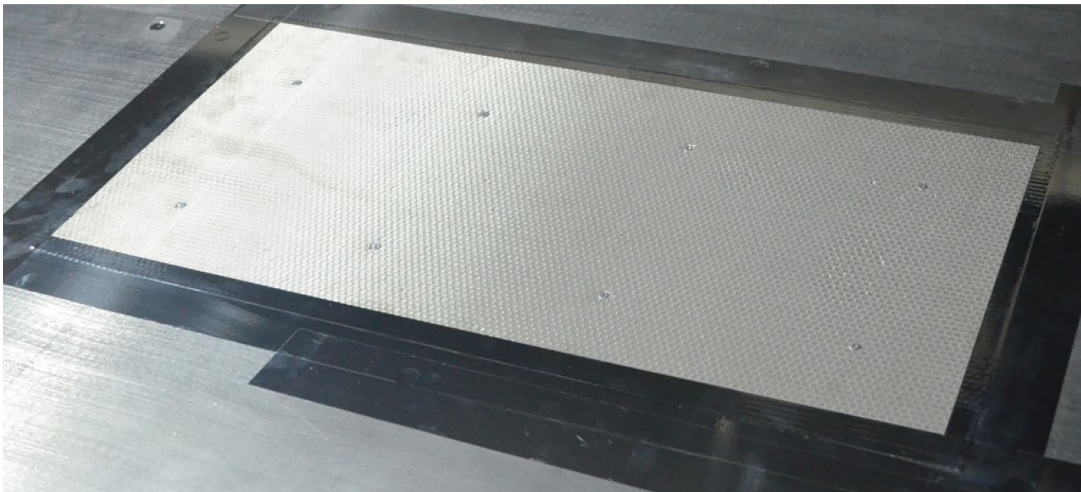


Figure 43.—Panel for rivet noise testing showing grid of eight fasteners.

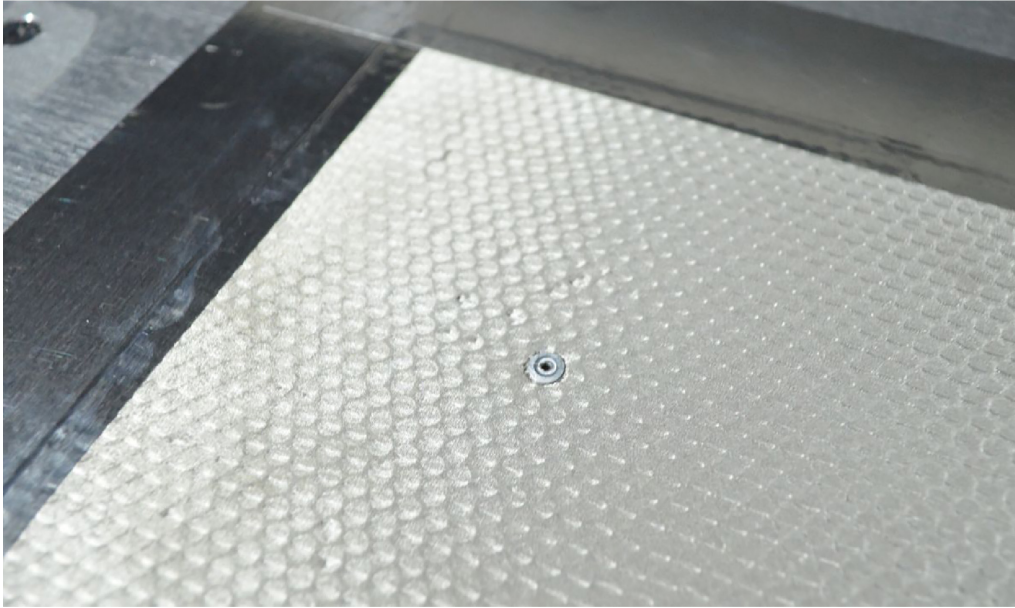


Figure 44.—Closeup of 1/8-in. rivet used with 5/32-in. perforate diffusion bonded panel.

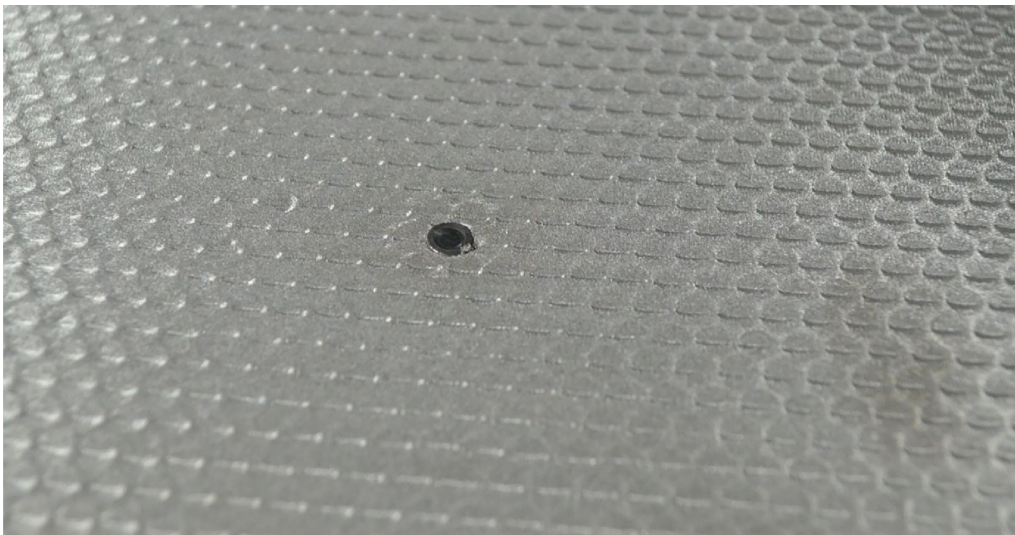


Figure 45.—Closeup of flow surface side of press-fit stud.

4.4 2016 Velocity Measurements

In order to help interpret the roughness noise measurement, we utilized hot wire anemometry to measure the near-wall flow field upstream and downstream of the test samples. There was difficulty making measurements directly over the perforate samples, so the complete data set was acquired 13 mm (0.5 in.) downstream of the sample. The upstream flow onto the sample plate was recorded with the smooth sample at 13 mm (0.5 in.) upstream of the sample or 140 mm (5.5 in.) downstream of the linear bump. All data were sampled at 51,282.1 Hz for 16 seconds. Figure 46 shows the boundary layer velocity measurement taken downstream of diffusion bonded panel 5. The panel edges are smoothed using aluminum tape. The flow direction is out of the picture.

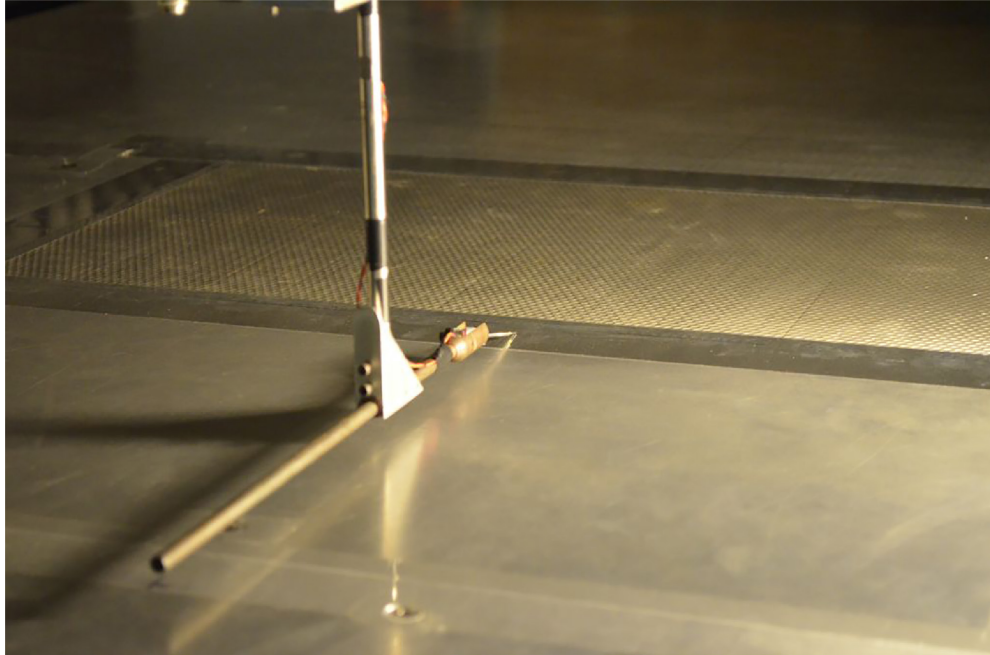


Figure 46.—Boundary layer measurement downstream of diffusion bonded panel 5.

TABLE 7.—TEST MATRIX FOR HOT WIRE MEASUREMENTS

Panel	Wire cloth	No bump	Bump	Downstream	Upstream
Sample A	None	x	x	x	x
Diffusion bonded panel 5	165 by 800	x	x	x	--
Sample L	325 by 325	x	x	x	--
Sample G	None	x	--	x	--

4.4.1 Test Matrix

A total of nine configurations of hot wire velocity measurements were acquired, as shown in Table 7. For each configuration, all five nozzle speeds shown in Table 2 were tested, for a total of 45 surveys. Each survey had a variable number of points in the wall-normal direction, usually around 90 samples between about 0.25 and 140 mm.

4.4.2 Upstream Unsteady Velocity Measurements

Figure 47 shows the mean velocity 13 mm (0.5 in.) upstream of the sample location and 140 mm (5.5 in.) downstream of the bump. The smooth plate was in place for these measurements, but it is assumed that the upstream measurements would be independent of the sample being tested. It can be seen that the bump pushes the peak velocity in the wall jet away from the wall somewhat, from about 15 to 25 mm. Around 10 mm from the wall, the bump creates a small velocity deficit of around 1 m/s, from 21.5 to 20.5 m/s. At the closest position (0.25 mm), the measured velocity increased from 14.1 to 14.6 m/s when the bump was added.

Figure 48 shows the normalized near-wall streamwise Reynolds stress, u^2/U^2 . As expected, the wake of the linear bump creates additional turbulence in the wall jet.

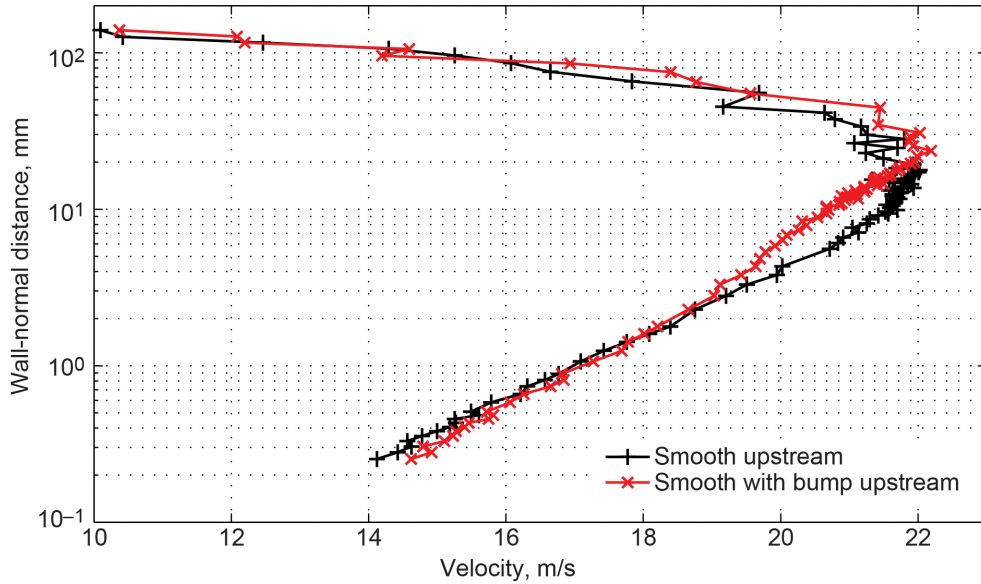


Figure 47.—Streamwise velocity measured 13 mm (0.5 in.) upstream of smooth solid plate (sample A). Jet exit velocity of 60 m/s.

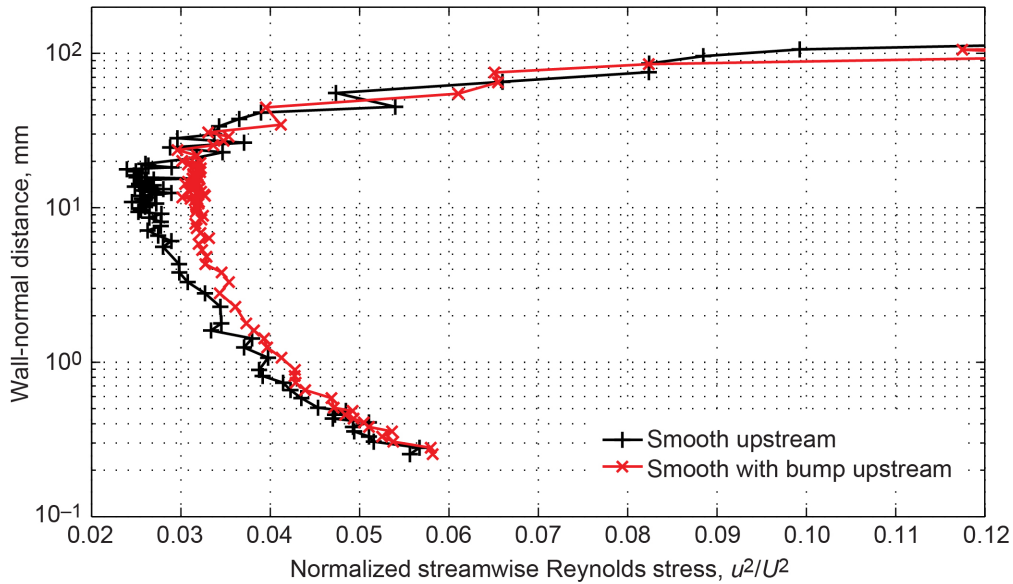


Figure 48.—Normalized streamwise Reynolds stress measured 13 mm (0.5 in.) upstream of smooth solid plate (sample A). Jet exit velocity of 60 m/s.

4.4.3 Downstream Unsteady Velocity Measurements

Figure 49 shows the mean velocity 13 mm (0.5 in.) downstream of the smooth plate with and without the bump. The outer part of the flow is minimally affected, but closer than about 30 mm, there is a 0.5 m/s velocity difference, with the bump wake being slower. Near the wall, the wake of the bump has a higher velocity, presumably due to continued mixing of the flow.

Figure 50 shows the normalized near-wall streamwise Reynolds stress downstream of the smooth sample. The near-wall velocity has a larger gradient for the smooth case, due to the well-formed boundary layer, and thus, the normalized shear stress is higher than when the bump is present.

Figure 51 shows the mean velocity 13 mm (0.5 in.) downstream of diffusion bonded panel 5 with and without the bump. Figure 52 shows the normalized near-wall streamwise Reynolds stress.

Figure 53 shows the mean velocity 13 mm (0.5 in.) downstream of the 325 by 325 wire cloth panel (sample L) with and without the bump. Figure 54 shows the normalized near-wall streamwise Reynolds stress. This panel has a bit more turbulence at around 1-mm height than diffusion bonded panel 5, although the difference is reduced with the bump.

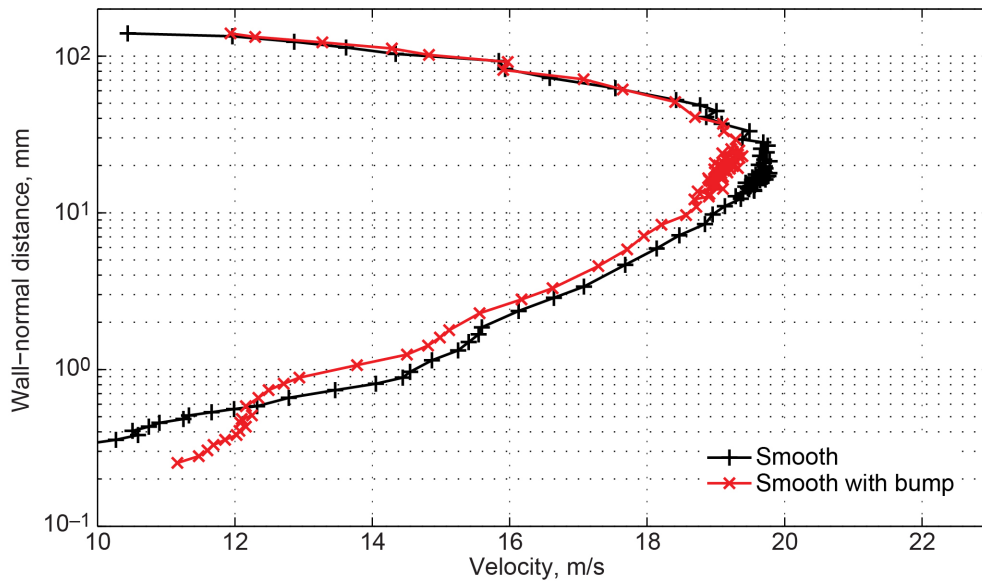


Figure 49.—Streamwise velocity measured 13 mm (0.5 in.) downstream of smooth solid plate (sample A). Jet exit velocity of 60 m/s.

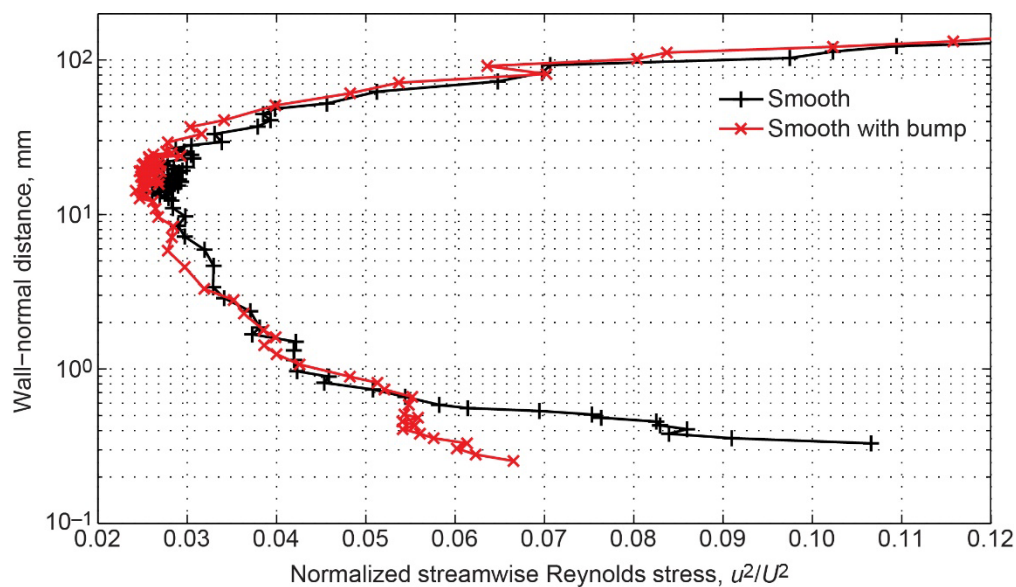


Figure 50.—Normalized streamwise Reynolds stress measured 13 mm (0.5 in.) downstream of smooth solid plate (sample A). Jet exit velocity of 60 m/s.

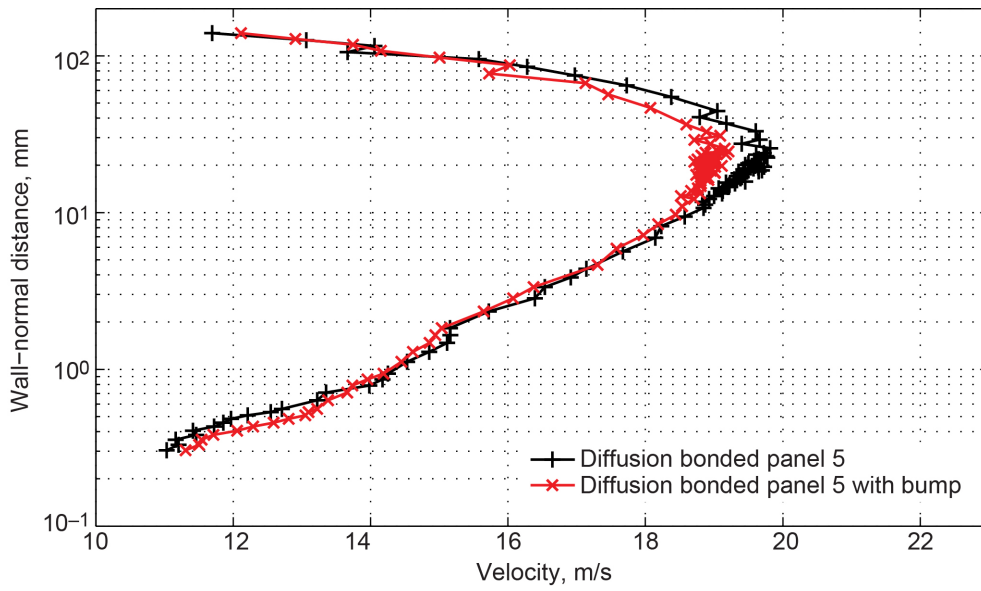


Figure 51.—Streamwise velocity measured 13 mm (0.5 in.) downstream of diffusion bonded panel 5. Jet exit velocity of 60 m/s.

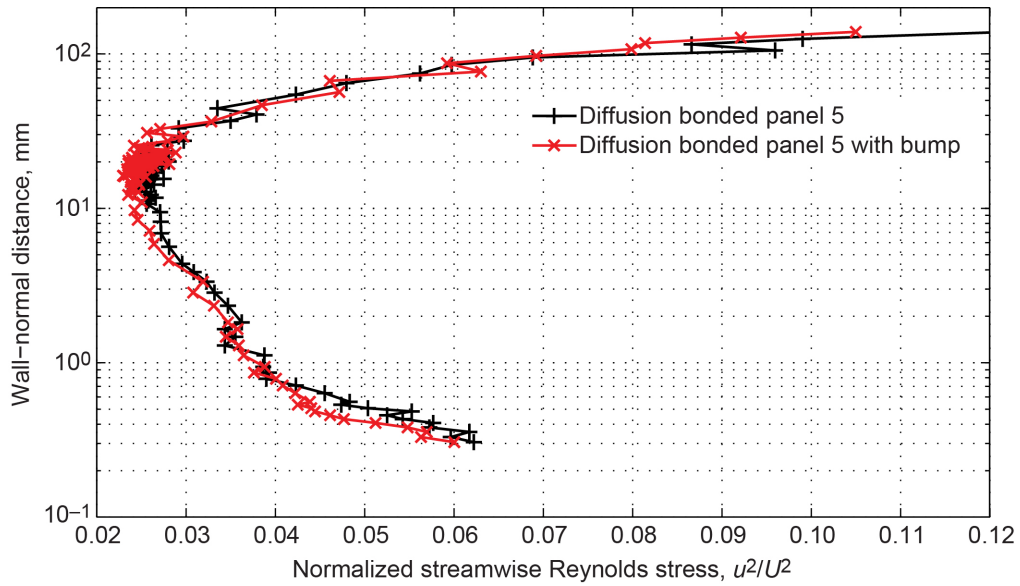


Figure 52.—Normalized streamwise Reynolds stress measured 13 mm (0.5 in.) downstream of diffusion bonded panel 5. Jet exit velocity of 60 m/s.

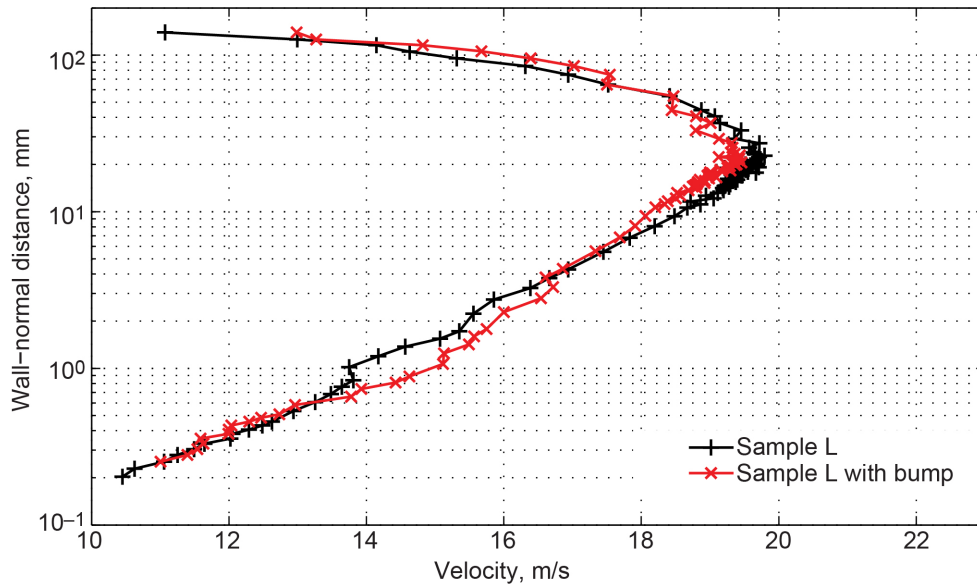


Figure 53.—Streamwise velocity measured 13 mm (0.5 in.) downstream of sample L. Jet exit velocity of 60 m/s.

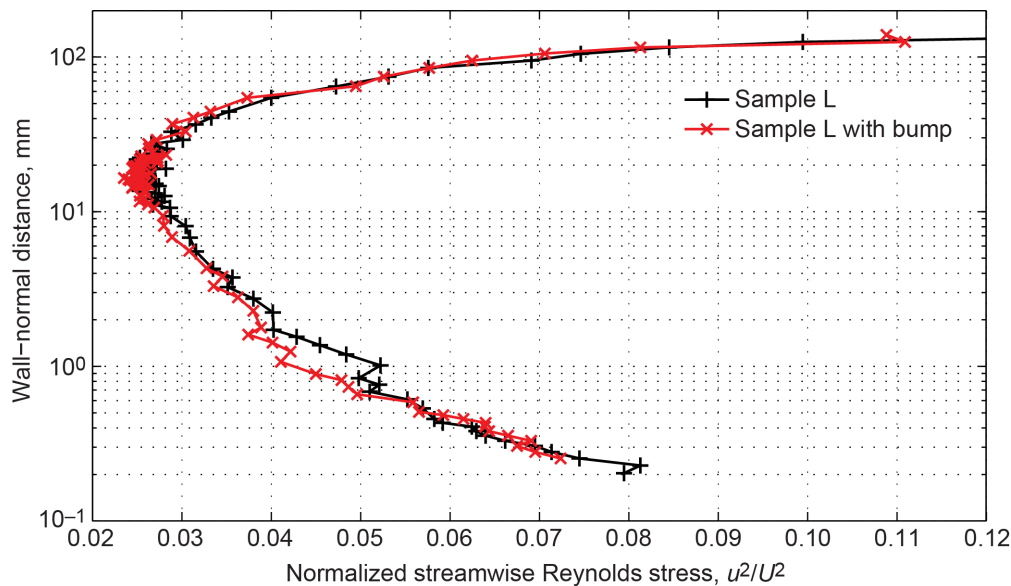


Figure 54.—Normalized streamwise Reynolds stress measured 13 mm (0.5 in.) downstream of sample L. Jet exit velocity of 60 m/s.

4.4.4 Effect of Wire Cloth on Unsteady Velocity Measurements

Figure 55 shows the mean velocity 13 mm (0.5 in.) downstream of the two panels that represent the before upgrade (open perforate, sample G) and after upgrade (diffusion bonded panel 5) condition in the 9×15 LSWT. Compared to all the other samples, the open perforate shows a huge velocity deficit for measurement locations closer than 2 cm. At 1 mm, the velocity with open perforate is 11.7 m/s compared with 14.2 m/s for the diffusion bonded panel. The open perforate also exhibits considerably more drag.

Figure 56 shows the normalized near-wall streamwise Reynolds stress, and it can be seen that the open perforate boundary layer is much more turbulent.

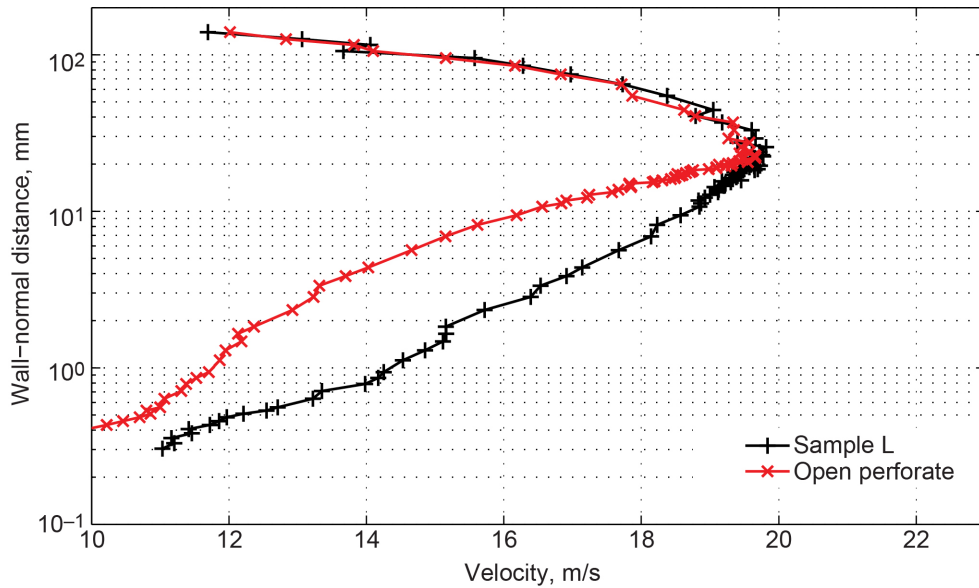


Figure 55.—Streamwise velocity measured 13 mm (0.5 in.) downstream of sample L compared with open perforate (sample G). Jet exit velocity of 60 m/s.

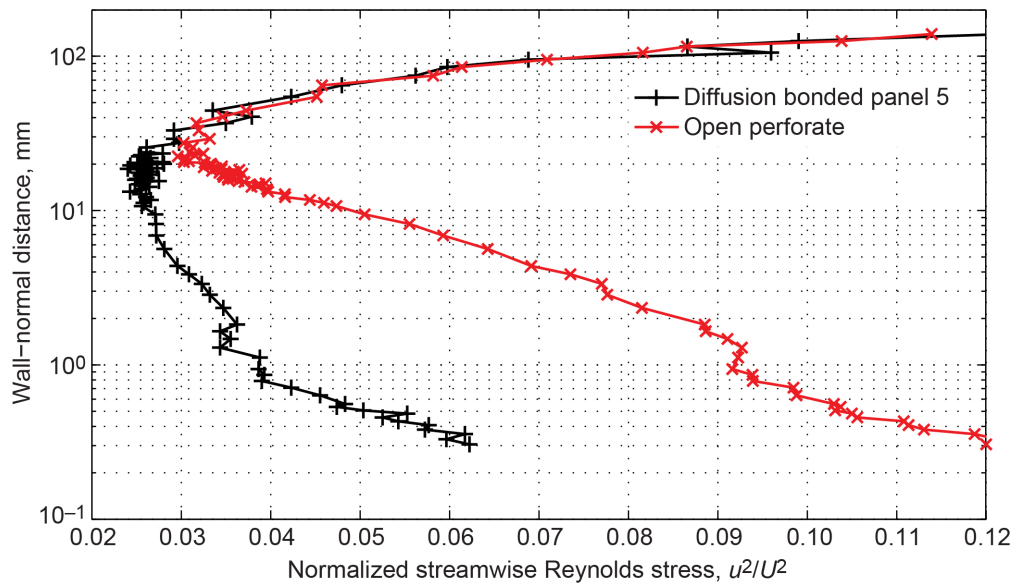


Figure 56.—Normalized streamwise Reynolds stress measured 13 mm (0.5 in.) downstream of diffusion bonded panel 5 compared with open perforate (sample G). Jet exit velocity of 60 m/s.

4.4.5 Velocity Spectra

Figure 57 shows the spectra of streamwise velocity, and it can be seen that the open perforate boundary layer is much more turbulent, although there is no narrowband content in the spectrum. Wall height is 0.965 mm.

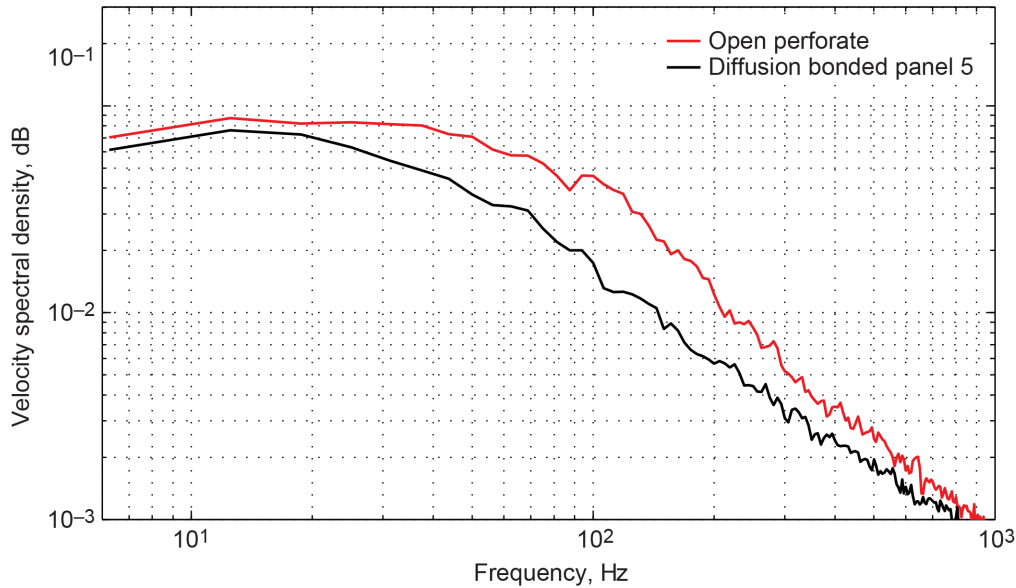


Figure 57.—Streamwise velocity spectra at wall height 0.965 mm.

5.0 Absorption Coefficient Testing

In order for the background noise improvement project to be a success, it had to maintain or improve the anechoic quality of the 9×15 LSWT test section. A dense, smooth flow surface would provide a quiet background noise level but would also have to allow sound into the bulk absorber.

5.1 Method

A convenient and useful test was described in the 40×80 WT improvement project publications (see Figure 18 of Ref. 8 and supporting text), which cites a series of reports by Wilby, White and Wilby, and Wilby and Wilby. We were unable to obtain copies of these reports, but the NASA Technical Publication contains enough information to illustrate the method and typical results.

The concept is to measure the acoustic reflection from a panel being tested. A speaker emits a short time chirp, which then reflects off of a panel and is measured by a microphone. If the incident sound on the panel is known, the reflection can be related to the acoustic qualities of the panel. Determining the uncertainty in these measurements was beyond the scope of the present effort.

5.1.1 Experimental Setup 2014

Since the experiment uses short time pulses, an anechoic environment is not strictly required for this measurement. A low background noise level is very helpful, because the short time signal from a speaker will not have very much energy and could be easily contaminated by ambient noise. Any sufficiently large and quiet space would be usable. These tests were all performed at the NASA Glenn ATL (Ref. 22).

The implementation of the method used for this report is described briefly. A speaker is pointed directly at and normal to the panel to be tested, with the largest practical distance between the two components used, as long as reflections from other surfaces (walls, floor, and ceiling) do not impact the measurement. A microphone is positioned between the speaker and the panel, approximately 2/3 of the way from the speaker to the panel. The microphone was pointed either at the panel or perpendicular to the axis between the two. The speaker is used to emit a short time sound signal, on the order of 3 ms, but dependent on the amount of space available. This sound would then pass over a microphone positioned

between the speaker and the panel being tested, reflect off the panel and then back to the microphone. The key is that the geometry of the room and the shortness of the time signal ensure that during the few milliseconds the reflected signal is received by the microphone, no other sound is also measured. Also, the positions and overall geometric relationship between the components must be maintained between different test panels that are to be compared. Obviously, the panels should be flat, which is not always the case when dealing with sheet metal.

The signal sent to the speaker was a white noise burst, and a different signal was sent as the process was repeated many times, typically 100. The same seeding was used for the random number generator so the 100 white noise signals were identical between tests. A virtual instrument was created in National Instruments™ LabVIEW software to conduct the experiment and record the data. A screen capture of the software is shown in Figure 58. Processing of the measurements was done in GNU Octave (Ref. 23).

As part of the data processing, a test with a solid steel panel, usually 16 ga, is always conducted to give a reference “absorption coefficient = 0” measurement. This is assumed to account for the finite size of the test panel, atmospheric conditions, microphone directivity response, and other practical concerns. The test with the solid panel must be conducted in the exact same geometric setup configuration as the panels being tested and as close in time as practical. This reflection from a solid panel also lets the experimenter determine the exact time window when the reflection is arriving, as it might be difficult with a highly absorptive panel and corresponding small return signal. During the 2014 test, the panel was suspended from string. In the 2016 test, discussed in Section 5.3, the solid panel was typically placed on a piece of foam to dampen any vibration and provide a flat surface on top of the metal floor grating of the facility.

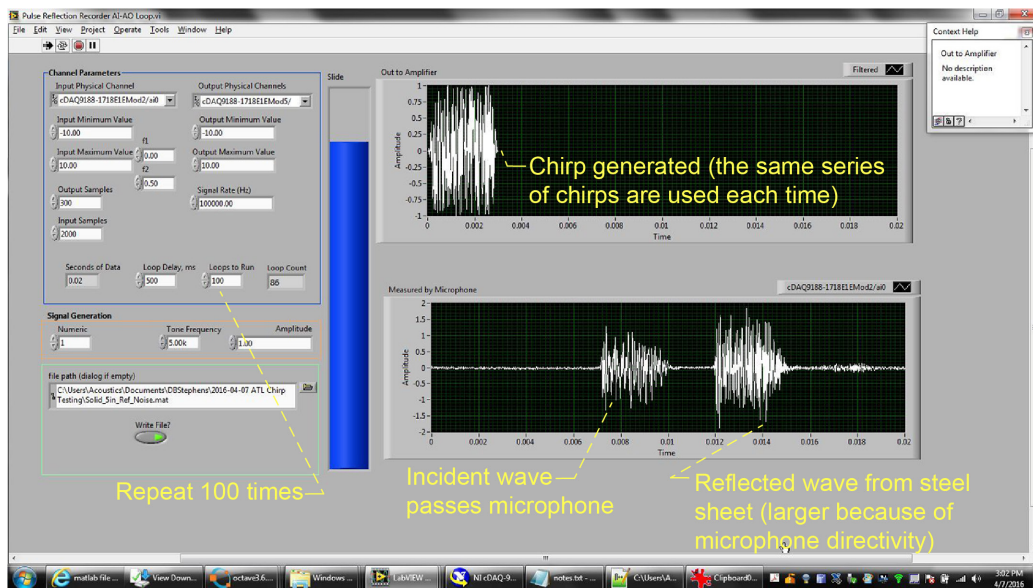


Figure 58.—National Instruments™ LabVIEW program developed for chrip testing.

5.1.2 Data Processing

The set of short signal pulses that were reflected off the panel and recorded by the microphone was processed in order to get a frequency-dependent spectral density function. The best practice for doing this was found to be windowing each sample reflection. These may only be a few hundred samples long at a recording frequency of 100 kHz. A chirp 1 ms long (100 samples at 100 kHz) creates a sound wave about 0.34 m long. It is necessary for the outward and reflected sound waves to have a quiet gap between them, as shown in Figure 58. This limits the length of the chirp to a few milliseconds, depending on the dimensions of the room being used. Next, the discrete Fourier transform of each reflected and windowed chirp is taken and the acoustic pressure spectrum is calculated using Welch's method (Ref. 24), giving $\overline{P^2(f)}$. In order to process the data, a solid steel panel was also tested and assumed to be perfectly reflective. This allows us to compute the absorption coefficient of the panel being tested as

$$C(f) = 1 - \frac{\overline{P^2(f)}_{\text{sample}}}{\overline{P^2(f)}_{\text{solid}}} \quad (2)$$

For measurements of absorption coefficient very close to 1.0 (say, above 0.95), background noise corrections might be appropriate. For example, even with no reflective sample present, the microphone may measure some ambient noise or residual noise from the speaker module.

The frequency resolution resulting from this method is a function of the sample rate (A/D and D/A were simultaneous, in this case) and the length of the sample. In the case of 200 samples at 100 kHz, the resulting frequency resolution is 500 Hz. Resolving high and low frequencies accurately depends on having a good signal-to-noise ratio. For low frequencies, this is difficult when very short time chirps (1 to 2 ms) are used. A lower limit of 500 Hz is achievable when using the ATL. The high-frequency limit is determined by the speaker output above the facility noise floor. This was around 40 kHz for the speakers used in this test series.

5.2 2014 Absorption Test

The first iteration of the setup was used to test the roughness noise sample panels from Virginia Tech. These were 1- by 2-ft perforated plates with various fabrics bonded to the surface, typically with spray adhesive. The set of panels tested in 2014, as described in Section 4.2, was shipped back to NASA Glenn and tested in the ATL using the setup pictured in Figure 59. These initial tests were conducted in December 2014. The equipment used for this testing included a Yamaha Corporation P7000S power amplifier, HiVi RT2H-A Planar Isodynamic Tweeter (Zhuhai Hivi Technology Company), and NI-9222 DAQ chassis with a cDAQ-9188 analog input card and cDAQ-9269 analog output card (National Instruments™). The microphone system was a Brüel & Kjaer 4939 Microphone with Falcon Range 2670 preamplifier.

The test samples were suspended in the room using tensioned string and folded wire fasteners. This facilitated quick and relatively repeatable exchanges of the panels being tested. No acoustic absorber was behind the panel except for the wedges of the ATL wall, which were several feet away.

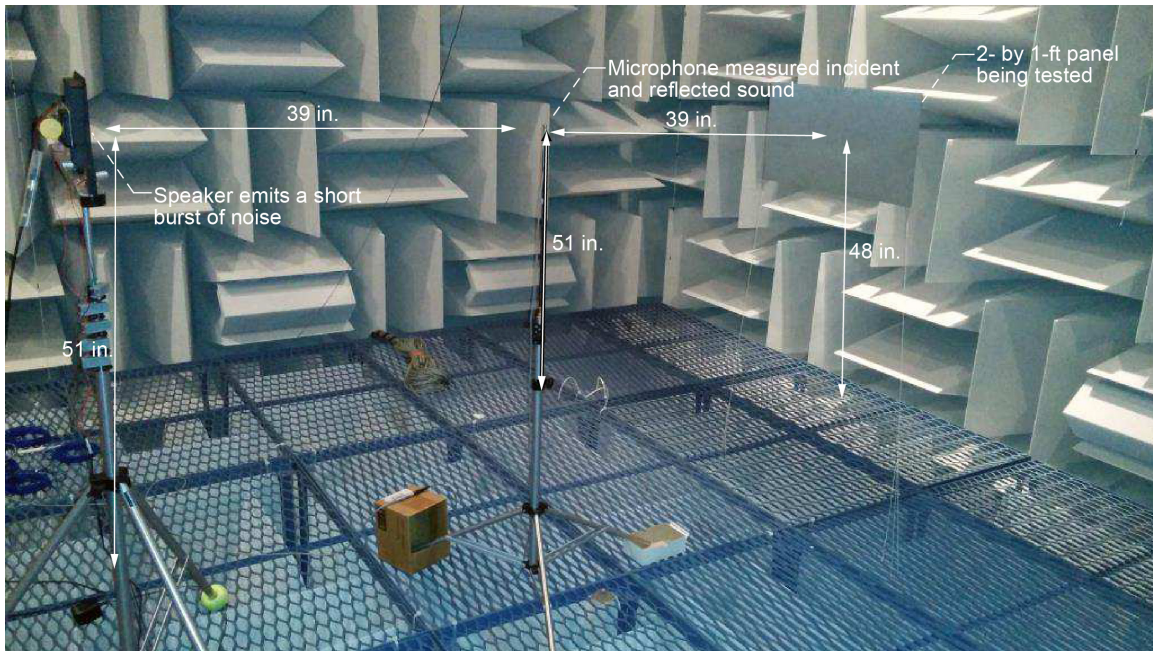


Figure 59.—NASA Glenn Research Center Acoustical Testing Laboratory 2014 absorption coefficient measurement setup.

5.2.1 Observations

The experimental setup in 2014 was fairly crude, but we quickly realized that there was a problem using the recommended fiberglass cloth solution. As shown in Figure 60, applying a layer of the fiberglass cloth over the perforate cut the absorption coefficient to around 60 percent of the bare perforate value. The value of an absorption coefficient less than zero implies some problem with the measurement. One possible explanation is that the reference solid panel was not perfectly flat and may have scattered sound away from the microphone. Verifying the geometry of the speaker, microphone, and panel was found to be difficult using the 2014 experimental setup.

By comparison, the panel supplied by NASA Ames from their 40×80 WT was measured to have a terrifically good absorption coefficient, as shown in Figure 61.

The additional samples of wire cloth over perforate were also quite educational. As seen in Figure 62, a few other major conclusions were drawn. The higher percent open area of the proposed panels (63 versus the 40 percent of the baseline) made a big difference. The 200 by 600 wire cloth was generally better than the 165 by 800 wire cloth and 4-mm (5/32-in.) holes were better than 8 mm (5/16 in.), especially at frequencies above 10 kHz. This combined result pushed us to focus on perforate with small holes (4 mm (5/32 in.) instead of 8 mm (5/16 in.)) with 200 by 600 wire cloth in preference to other combinations.

5.2.2 Diffusion Bonded Panel With Fiber Contamination

We also confirmed that the first diffusion bonded panel we had made in 2014 was contaminated with fiber. In addition to being a source of roughness noise, it was also an acoustic quality problem. As seen in Figure 63, the panel performed significantly worse than the sample made with spray adhesive. The manufacturing process would have to be improved upon. It obviously could be done because the NASA Ames 40×80 sample was terrific.

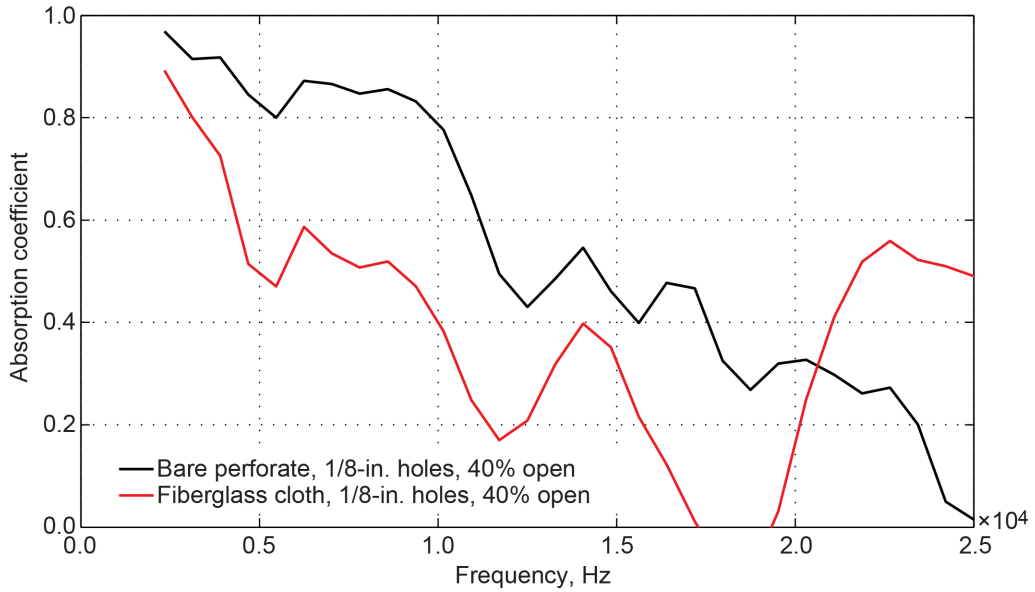


Figure 60.—Absorption coefficients measured on baseline 9- by 15-Foot Low-Speed Wind Tunnel perforate sample and same material covered with fiberglass cloth.

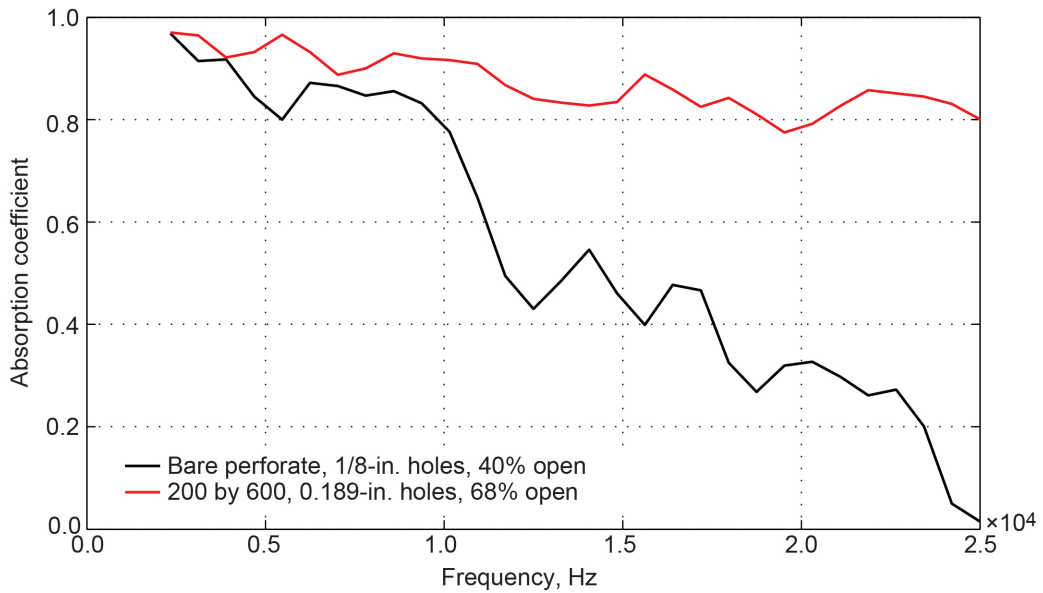


Figure 61.—Absorption coefficients measured on baseline 9- by 15-Foot Low-Speed Wind Tunnel bare perforate sample compared with sample of 200 by 600 wire cloth diffusion bonded panel from NASA Ames Research Center 40- by 80-Foot Wind Tunnel.

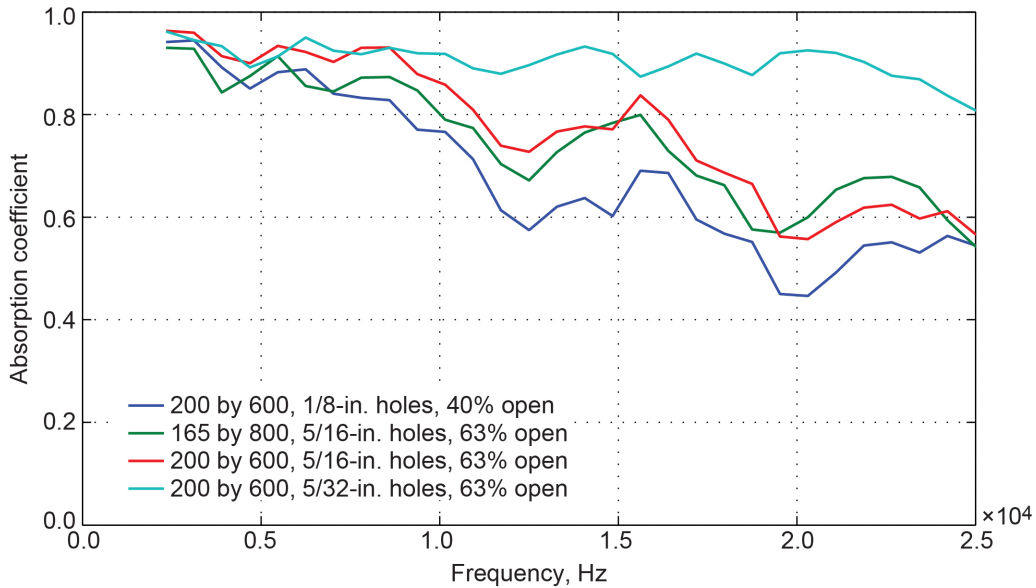


Figure 62.—Absorption coefficients measured with several combinations of wire cloth weave and perforate plate parameters.

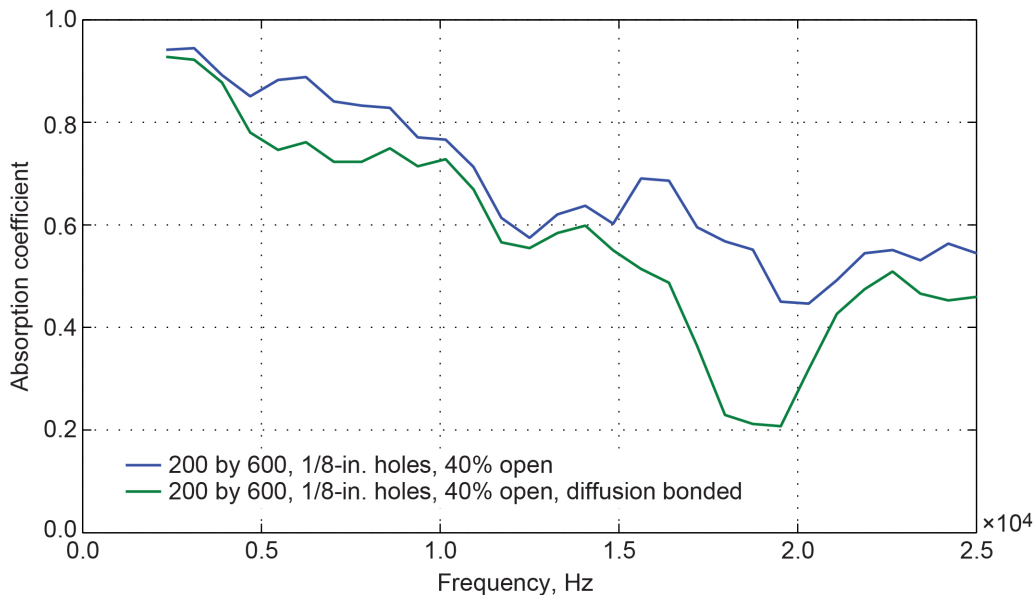


Figure 63.—Absorption coefficients from baseline perforate with 200 by 600 wire cloth. Sample made with spray adhesive compared with fiber contaminated diffusion bonded panel.

5.2.3 Effect of Oil Contamination and Cleaning

We verified that a wire-cloth-covered panel contaminated with oil would have considerably degraded acoustic properties. Micronic wire cloth could become contaminated with the oil used for lubricating rotating machinery being tested in the wind tunnel. Some of the oil was spread on a micronic wire cloth panel using a paper towel. Cleaning the panel with acetone did not restore the acoustic properties but spraying each perforate hole with shop air did. Results are shown in Figure 64. A similar finding was discussed in Reference 8 where the contamination was with jet fuel soot. Cleaning methods for the panels will likely be important, in addition to the development of an acoustic test that can be performed in the wind tunnel facility rather than in the ATL.

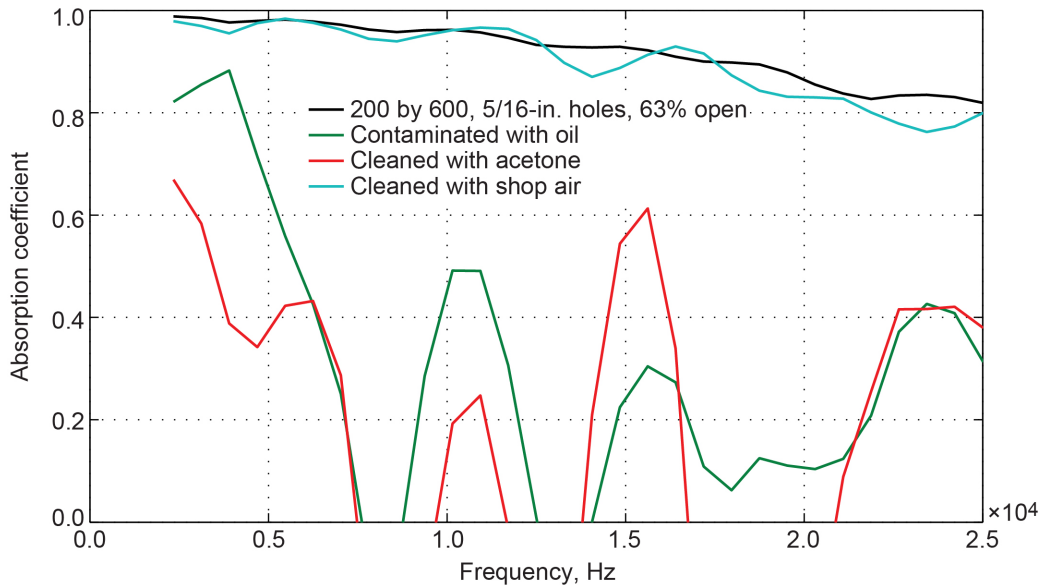


Figure 64.—Absorption coefficients from baseline perforate with 200 by 600 wire cloth, effect of oil contamination and cleaning.

5.3 2016 Absorption Testing

A second generation of testing at the ATL was conducted in April, May, and June 2016. With the design of the acoustic box surface decided, our attention turned to the acoustic absorber inside the box. A rigorous experimental and theoretical study had been conducted by Dahl and Rice (Ref. 25). In their conclusion: “For the 9- by 15-Foot Wind Tunnel, an absorptive lining was chosen for installation consisting of two layers each 17.2-cm (6.75-in) thick with the first layer having a nominal density of 6.4 kg/m³ (0.4 lbm/ft³) and the second layer having a nominal density of 17.7 kg/m³ (1.1 lbm/ft³).”

This two-layer bulk absorber was used in the 1986 upgrade of the 9×15 LSWT test section along with 40 percent open perforate on top and separating the two layers, as shown in Figure 2 of Reference 5.

The 2016 test campaign surveyed a wide variety of materials to understand the acoustic performance with the intent of comparing with the original design.

5.3.1 Experimental Setup

A few changes to the experimental setup were implemented for the testing in 2016. In order to more easily test large samples of acoustic insulation material, the speaker was mounted on an overhead rail near the ceiling of the ATL, about 12 ft above the floor. A microphone was suspended from a string stretched across the room, about 4 ft from the floor. Test samples were placed on the ATL floor, which is a steel grating above the acoustic wedges. A JBL 2426H horn driver (Harman) with a Selenium HL14-25 horn (Harman) was used as the sound source. This combination was chosen as it handled a wide frequency range and substantial signal levels. The panel size was increased from the 1- by 2-ft samples that were used in the Virginia Tech roughness noise facility. Typical samples now tested were 4 by 3 ft. The setup was used for testing throughout 2016, 2017, and 2018, and some incremental improvements were made. For very high absorption coefficient samples, the reflection from the test chamber floor grating became measurable, so the sample was surrounded by melamine wedges. It was also found that using multiple microphones and taking a median or average of the absorption coefficients was a way to reduce ripples in the frequency-dependent result. The ripples are believed to be due to the specific geometry of the setup, including the finite size of the panel being tested. The multiple microphone method resulted in smoother

spectra and more repeatable results. The background noise of the ATL was excellent and is not believed to have had a negative influence on the results. The experimental setup is shown in Figure 65.

5.3.2 Melamine Foam

A popular modern acoustic absorber material is melamine foam and several samples were procured for testing. The density was 11 kg/m^3 (0.7 lbm/ft^3) and panels in thicknesses of 50 mm (2 in.), 76 mm (3 in.), and 102 mm (4 in.) were available in solid pieces of 4-ft square size. The test results are shown in Figure 66, with the foam placed over a steel sheet. It was hoped that these results would collapse with nondimensional frequency based on thickness, but perhaps measurement uncertainty and coarse frequency resolution preclude finding this.

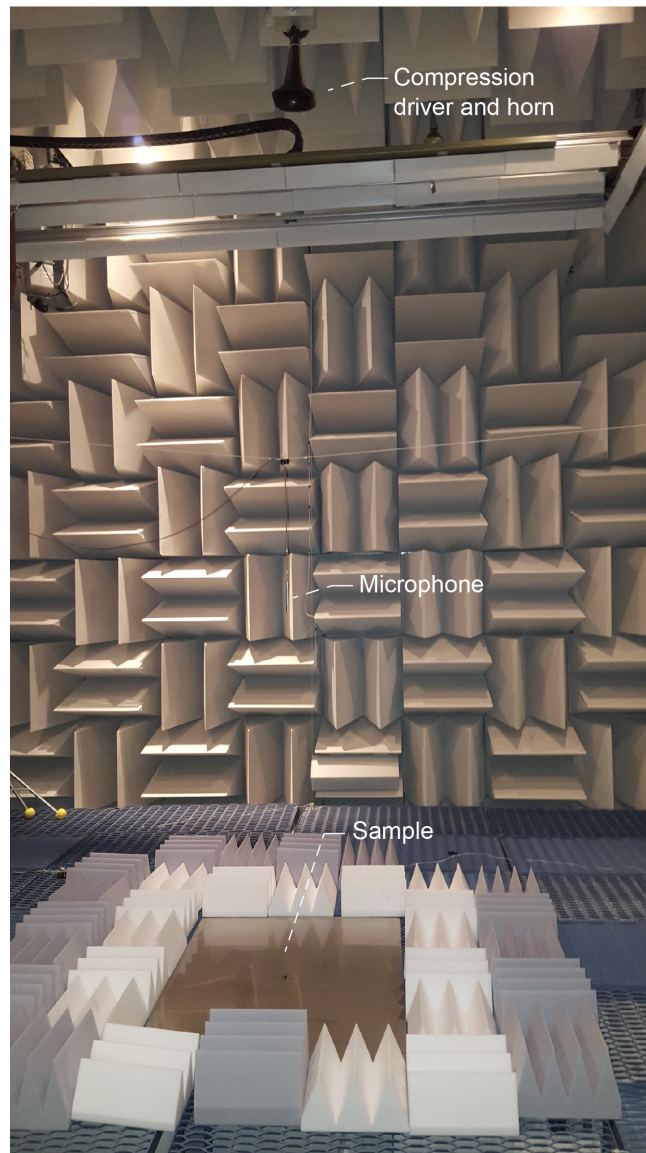


Figure 65.—Second-generation acoustic absorption measurement setup.

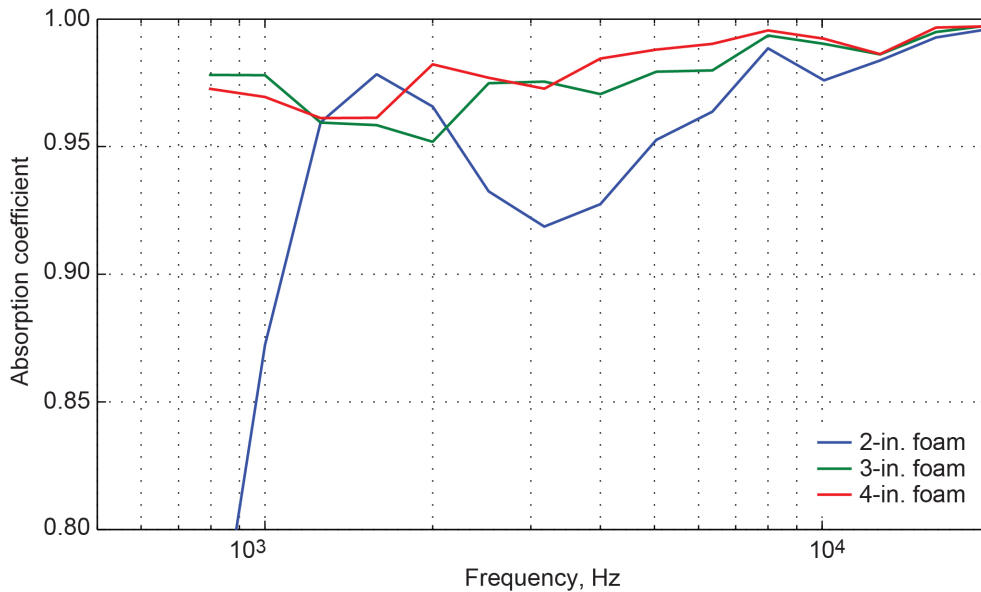


Figure 66.—Absorption coefficients measured with various thicknesses of melamine foam over solid panel. No top perforate surface.

5.3.3 As-Built 1986 Acoustic Absorber

While not the main focus of the test campaign, we did build a simulated 2D acoustic box following the design intent from Dahl and Rice (Ref. 25). Without a sheet metal frame, it was difficult to compress the lower layer of Kevlar[®], which has considerable mechanical energy to overcome. A frame was built from welded wire fencing to hold the lower Kevlar[®] layer. It was stitched using wire poked through the Kevlar[®] to hold 18 layers of batting into a 7.5-in. depth. Even poking a welding wire through 18 layers of Kevlar[®] is challenging. The upper layer, by contrast, had to be protected from compression using pins holding up the top perforate sheet to maintain a 7.5-in. depth. The final product is shown in Figure 67. Measurements from this sample, along with the case of the Kevlar[®] only (no top perforate plate) are shown in Figure 68. Below 1,600 Hz, no effect of the top perforate plate is observed. The absorption coefficient is maintained above 0.98 up to 4,000 Hz, so this kind of treatment is quite effective in a certain frequency range. At higher frequencies, the absorption coefficient falls very quickly and is down to 0.8 at 13.6 kHz.

5.3.4 Thin Acoustic Absorber

We became concerned that the thin acoustic treatment over the tunnel beams was a source of reflections in the 1986 design of the 9×15 LSWT test section. We built a simulated thin acoustic panel, as shown in Figure 69. This is approximately 2 in. of Kevlar[®], composed of two layers of the batted material. The results are shown in Figure 70, and it is found that the thin Kevlar[®] is a poor acoustic absorber. The addition of the perforate panel has the interesting effect to “tune” the depth of the material a bit like a resonator. This effect was evidently damped by the increased resistivity of the lower layer in the full-box case. It is clear that this implementation of a thin absorber was not intended and potentially disrupts the acoustic environment of the 9×15 LSWT test section.

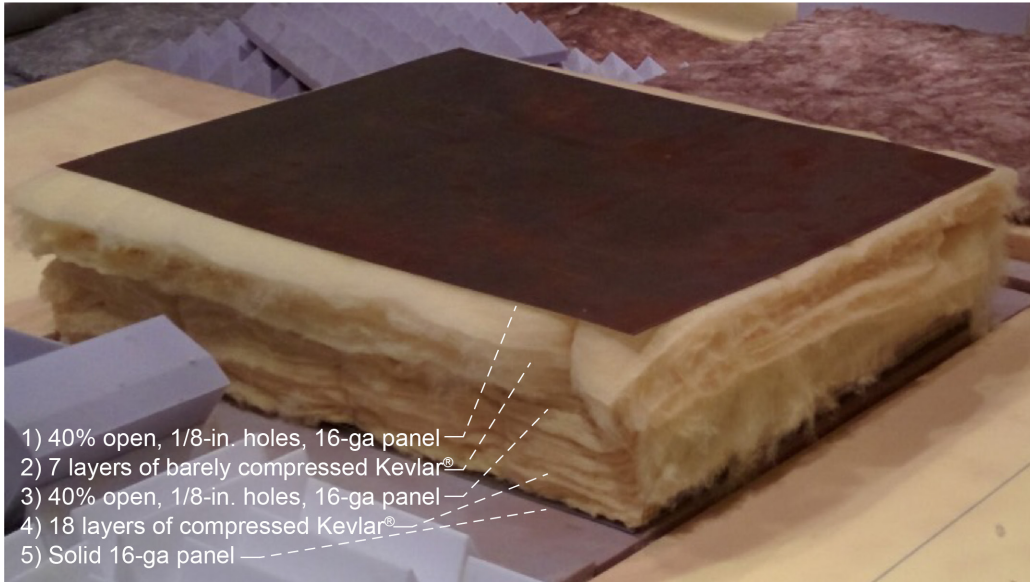


Figure 67.—Simulated 1986 acoustic box using as-designed criteria.

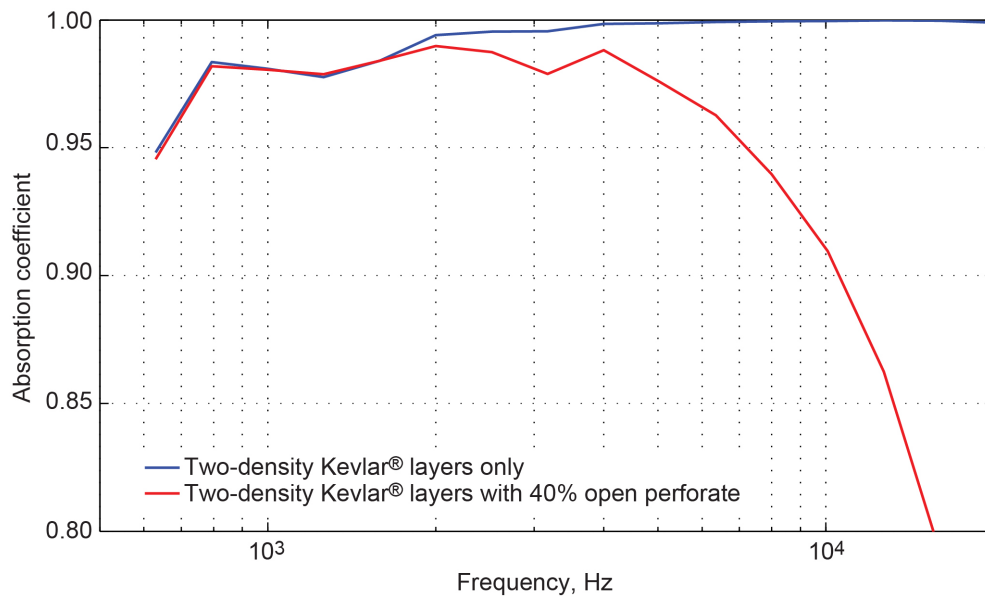


Figure 68.—Absorption coefficients measured with simulated 1986 acoustic box, 33-cm (13-in.) Kevlar® (DuPont™) bulk absorber (variable density, described at top of Section 5.3), with and without perforated face sheet over solid panel. Interior perforate sheet shown in Figure 67 is present in both configurations.



Figure 69.—Simulated 1986 acoustic treatment used over beams.

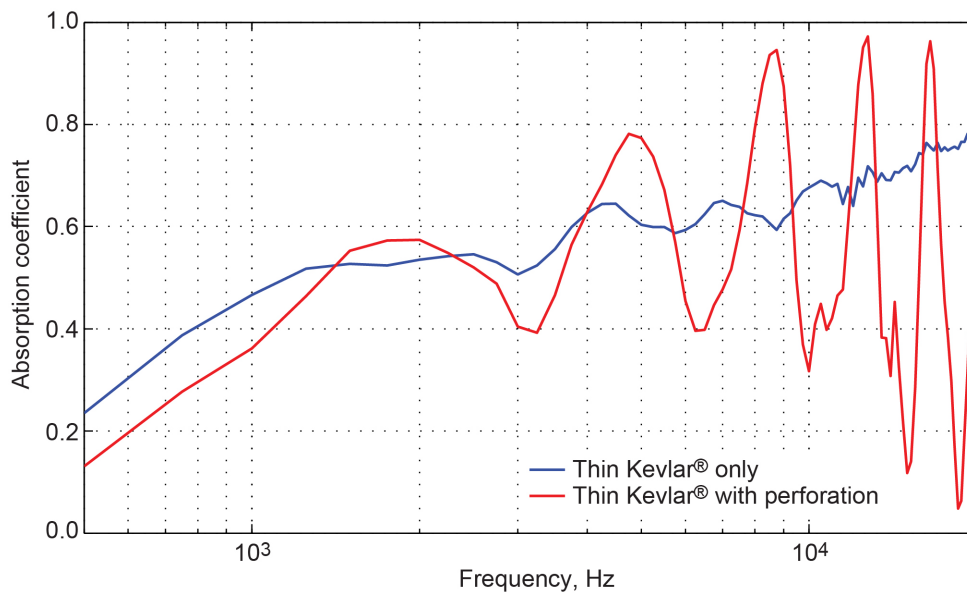


Figure 70.—Absorption coefficients measured with 5-cm (2-in.) Kevlar® (DuPont™) bulk absorber (6.4 kg/m³ (0.4 lbm/ft³) density) over solid panel. Note change in axis range to account for very low absorption coefficient.

5.3.5 Layered Bulk Absorbers

We were interested in evaluating alternative bulk absorbers, if improvements to the acoustic performance of the facility could be made with a relatively simple change. The prior assessment by Dahl and Rice (Ref. 25) and Dahl and Woodward (Ref. 4) (see Appendix C) lead to the 1986 design specification, see Table 3 of Reference 4. Specifically, the upper layer is intended to be 6.4 kg/m³ (0.4 lbm/ft³) and the lower layer 17.7 kg/m³ (1.1 lbm/ft³). Each layer is 17.2 cm (6.7 in.) thick. The fiber diameter is 1.254×10⁻⁵ m (5×10⁻⁷ in.) with a fiber density of 1,440 kg/m³ (89.9 lbm/ft³).

Relationships between bulk density, fiber size, and flow resistivity are typically provided in figures, such as Figure 10.4 of Ver and Beranek's book on Noise and Vibration Control (Ref. 26) and Figure C.3

of Engineering Noise Control (Ref. 27), although depending on the combination of fiber size and density, determining flow resistivity may require extrapolation. Empirical relationships are also typical, such as Equation C.8 of Reference 27. For example, the upper layer of Kevlar® in the 1986 design should have a flow resistivity around 350 Rayls/m, while the lower layer should be around 1,500 Rayls/m. Note that 1 MKS Rayl equals 1 pa·s/m, so the flow resistivity has units of pascal-seconds per meter squared.

We also reviewed the multilayer acoustic absorber calculations given by Allard and Atalla (Ref. 28). We purchased a selection of fiberglass insulation in various densities and tested a number of arrangements. The unwoven Kevlar® batting and melamine foam were also used. Again, the ATL absorption coefficient test setup was used to evaluate acoustic performance of layers of various bulk absorbers over a 16-ga sheet of steel, see Figure 71. We quickly determined that the fiberglass insulation sold as “aerospace grade” is low density but utilizes fiber sizes much smaller than ordinary fiberglass insulation and had a correspondingly higher resistivity. Since weight of acoustic insulation is not a factor for our wind tunnel, we determined this material was not especially useful. A fiberglass batting of density 0.6 lbm/ft³ (9.6 kg/m³) was found to be a suitable replacement for the lower layer of Kevlar® and did not need to be compressed. This had the advantage that the middle layer of perforate (needed to hold the Kevlar® in compression) could be replaced with a wire screen, which we believed only served to keep the fiberglass in place when used on a wall or ceiling installation. The estimated flow resistivity value for this layer is 3,000 Rayl/m, assuming a fiber size of 230 μm, or 6 μm.

After a large number of tests, we essentially confirmed that the original bulk absorber design was excellent (Figure 72). Fiberglass stack 52 was 7 layers (6.5 in.) of Kevlar® over 6.5 in. of 0.6 lbm/ft³ fiberglass, with a diameter of around 6 μm, or 2.3×10^{-4} in.



Figure 71.—Stack of batted fiber bulk absorbers over steel sheet placed on top of piece of gray melamine foam.

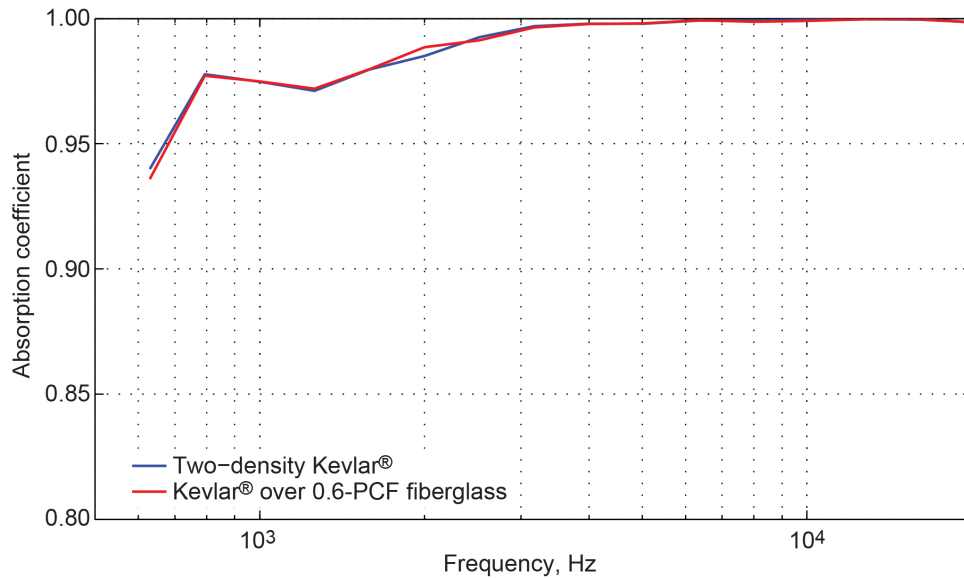


Figure 72.—Absorption coefficient of best new stack of bulk absorber (Kevlar® (DuPont™) over 0.6 lbm/ft³ fiberglass) without middle perforate sheet, compared with original Kevlar® two-density design, including middle perforate sheet. No upper perforate sheet for either configuration.

5.3.6 Effect of Perforated Plate Thickness

The build of the 9×15 LSWT acoustic treatment in 1986 used the same 16-ga-thick perforate on the walls, floor, and ceiling. We realized the high-frequency acoustic transparency of the multilayer treatment is controlled by the face sheet far more than the bulk absorber. Measurement of acoustic absorption with 24-ga face sheet was found to be dramatically better at high frequencies, but the flexibility of this material led to concerns about flatness and durability. The face sheet material we were investigating (16 ga, 63 percent open, 4-mm (5/32-in.) holes, 316 stainless) was also available in 20 and 22 ga, so a comparison test could be performed. Unfortunately, these materials were not all available simultaneously, and so were not tested back-to-back. Some differences in the test setup were evident. There was also the difficulty of keeping the thin perforates flat, which is required for accurate testing using this method. Nonetheless, a consistent pattern was found, as seen in Figure 73. The absorption coefficient at 20 kHz was increased from 91 to 96 percent, just by going from 16 to 20 ga.

Measurements were found to match the model by Phong and Papamoschou (Ref. 29) quite well, as seen by comparing Figure 73 with Figure 74. For reference, the 16-, 20-, 22-, and 24-ga stainless perforate sheets were 60, 36, 30, and 24 thousandths of an inch thick, respectively. The predicted values for absorption coefficient at 20 kHz were 92 percent for the 16-ga panel and 97 percent for the 24-ga panel. This agreement helps confirm the accuracy of the test method and adds confidence to further use of the prediction method. The floor of the 9×15 LSWT would be built with 16-ga perforated plate to handle walking loads, but the walls and ceiling were built with 20-ga perforated plate for the anechoic quality benefit. Thinner perforated sheets were found to be too thin to work with.

5.4 Effect of Micronic Wire Cloth

Existing literature on the effect of micronic wire cloth on top of perforate was found to be limited, although one study from Rice at NASA Lewis Research Center[†] is available (Ref. 30). The focus of the

[†]Now NASA Glenn Research Center.

present effort was to reduce background noise due to flow over perforate, so the added penalty of having a wire cloth over the perforate was going to be accepted. This penalty could be evaluated by comparing absorption coefficient (or, one minus the reflection coefficient) of the perforate alone to a similar perforate with a wire cloth diffusion bonded to the surface. The result is seen in Figure 75. This shows a loss of around 5 percent in absorption coefficient, although we later realized there was some variability in the acoustic transparency of the diffusion bonded panels.

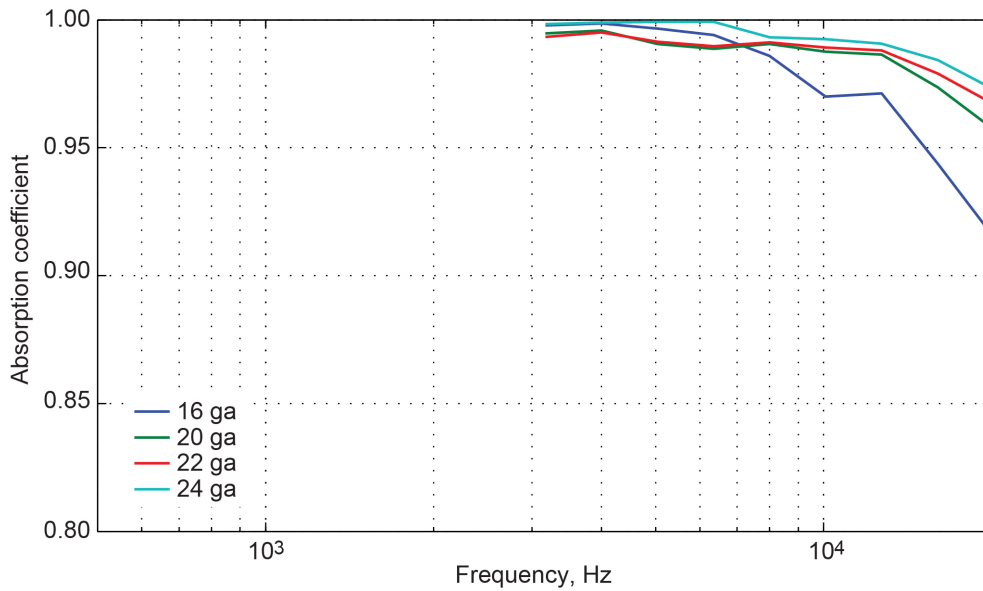


Figure 73.—Measurements of absorption coefficient for perforate of various thickness. No wire cloth.

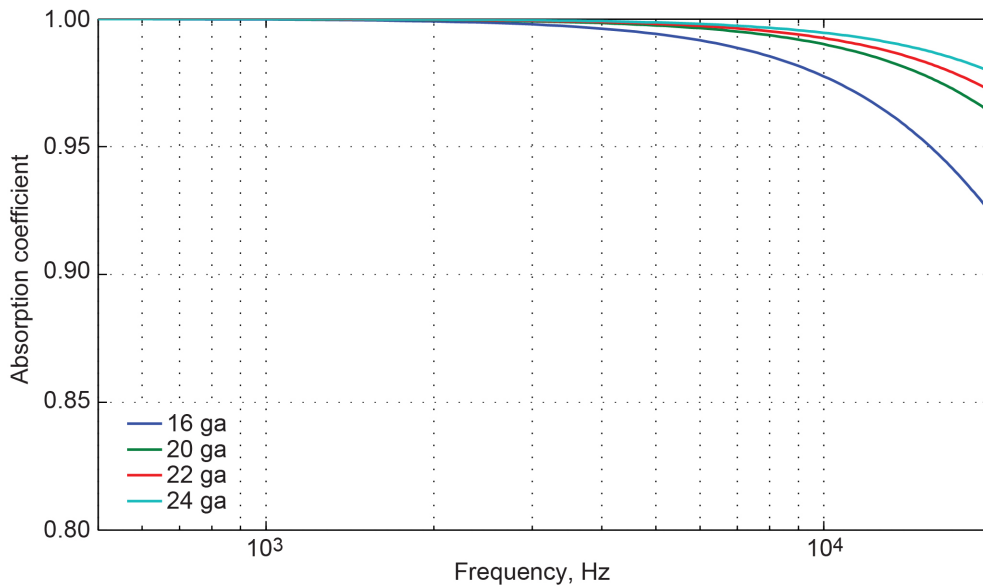


Figure 74.—Prediction of absorption coefficient for perforate of various thickness using methods from Reference 29. No wire cloth.

5.5 Final Design

The overall acoustic impact of the low roughness noise surface is shown in Figure 76. For frequencies below 4 kHz, there is a penalty to the acoustic performance due to the added resistance of the micronic wire cloth. At 1,590 Hz, the measured absorption coefficient is reduced from 0.997 to 0.972, which is approximately a nine-fold increase in reflection coefficient. Above 4 kHz, the acoustic performance is improved, due to the higher percent open area of the perforate plate. The absorption coefficient at 10 kHz improved from 0.87 to 0.94, corresponding to a reflection coefficient that is cut in half. The impact of the absorption coefficient is evaluated in an analysis given in Section 8.0.

5.6 Prototype Box Evaluation

A prototype acoustic box was delivered to NASA Glenn in late 2017. Acoustic fill was as prescribed, and the face sheet was a diffusion bonded panel from the previous batch. A photograph of the box is shown in Figure 77. The box is assembled as two halves, roughly 7 in. high each. The seam is in the middle, covered with aluminum tape. The top (flow-surface) side is filled with the low-density Kevlar[®] fill while the lower half is filled with the denser fiberglass bulk absorber.

The interior of the box is shown in Figure 78. The design of the box is essentially what was used in the final construction. It includes around four-dozen press-fit studs that are pushed through the diffusion bonded panel and are threaded on the inside. These are fastened with a nut to an internal grid of reinforcing sheet metal struts with roughly 30-cm (1-ft) spacing. The Kevlar[®] fill inside the surface panel is cut to roughly 30-cm (1-ft) squares to fit between the reinforcing struts. Beyond this layer, the Kevlar[®] is in full 3- by 4-ft sheets.

Test results are shown in Figure 79. The new design stack measurement from Figure 76 is also shown. The good agreement indicates that the mechanical design successfully avoided compromising the acoustic performance. In late 2018, a large number of acoustic boxes were tested as they were delivered for installation in the 9×15 LSWT. The median result at each frequency was plotted as a curve in Figure 79. This shows the acoustic quality was essentially maintained during the manufacturing process.

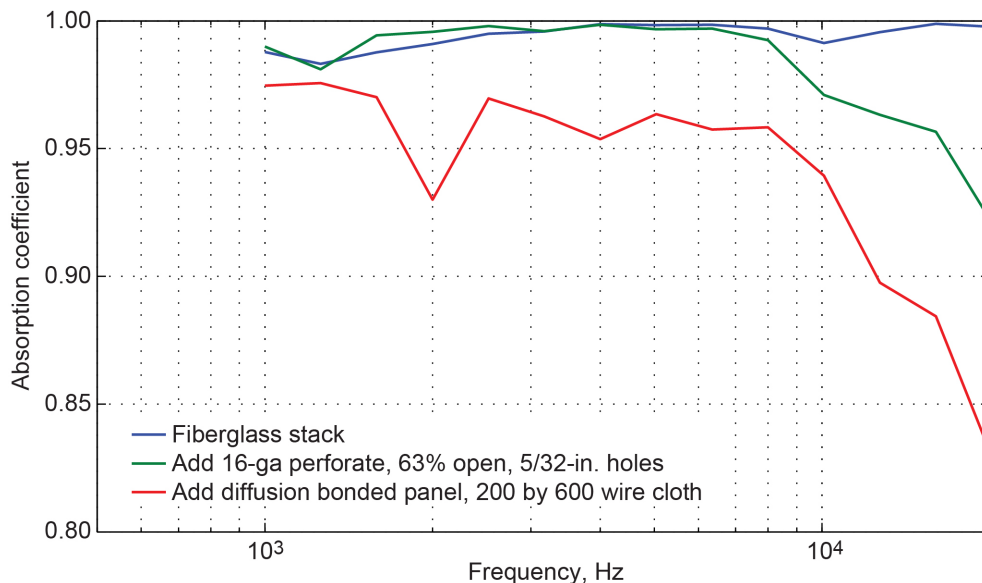


Figure 75.—Absorption coefficient measurements showing effect of adding wire cloth.

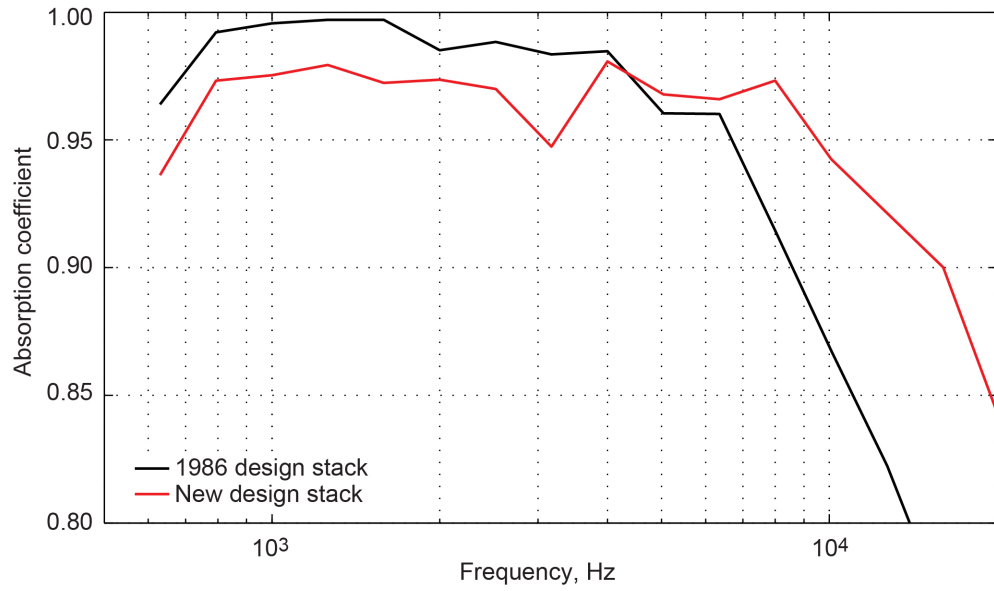


Figure 76.—Measured absorption coefficient for “baseline” and “new” acoustic treatment, including two-layer bulk absorber and flow surface perforated steel sheet. These results are for layered stack of materials rather than full box with sides, stiffeners, and fasteners.



Figure 77.—Prototype acoustic box tested in NASA Glenn Research Center Acoustical Testing Laboratory in December 2017.

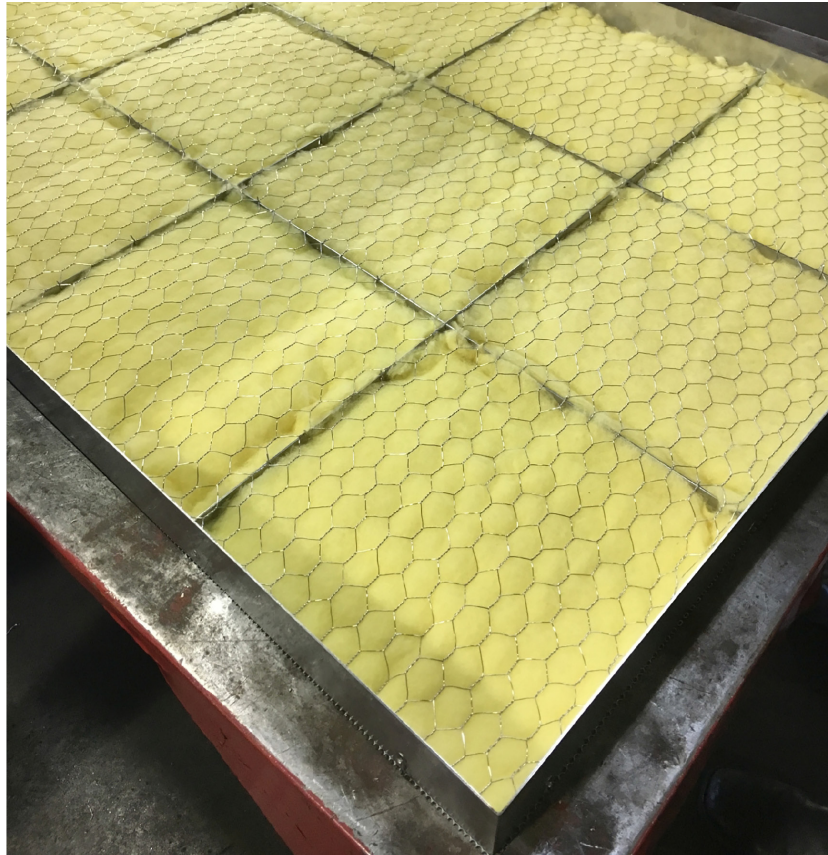


Figure 78.—Inside upper surface of prototype acoustic box from December 2017.

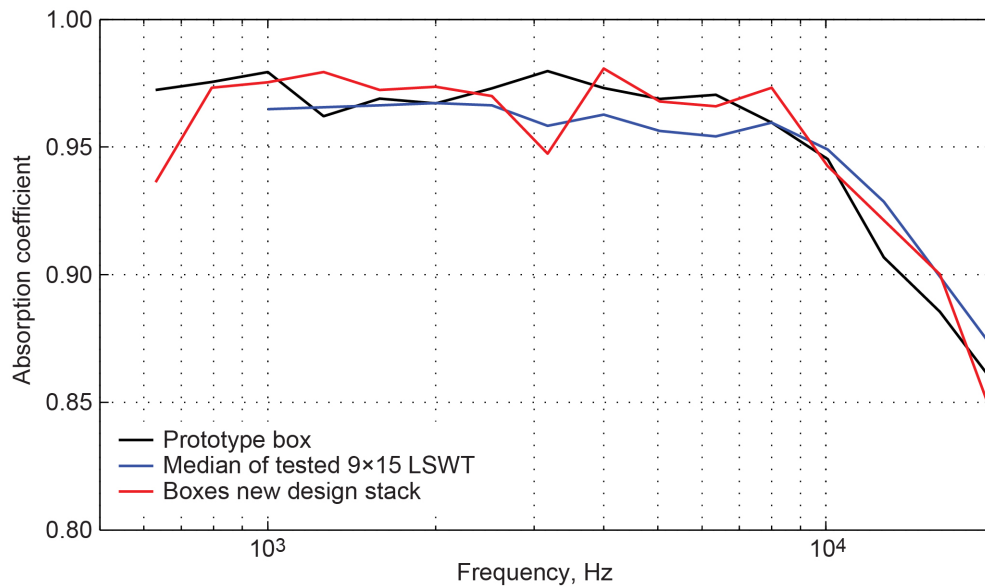


Figure 79.—Absorption coefficient of prototype acoustic box tested in December 2017 compared with median result from production boxes. Production boxes were subsequently installed in 9- by 15-Foot Low-Speed Wind Tunnel (9x15 LSWT) in December 2018.

6.0 Testing at NASA Langley Research Center

During the early part of the wind tunnel improvement project, we were interested in utilizing the established facilities at NASA Langley that were designed and built for testing engine liners. The idea is that engine acoustic liners are qualitatively similar to the kind of wind tunnel lining we wished to use for the 9×15 LSWT. The two main facilities of interest were the Normal Incidence Tube (NIT) and the Curved-Duct Test Rig (CDTR), although the Grazing Flow Incidence Tube may have been of use for this project also.

6.1 Normal Incidence Tube

A facility used for acoustic treatment studies is the NASA Langley NIT (Ref. 31). This accepts a sample that is 51-mm (2-in.) square and adjustable in depth. The NIT requires only plane waves to be present in the duct, so the test frequency is limited to 3,000 Hz or less. This is a major limitation for evaluating acoustic treatment to be used with scale models where frequencies up to 50 kHz are frequently of interest.

A ready-made sample holder of 10-in. depth was available, so we cut a perforate plate front surface to size and filled the sample holder with Kevlar® to approximately the specified density for the upper layer of the 9×15 LSWT acoustic treatment of 6.4 kg/m³ (0.4 lbm/ft³). The tunnel boxes were specified in the 1986 build to have a two-layer Kevlar® fill with the lower layer compressed by approximately a factor of three. Keeping the lower layer in compression in the NIT sample chamber was judged to add to the complexity, so the treatment was uniform. Several perforate plate samples were tested, Figure 80 shows results for three of them. The reference sample has 40 percent open perforate and 3-mm (1/8-in.) holes. This was the original 1986 9×15 LSWT flow surface. Also shown are variations with 200- by 600-thread-per-inch wire cloth, then also with the upgraded 63 percent open, 4-mm (5/32-in.) hole size. The test was conducted in January 2015.

The cases with the wire cloth are seen to be more strongly tuned to resonate at odd multiples of the quarter wavelength depth mode of the 10-in.-deep sample holder, leading to a resonance every 700 Hz or so. This effect would be dramatically reduced with a multilayer acoustic absorber where the lower layer was much denser. The use of only the low-density Kevlar® layer evidently allowed standing waves to form in the test sample. The oscillations are thus an artifact of the test. The impact of switching the face sheet seems to be about a 1-percent loss in acoustic absorption at the frequency range tested, from an average of 0.98 to 0.97.

6.2 Curved-Duct Test Rig

The CDTR at NASA Langley is a specialized facility for testing acoustic liners in the presence of flow (Refs. 32 and 33), specifically to mimic the physics of sound waves in the annular bypass duct of a turbofan engine. A set of acoustic drivers generates rectangular duct modes upstream of the sample to be tested. Mode measurement arrays of microphones are placed on either side of the sample to document the incident, reflected, and transmitted sound field. The facility would enable the testing of proposed 9×15 LSWT flow surfaces in the presence of the actual Mach numbers experienced in the tunnel. The results would be quantified as transmission loss for various rectangular acoustic modes. There was also the possibility of measuring roughness noise in this facility, although this was not the intent of the apparatus. The mode measurement and control system was limited to frequencies between 400 and 3,000 Hz. The data acquisition rate was 25 kHz with approximately a 10-kHz bandwidth. The test at NASA Langley took place Dec. 8 and 10, 2015. Personnel from NASA Glenn traveled to NASA Langley to participate in the test.

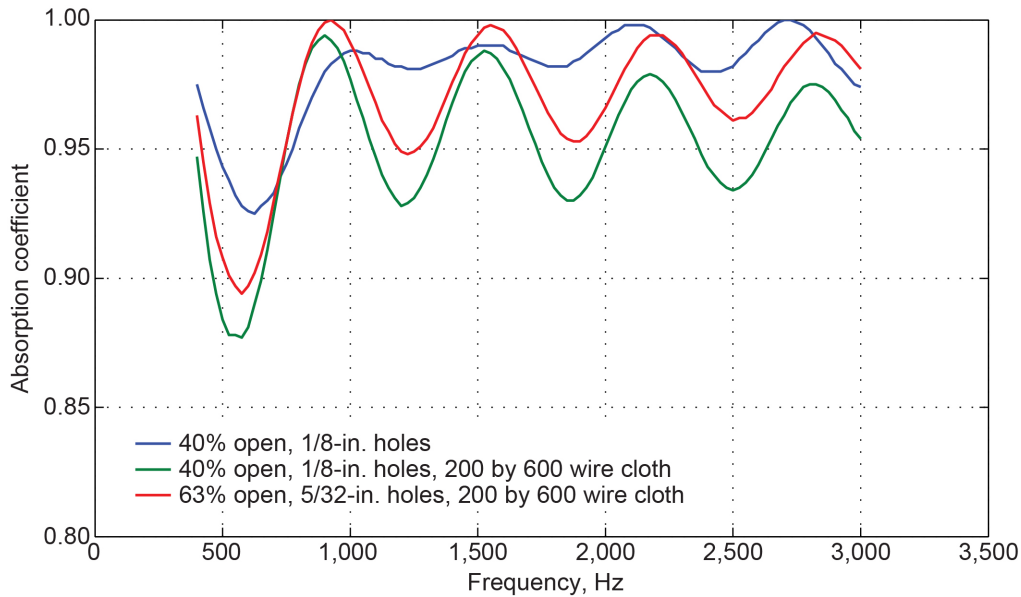


Figure 80.—Absorption coefficient of baseline and proposed flow surface measured using normal incidence tube method.

6.2.1 Curved-Duct Test Rig Test Sample Design

The test section of the CDTR is rectangular, 152 by 831 mm (6 by 15 in.), intended to represent an unwrapped engine bypass duct. The test section is configurable to allow this shape to be a rectangular “S-Duct” (see Figure 3 of Ref. 34 for an example) or it can be straight, as used in the present experiment. The 6-in. height represents the gap between the inner and outer radii of a bypass duct while the 15-in.-high walls are the inner and outer duct surfaces where acoustic treatment can be placed. The test section is 36 in. long. Two arrays of 63 microphones each are used upstream and downstream of the test section to measure the modal content of the sound field at these locations. A line array of 32 microphones is placed in the lid of the test section.

We decided to utilize the 305- by 610-mm (1- by 2-ft) perforate samples previously tested for roughness noise at Virginia Tech. The sample would be placed lengthwise in the CDTR, with 38 mm (1.5 in.) of untreated sidewall upstream and downstream. A rendering of our test sample is shown in Figure 81. The bulk of the part is made from a dense 192 kg/m^3 (12 lbm/ft^3) machinable foam block, specified by the CDTR facility staff and assumed to be acoustically hard. A 13-mm- (1/2-in.-) thick aluminum back plate provides structure and has threaded holes for anchoring to the test facility walls. A 16-ga top plate has a hole for accepting the panel being tested. The 25-cm (10-in.) box depth is filled with Kevlar[®] bulk absorber of uniform density at 6.4 kg/m^3 (0.4 lbm/ft^3), to match the NIT experiment. A set of six pins (red) are pushed through the Kevlar[®] to help support the bulk absorber while the box is turned on its side during testing. The green anchors were intended to be fastened to the perforate surface, but this was found to be unnecessary as the sample would only be tested to Mach 0.20. The perforate sample being tested was secured to the box with aluminum tape along the edges. The circles visible on the near surface are aluminum anchors glued into the assembly. These provide a place to attach handles for raising and lowering the sample into the test chamber.

A photograph of the test fixture is shown in Figure 82 with the baseline perforate, with 40 percent open area and 3-mm (1/8-in.) holes. Yellow Kevlar[®] bulk absorber is visible inside. The alignment of the holes is staggered in the cross-stream direction, which is not the intent of the final design.

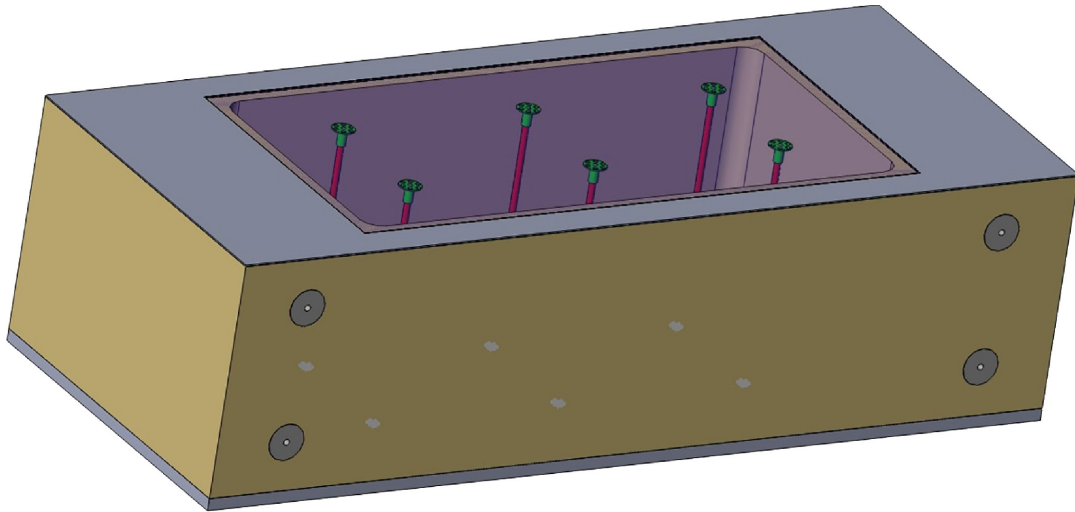


Figure 81.—Render of NASA Glenn Research Center test sample for use in Curved-Duct Test Rig. Flow surface is shown on top. During testing, flow will be lengthwise.

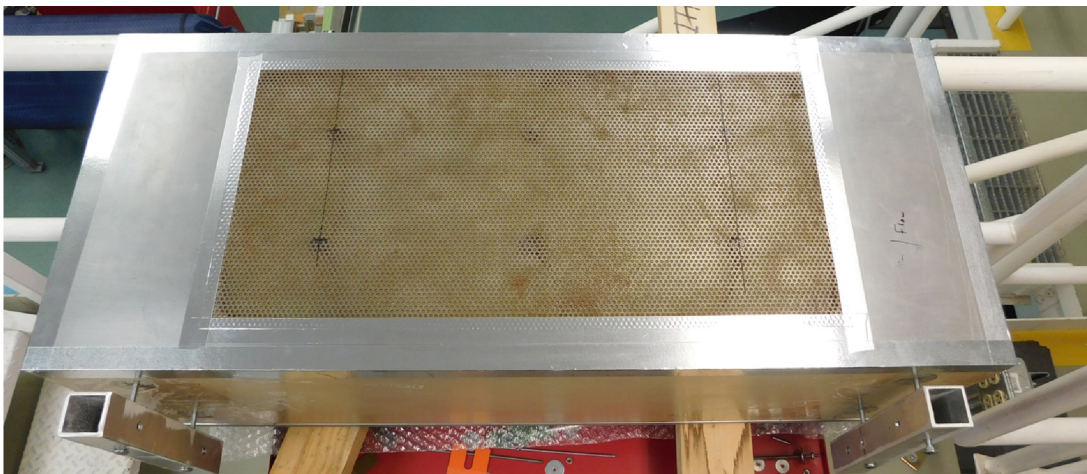


Figure 82.—Assembled test sample with baseline perforate. Square tube handles installed on previously mentioned anchors.

A photograph of the installed test fixture is shown in Figure 83. This view is top looking down, with flow and acoustic signal from right to left. The channel side closest to the observer has a hard wall. The side away from the observer has the liner to be tested.

A photograph of the CDTR facility test fixture is shown in Figure 84. The lid of the test chamber is populated with 32 microphones in white holders. The CDTR facility is rather tightly integrated in the NASA Langley laboratory and is difficult to photograph.

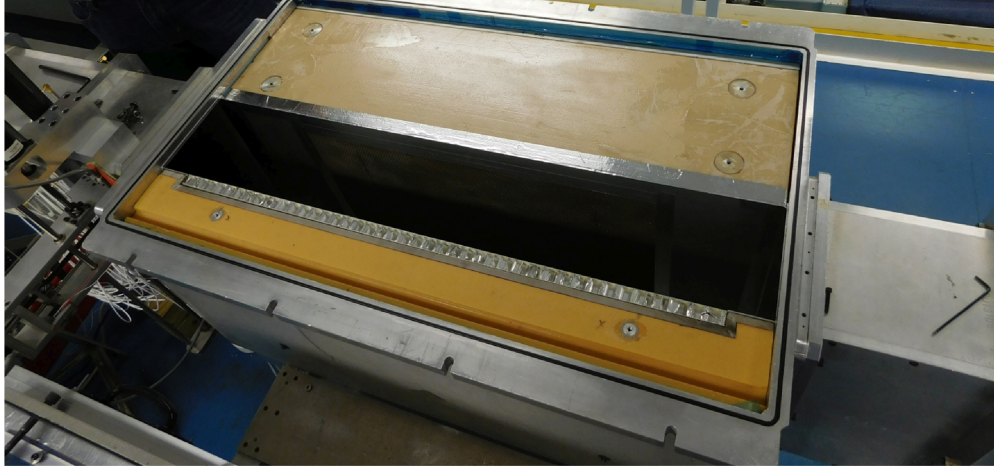


Figure 83.—Normal incidence comparison of baseline and proposed flow surface.



Figure 84.—Sample ready to test at NASA Langley Research Center facility. Flow is from right to left.

6.2.2 Experimental Results

Mode power was calculated from microphone measurements upstream and downstream of the test sample for each condition and delivered by the NASA Langley research team as part of the test data. Six modes were measured for each test configuration. Insertion loss was calculated for each mode by subtracting the transmitted duct sound power from the sound power input into the test section. A subset of results is shown as in Figure 85. Modes are listed as “DXY” where “D” is the mode designation and “X” is the vertical (15-in. direction) mode order (number of nodes) while “Y” is the horizontal direction mode order. The subset of modes shown is representative and chosen basically for plotting convenience. The wire cloth configuration provides essentially the same absorption as the baseline, suggesting the anechoic quality should not be adversely affected by the flow surface modification.

A data set was also acquired with a random signal sent to each of the drivers, in order to generate broadband noise in the duct between 300 and 4,000 Hz. The acoustic compression drivers are coupled to the rectangular duct with hollow tubes, so a truly white noise field is not expected. The measurement was converted to one-third octave bands to reduce the ripples pervading the measured spectra. Again, the principal comparison is between the insertion loss of the baseline flow surface and the new flow surface with wire cloth. In this case, the insertion loss was calculated by comparing the pressure spectrum from the first and last lid microphones. Results are shown in Figure 86. It appears the new treatment performance is similar, perhaps with a small penalty in the frequency range tested.

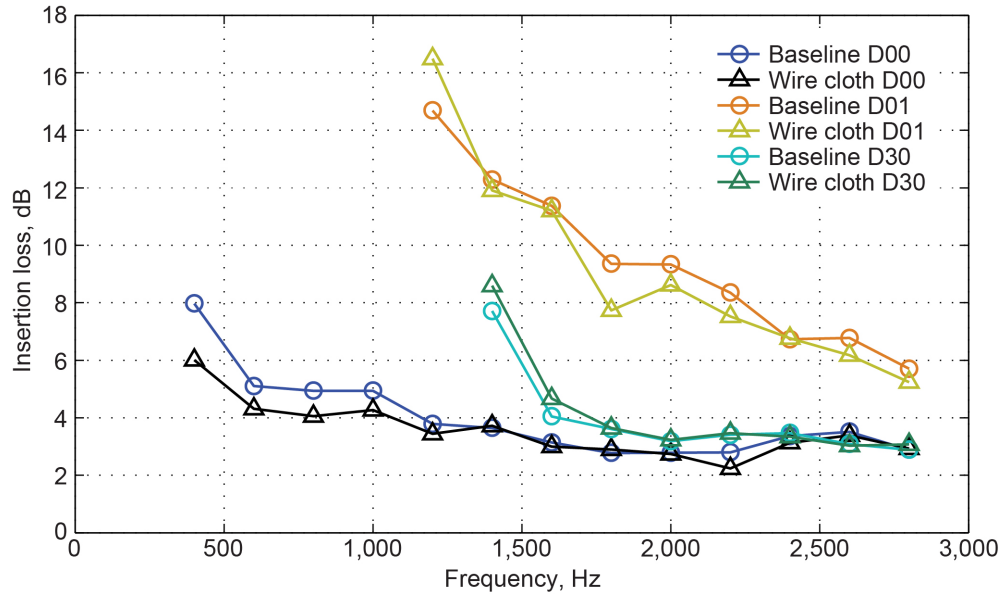


Figure 85.—Insertion loss for selection of modes tested. Mach 0.20. Mode D00 is plane wave, D01 is first horizontal mode, and D30 is third vertical mode.

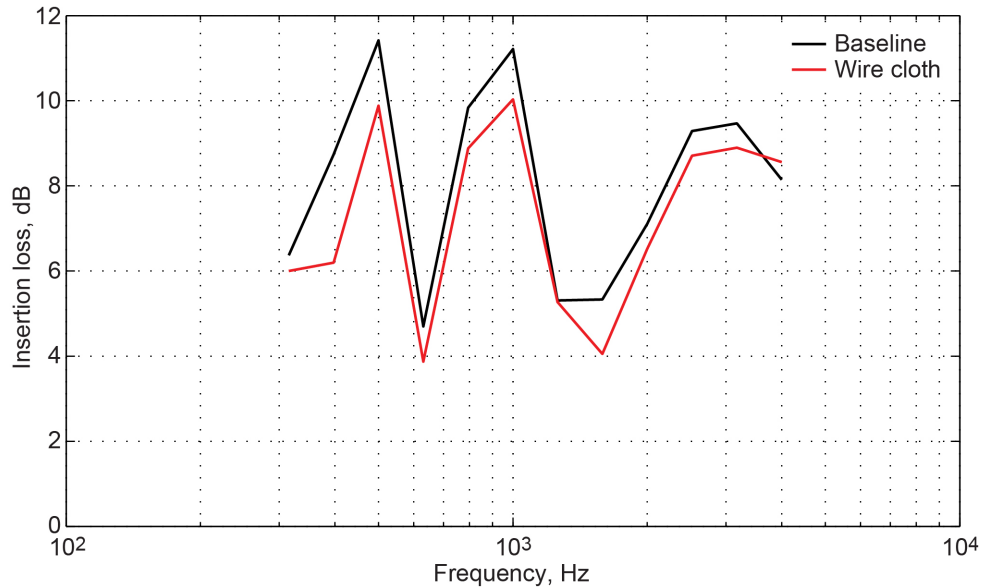


Figure 86.—Insertion loss for broadband incident signal. Mach 0.20.

7.0 Computational Study

As technology improvements are implemented and test model noise levels decrease, the level of these signals above the background noise in the test section of the 9×15 LSWT is decreasing. In addition to quantifying the lower signal-to-noise ratio, the character and distribution of the background noise in the test section is of interest. The 1986 design’s spatially nonuniform acoustic treatment, with varying depth and untreated sidewall slots, is expected to have an impact on the background noise distribution, but the level of impact on the measurement uncertainty is unknown, and spatial details of the test section background have not been previously assessed.

A computational assessment of the test section was undertaken to provide an estimate for the reflections and their impact on test uncertainty. This section of the report details the modeling of the test section in the old, or 1986 configuration, and concepts for the upgraded configuration of 2016.

The 1986 acoustic design of the test section has flow relief slots in the walls and variable depth acoustic treatment. For the 2016 redesign, the slots were removed, and the treatment changed to improve the wall attenuation. In 1990, the 1986 treatment was evaluated using both time domain spectrometry, to capture reflections off of surfaces, as well as decay with distance measurements (Ref. 4). These measures define overall behavior of the treatment, but do not quantify the spatial magnitude of the reflection ripple, which contributes to measurement uncertainty.

To better characterize the reflection ripple component of test uncertainty, before and after the upgrade, the test section was modeled with the software COMSOL Multiphysics™ (Ref. 35) using the “acoustic pressure (acpr)” physics on tetrahedral (three-dimensional (3D)) or triangular (2D) mesh with the default quadratic elements. For each frequency analyzed, the maximum element size was set to provide at least six points per wavelength. This value was set based on a grid density study on the model in a no-wall simulation (all boundaries are spherical radiation). Using (6, 8, and 10) points per wavelength produced the same 30-cm (1-ft) lossless sound pressure level along the sideline traverse. Using four points per wavelength was slightly different, by about 0.02 dB.

An approximation used in all analyses is to use spherical or cylindrical spreading as the nonreflecting boundary condition. This boundary condition is best for waves approaching perpendicular to the boundary and only approximate for angled or reflected waves. Plots of the sound field did not show noticeable error, except possibly in the downstream corners where the sidewall (reflecting) and rear face (spherical radiation) conditions meet. This approximation eliminates the need for the large amount of grid needed for a perfectly matched layer (PML) boundary. Evaluating 30-cm (1-ft) lossless sound pressure level along the sideline traverse for a no-wall (all boundaries using spherical or cylindrical radiation conditions) case, the solution ripple was <0.2 dB for 500 Hz and <0.1 dB for 1,000, 1,500, and 3,500 Hz. These values set a lower bound on predicted reflection effects.

The computational model used a small sphere with an arbitrarily selected surface pressure (for 120 dB, using $20 \times 10^{-6} \text{ [Pa]} \times 10^{(120/20)}$) to represent the tube or speaker ball source used in the experiment. Because of the pressure used, only the relative differences (ΔdB) are important. Measured treatment characteristics were applied as boundary conditions on the treatment box face locations, with nonreflecting boundary conditions applied to the bleed slots and the upstream and downstream boundaries. The reflection ripple is assessed primarily on the 2.26-m (89-in.) sideline path used for measurements during testing.

7.1 Model Geometry

The 9×15 LSWT test section was originally hard wall, used for V/STOL aerodynamic testing. The 1986 acoustic upgrade put acoustic treatment, roughly 4-cm (1.5-in.) deep, over the steel test section support frame and 33-cm- (13-in.-) deep treatment in the cavities between beams. The 1986 flow surface was thus inset from the original flow surface by roughly 5 cm (2 in.) on all four sides. The original 2.74-

m-high by 4.57-m-wide (108- by 180-in.) test section of the 9×15 LSWT thus became 2.64 m high by 4.47 m wide (104 by 176 in.) at the entrance to the test section. Where steel support beams are exposed in the flow relief slots, they were covered with gray foam to provide some acoustic attenuation.

Figure 87 shows the test section, with acoustic treatment boxes (yellow and/or gray), the floor-mounted sideline microphones (traversing and fixed) for acoustic testing, and flow relief or bleed slots on the sidewalls. Note that the test section vertical support beams are visible in the sidewall slots.

Figure 88 details the steel frame supporting the test section. This is the same beam configuration as for the V/STOL test section before there was acoustic treatment. The 1986 acoustic treatment is 33 cm (13 in.) deep between frame members, but only 4 cm (1.5 in.) deep between the flow surface and the I-beams. This characteristic is shown in the image of an acoustic box in Figure 4. This variable treatment depth (none, 4-cm, and 33-cm) was hypothesized to compromise the attenuation at low frequencies, allowing noticeable reflections to reach the sideline microphones shown in Figure 87.

The test section was built with a 7.6-cm (3-in.) flare in width. The sidewall flare was intended to account for area reduction of the free stream due to boundary layer growth on the walls, floor, and ceiling. The objective of this is to maintain a uniform axial speed through the test section. The opening in the first frame is 4.57 m (180 in.) wide, while the last frame is 4.65 m (183 in.) wide. To simplify the geometry for the COMSOL acoustic models of the test section, this small test section flare was not included.

Acoustic treatment properties were measured and reported in Reference 4. The resistance and reactance for the full depth are in Figure 6a of Reference 4. The characteristics of the shallow treatment are in Figure 6f of Reference 4. Figure 89 and Figure 90 in this report are replots of those resistance and reactance values, digitized from the earlier report.



Figure 87.—Forward looking aft at 9 by 15-Foot Low-Speed Wind Tunnel test section with representative model and microphones, 1986 configuration. Test section support frame is visible in slots, covered with foam.

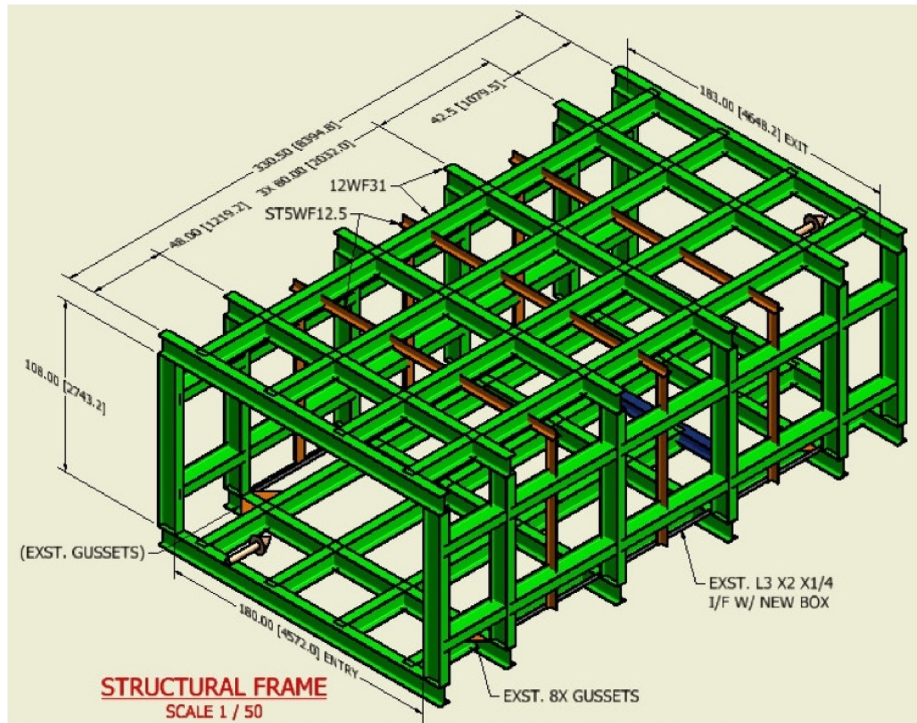


Figure 88.—Oblique view of original test section structural support beams.

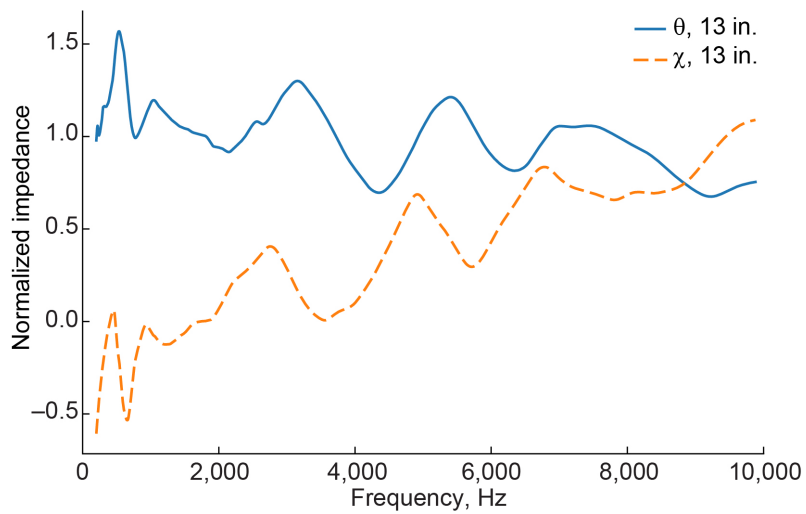


Figure 89.—Measured resistance θ and reactance χ for 33-cm (13-in.) depth of 1986 design acoustic treatment (Ref. 4).

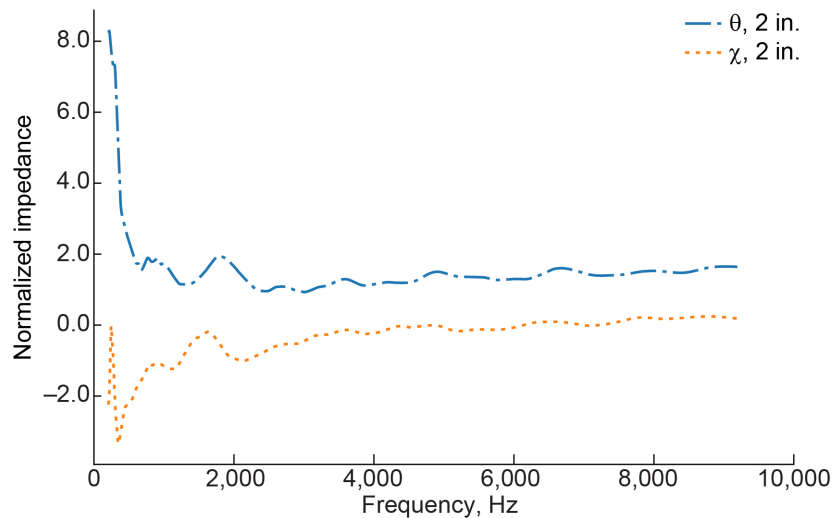


Figure 90.—Measured resistance θ and reactance χ for 4-cm (1.5-in.) depth of 1986 design acoustic treatment (Ref. 4).

7.2 Three-Dimensional Model Details

For the acoustic analyses, a small pulsing source was placed at the location where the fan center would be, shown in Figure 91 as the point where the fan balance centerline intersects the fan axis. This location is also the reference location for the model station coordinates (0,0,0).

In the 1986 test section, the drive rig centerline position is vertically about 5 cm (2 in.) above the centerline of the test section. When the acoustic treatment was added, the drive rig strut length was not adjusted, so with the turntable flush on the floor, the centerline is about 5 cm high. This vertical offset was not included in the acoustic model.

When operating, the test section has a flow speed ranging between Mach 0.05 and 0.22. The effect of the flow can be included in the COMSOL acoustic analysis using the linearized Navier-Stokes equations, “lnsf” physics. The impact of grazing flow on the acoustic liner properties as a function of the grazing flow Mach number is discussed by Rice (Ref. 36) and Malmary et al. (Ref. 37). The grazing flow effect was expected to be small for the low Mach numbers considered here and so was not included in the analysis.

Including flow effects for flow speeds higher than Mach 0, the only changes are the wavelengths and pattern locations without a significant change to the magnitude of the reflection ripples. Therefore, the no-flow acoustic pressure frequency domain (acpr) physics was used to reduce memory requirements (a problem with a large domain and high frequencies) and enable higher frequency analyses.

Boundary conditions used with the 3D (acpr) modeling are

- Upstream and downstream boundary: spherical wave radiation for this nonreflecting boundary
- Treated box faces: the 1986 as-built and measured resistance and reactance applied at the face
- Bleed slots: nonreflecting spherical wave radiation
- Downstream diffuser walls: hard wall (reflecting)

A horizontal symmetry plane through the source was used to reduce the model domain by half and speed the calculations. Even with this reduction, the highest frequency that could be run in 64 GB of random access memory (RAM) was 400 Hz. The RAM needed to reach 10 kHz with this modeling approach is estimated to be over 1,000 TB and not feasible.

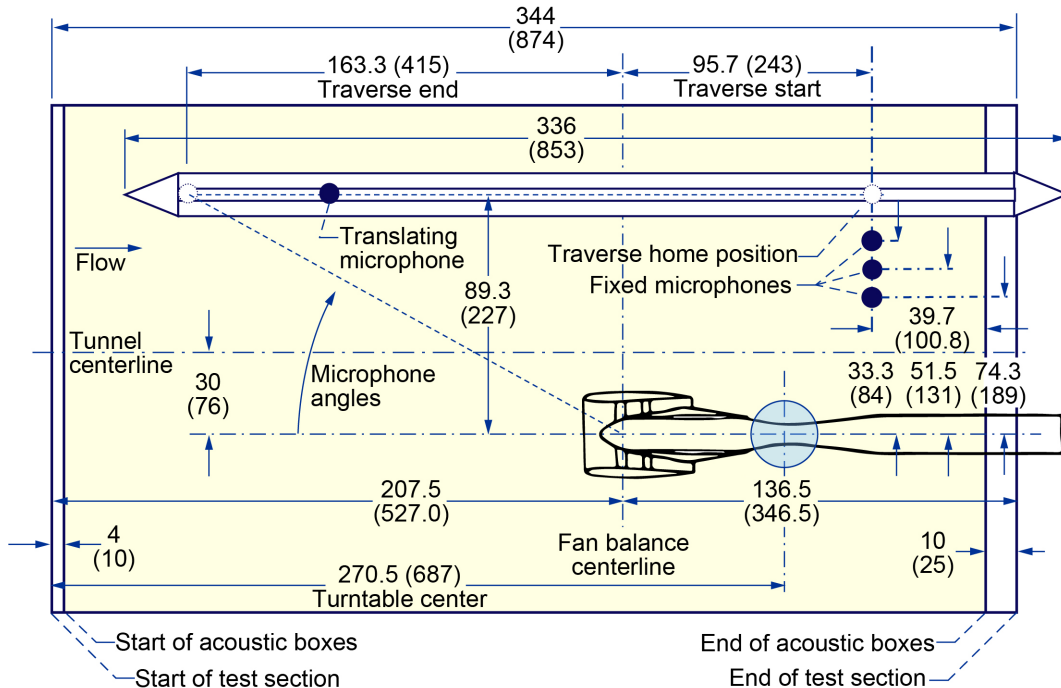


Figure 91.—Select dimensions of standard acoustic measurement locations in 9- by 15-Foot Low-Speed Wind Tunnel, 1986 configuration. Flow from left to right. Not to scale. Locations are approximate. All dimensions are in inches (centimeters).

7.3 Two-Dimensional Model Details

The next investigation used a 2D planform slice, to reduce RAM and reach higher frequencies, but with the knowledge that this will make the estimated reflection effects stronger. Predictions for the uncertainty using the 2D models are therefore more conservative (larger). With the 2D model, frequencies up to 3,500 Hz can be run in 256 GB of RAM. With the available 1 TB of RAM, the maximum frequency is 6,900 Hz.

Boundary conditions used with the 2D (acpr) model are

- Upstream and downstream flow surface: cylindrical radiation (nonreflecting)
- Upstream contraction: hard wall (reflecting)
- Treated box faces: as-built measured impedance for 33-cm- (13-in.-) deep treatment
- I-beam location faces: as-built measured impedance for 4-cm (1.5-in.-) deep treatment
- Downstream diffuser walls: hard wall (reflecting)

Figure 92 shows a representative result for the as-built geometry, on a 2D representation of the 1986 test section, with as-measured impedance for the 33-cm- (13-in.-) deep boxes and the 4-cm- (1.5-in.-) deep treatment over the beams. In the figure, the sound pressure level has been corrected for cylindrical spreading to a 30-cm (1-ft) distance (30-cm (1-ft) lossless), similar to correcting for spherical spreading as done with experimental data. Reflections from the boxes and beams can be seen, as well as reflections from the impedance jump at the junction with both the hard-wall contraction upstream and the hard-wall diffuser downstream. The sound pressure level range for the actual (3D) test section with a point source is expected to be much lower than the ± 10 -dB range shown in the figure. The absolute decibel level shown is not important as this is an arbitrary source strength, and the ripple levels should be independent of source strength.

The sound pressure level was extracted along the 2.26-m (89-in.) sideline traverse path from this solution to characterize the perturbations that might be seen by the traverse. Figure 93 presents the 30-cm (1-ft) lossless

sound pressure level for four frequencies. The predicted reflections decrease with frequency, due to the treatment being more effective at higher frequencies. An upper bound on reflection ripple in a measured signal can be inferred from this figure. For the noise source at 500 Hz, the minimum to maximum excursion is 8 dB, for an estimated uncertainty of less than ± 4 dB. For 1,000 Hz, uncertainty is less than ± 3 dB; for 1,500 Hz, uncertainty is less than ± 1.5 dB (away from the inlet contraction); and for 3,500 Hz, uncertainty is less than ± 1 dB (away from the inlet contraction). At 3,500 Hz, the impedance jump at the inlet contraction has twice the ripple effect as wall treatment. Due to these results, a model refinement study was carried out to minimize reflections and numerical error from the modeling process (grid density and boundary conditions). More detail on that study is below in Sections 7.5 and 7.6. These ripples have been investigated multiple times in the 9×15 LSWT test section by draw-away assessments, including in 1986 by Dahl and Woodward (Ref. 5) and in 2016 by JGS Consulting and ETS-Lindgren (Ref. 38). Qualitatively, the findings are practically all identical. Quantitative comparisons between the various efforts are beyond the scope of the present work.

7.4 Configuration Options Evaluated

Similar to the study of the 1986 as-built geometry outlined previously, the same COMSOL modeling process was used to evaluate a number of treatment options:

- “Slab13”: 33-cm- (13-in.-) deep treatment on all the sidewalls
- “Tbeam”: the I-beam flange was removed on the flow side, leaving a 6-mm (0.25-in.) beam face with 4-cm (1.5-in.) treatment; 33-cm treatment elsewhere
- “Tbeam+td02”: derived from Tbeam, with a treated diffuser using 4-cm treatment
- “Tbeam+td13”: derived from Tbeam, with a treated diffuser using 33-cm treatment
- “Slab13+td13”: derived from Slab, with a treated diffuser using 33-cm treatment

This set of studies showed that none of the options with thin treatment over the beams would sufficiently reduce the low frequencies. Based on these findings and other studies presented in this report, the test section frame was replaced with a new frame of larger dimensions, such that the beams are now outside the acoustic treatment.

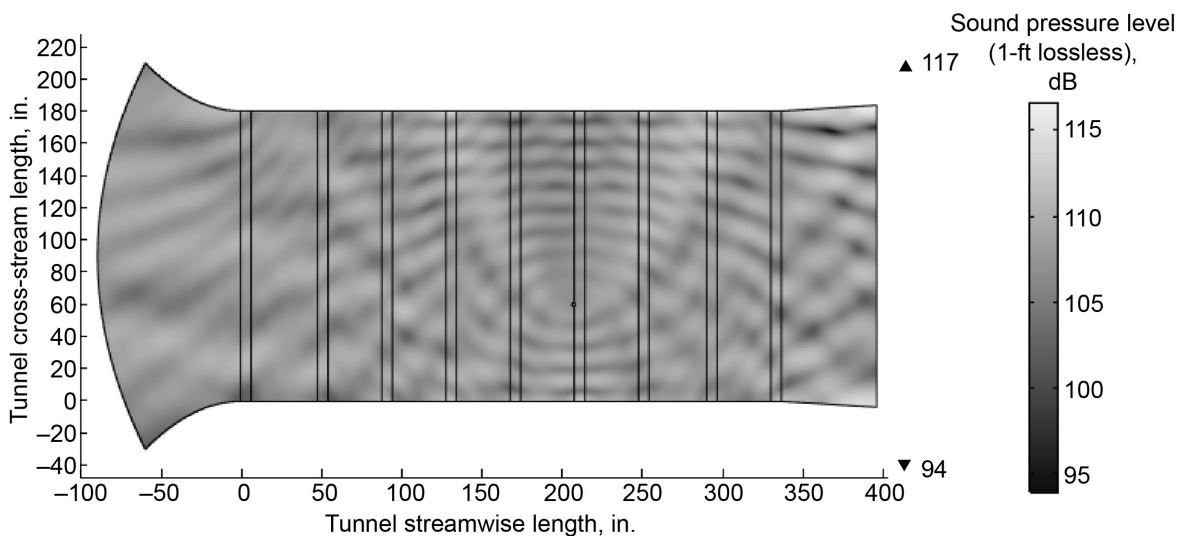


Figure 92.—Predicted 30-cm (1-ft) lossless sound pressure level (SPL) in dB at 500 Hz for 1986 as-built geometry, using two-dimensional model. Source location is dot at roughly (200,60). Beam locations are represented by close-spaced pairs of vertical lines. The (over) estimated uncertainty bounds are roughly ± 10 dB in SPL.

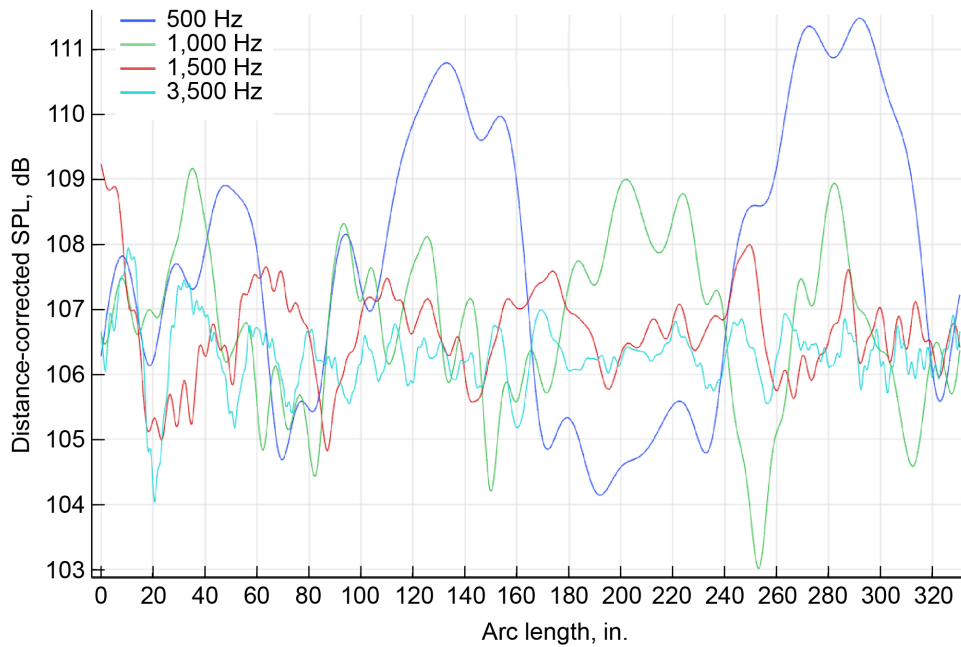


Figure 93.—Predicted lossless sound pressure level (SPL) along the 2.26-m (89-in.) sideline, for 500, 1,000, 1,500, and 3,500 Hz, using the 1986 as-built geometry.

7.5 Selected Option: Lengthen Test Section by 5 Ft

In April of 2016, a 5-ft extension to the downstream end of the test section was proposed to obtain better data at aft measurement angles from the model. The following analyses also supported an additional change: treating the diffuser to further reduce the level of reflections for aft angles.

Because of large reflections found in the previous model, at this point a grid refinement study was performed to minimize spurious numerical errors that would be misinterpreted as reflections. The grid study was performed with the 2D model to find the set of grid parameters to minimize ripple from the solver for the case where there are no reflective walls (PML boundary conditions on all walls). The grid density near the source was driven by the size of the source, a very small fraction of the smallest wavelength, and is denser than in the field. In the field, the grid density was driven by the number of points per wavelength (6, 8, 10, 12, and 14 were tried). Balancing solution quality against required memory, eight points per wavelength was selected. This is a finer grid than previously used for the solution shown in Figure 93.

With the improved numerical modeling approach, the lengthened test section was modeled with treatment on the diffuser, and a uniform 33-cm- (13-in.-) deep treatment on the walls. The magnitude of the ripple, presented as sound pressure level corrected for distance to 30 cm (1 ft), is shown in Figure 94. With this improved model the reflection ripple is reduced, putting the lower bound on solution uncertainty at less than 0.3 dB across most of the test section.

To illustrate the impact of acoustic treatment in the diffuser, Figure 95 presents the difference between the diffuser having a hard-wall versus a 33-cm- (13-in.-) deep treatment, along the 2.26-m (89-in.) sideline position. This Δ dB plot shows that diffuser treatment has no more than a ± 0.5 -dB impact on measurements along the sideline traverse in the test section. In the final design of the renovated 9×15 LSWT, the diffuser treatment varied in depth as the final design has multiple components and a somewhat complicated shape. Near the test section, the average depth is approximately 15 cm (6 in.).

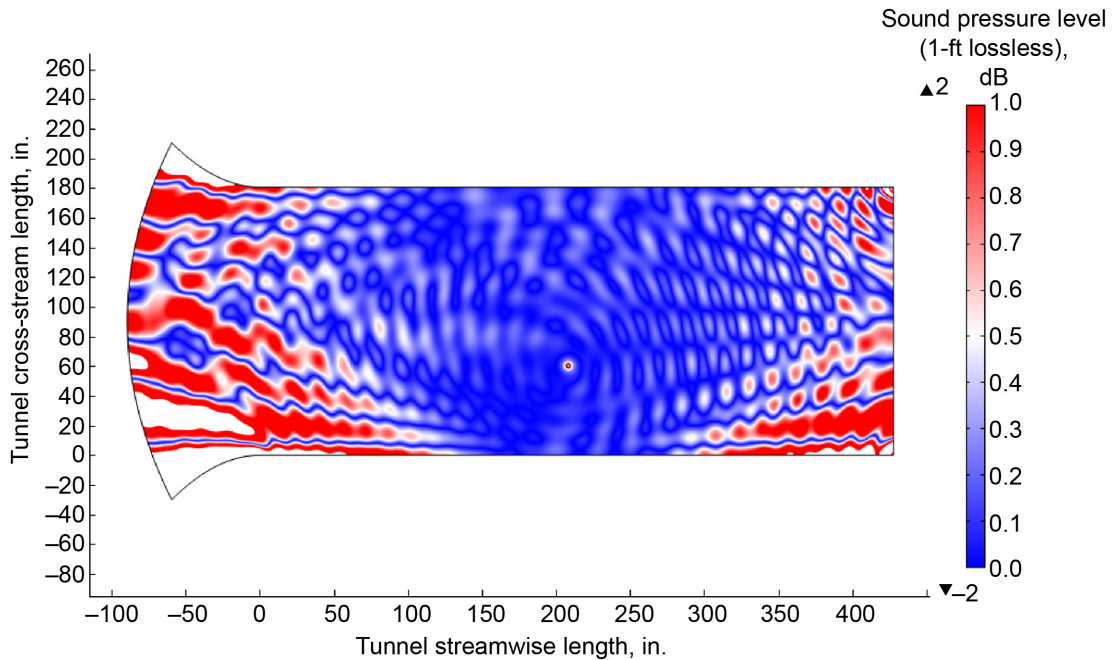


Figure 94.—Predicted 30-cm (1-ft) lossless sound pressure level ripple across test section at 500 Hz for 1986 as-built geometry. For most of test section, lower bound on solution uncertainty is 0.3 dB.

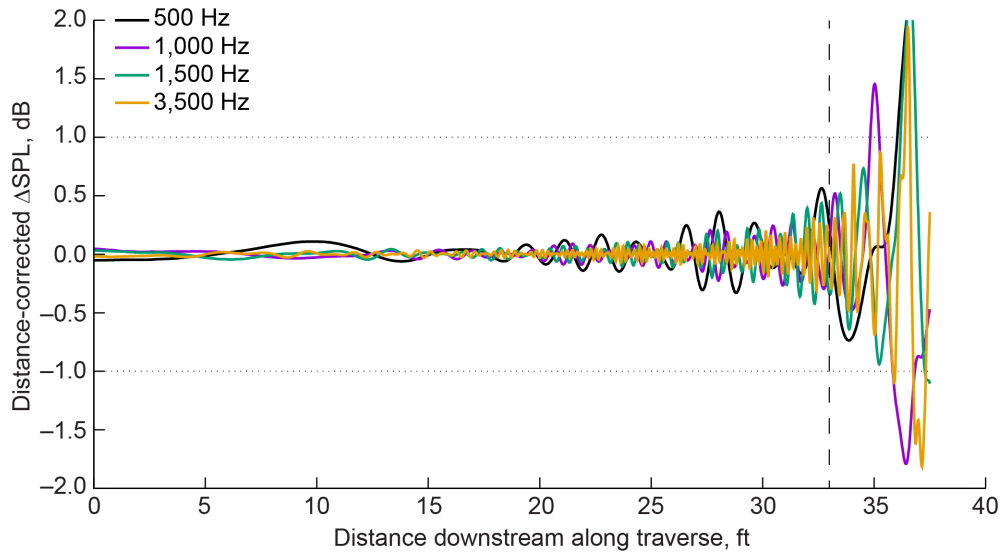


Figure 95.—Change in 30-cm (1-ft) lossless sound pressure level (SPL) along 2.26-m (89-in.) sideline traverse due to adding acoustic treatment to hard-wall diffuser. Diffuser treatment reduces test section aft end reflections by about 0.3 dB. Test section end at 33 ft.

7.6 Nonreflecting Boundary Condition

At this point in the analysis, the model was rechecked to see if the cylindrical radiation boundary condition was sufficiently accurate as a nonreflecting boundary, or if a PML would give a better, but more computationally expensive, answer. In this evaluation, all boundaries use either the cylindrical radiation or PML. Two approaches to the PML were tried, “PML” and “PML2,” differing by the number

of cells in the layer. Figure 96 to Figure 99 present the predicted sideline 30-cm (1-ft) lossless sound pressure level for four frequencies.

In summary, the cylindrical radiation boundary condition seems to result in more reasonable solutions with less spurious fluctuation. Even with the cylindrical radiation condition, the predicted solutions have up to ± 0.7 -dB variation about the mean at the inlet and exit ends with ± 0.4 dB over most of the range, while analytically it should be zero. This result is an assessment of the uncertainty in the numerical model. From this point on, the impact of physical changes on the solution should be compared to some baseline solution, for example, where all walls are set to be nonreflective.

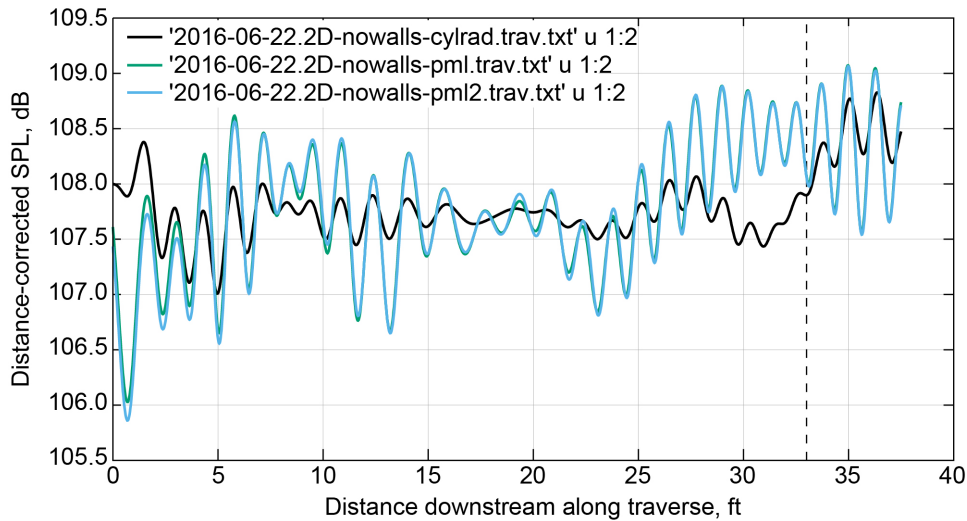


Figure 96.—Comparison of three nonreflecting boundary conditions on all walls for 30-cm (1-ft) lossless sound pressure level (SPL) on 2.26-m (89-in.) sideline at 500 Hz. Cylindrical radiation condition, “cylrad” in black, has least spurious noise. Two perfectly matched layers (PMLs) differ by number of layers in PML and produce roughly same result. Test section end at 33 ft.

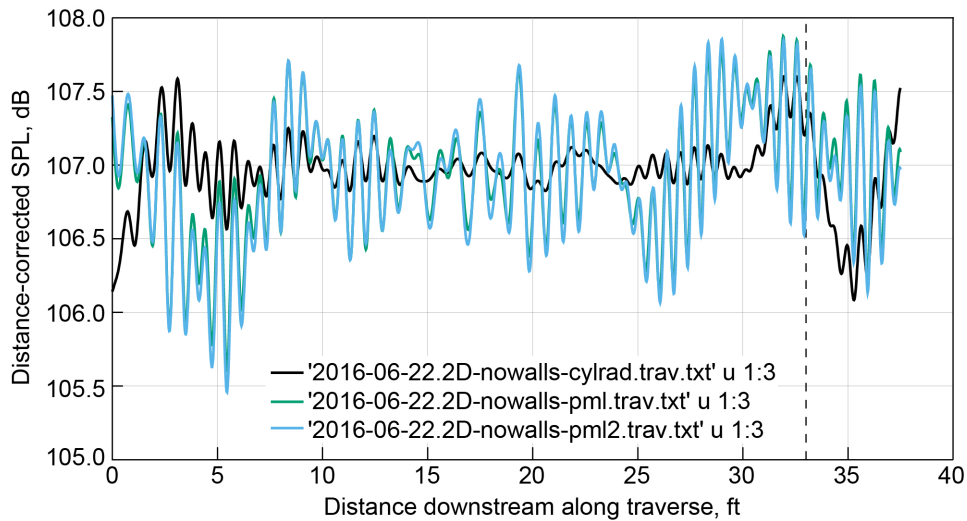


Figure 97.—Comparison of three nonreflecting boundary conditions on all walls for 30-cm (1-ft) lossless sound pressure level (SPL) on 2.26-m (89-in.) sideline at 1,000 Hz. Cylindrical radiation condition (cylrad). Two perfectly matched layers (PMLs). Test section end at 33 ft.

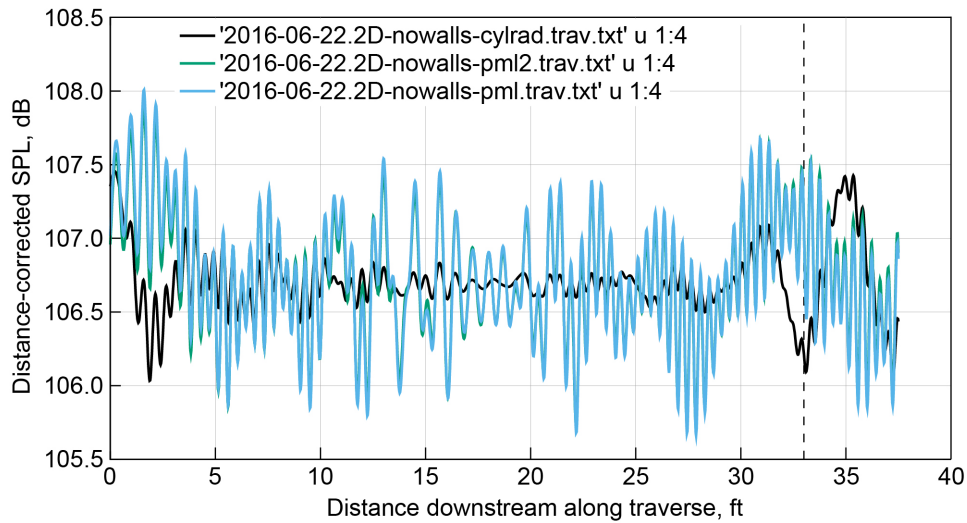


Figure 98.—Comparison of three nonreflecting boundary conditions on all walls for 30-cm (1-ft) lossless sound pressure level (SPL) on 2.26-m (89-in.) sideline at 1,500 Hz. Cylindrical radiation condition (cylrad). Two perfectly matched layers (PMLs). Test section end at 33 ft.

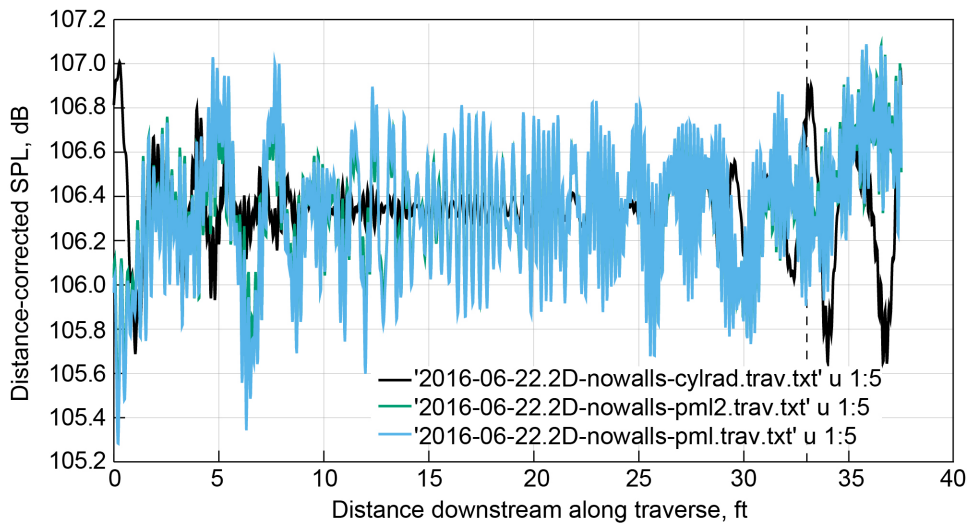


Figure 99.—Comparison of three nonreflecting boundary conditions on all walls for 30-cm (1-ft) lossless sound pressure level (SPL) on 2.26-m (89-in.) sideline at 3,500 Hz. Cylindrical radiation condition (cylrad). Two perfectly matched layers (PMLs). Test section end at 33 ft.

7.7 Evaluation of Wall Treatment

Figure 100 to Figure 103 present a comparison of solutions: “no walls,” where all walls are nonreflecting; “13-13,” where there is 33-cm- (13-in.-) deep treatment on both the walls and the diffuser; and “13-hard,” where the test section has 33-cm-deep treatment on the walls coupled with a hard-wall diffuser. These are to assess the upper bound on solution ripple due to the diffuser treatment. The most useful comparison is between 13-13 and 13-hard.

In summary:

- Treating the diffuser decreases the ripple in the test section by less than 0.2 dB, except for the aft end of the test section at low frequencies, where there could be a 0.5-dB improvement.
- Using the 1986-designed full-depth treatment on all walls reduces the measurement uncertainty due to reflections down to ± 0.4 dB, which was considered acceptable.
- Further reductions in the reflections at the upstream end require acoustic treatment on the currently hard-wall inlet contraction.

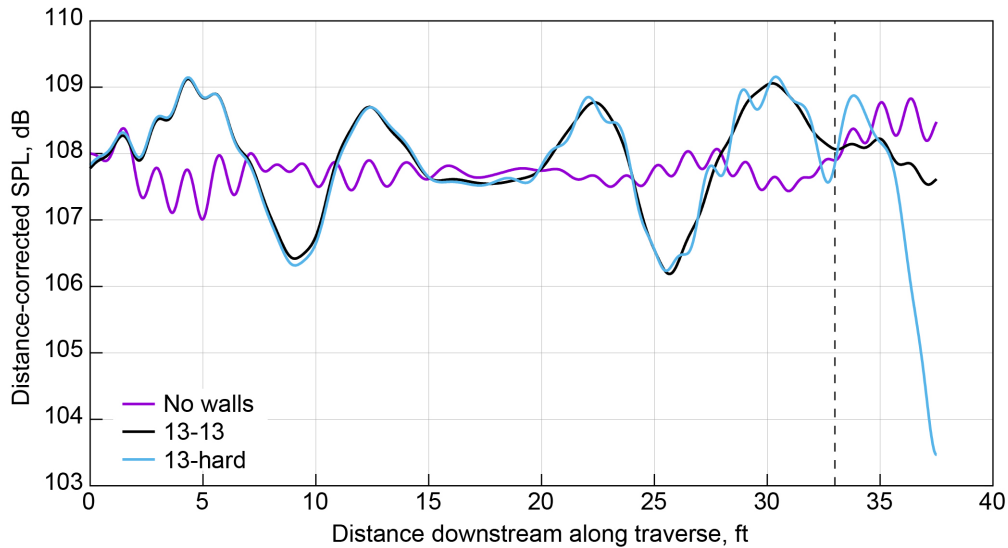


Figure 100.—Impact of diffuser acoustic treatment on test section 2.26-m (89-in.) sideline 30-cm (1-ft) lossless sound pressure level (SPL) at 500 Hz. Test section end at 33 ft.

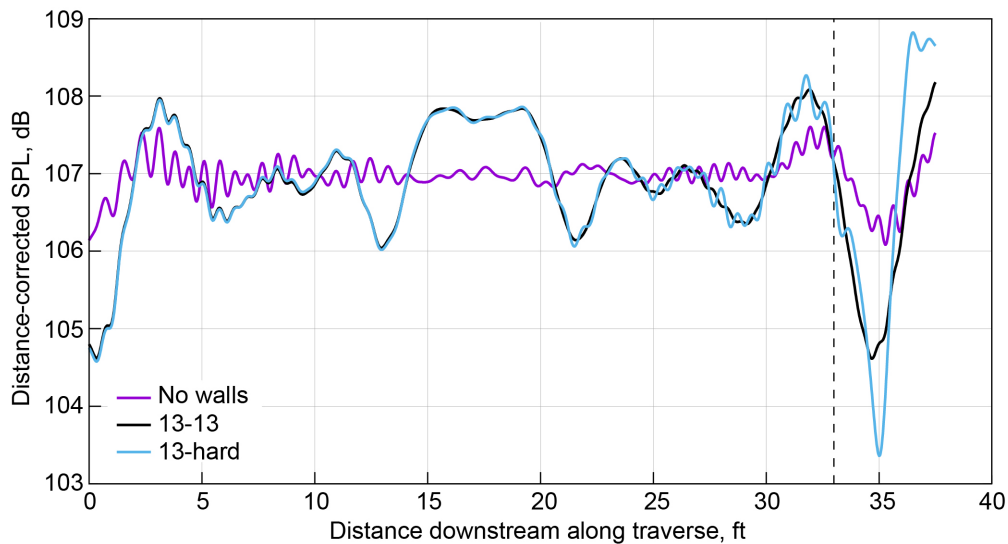


Figure 101.—Impact of diffuser acoustic treatment on test section 2.26-m (89-in.) sideline 30-cm (1-ft) lossless sound pressure level (SPL) at 1,000 Hz. Test section end at 33 ft.

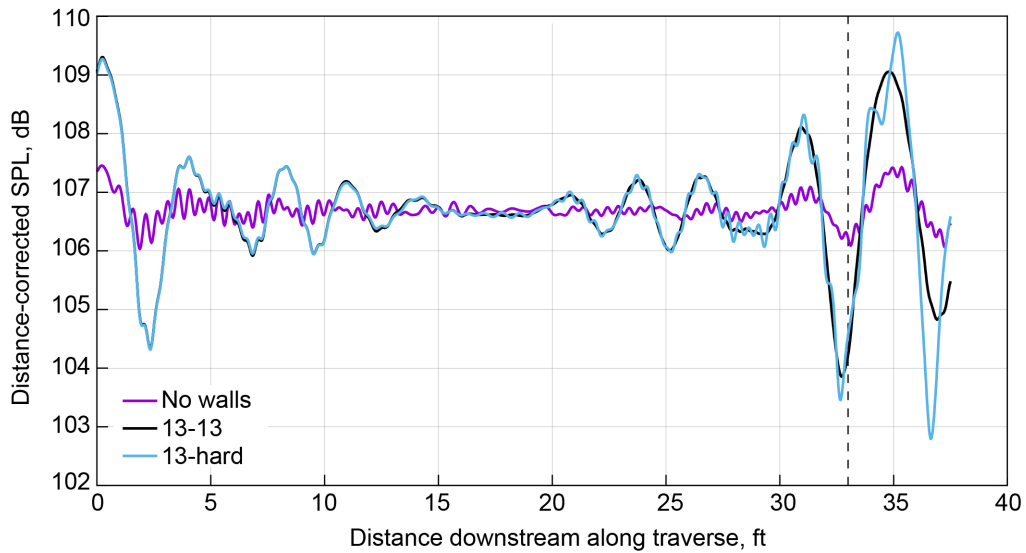


Figure 102.—Impact of diffuser acoustic treatment on test section 2.26-m (89-in.) sideline 30-cm (1-ft) lossless sound pressure level (SPL) at 1,500 Hz. Test section end at 33 ft.

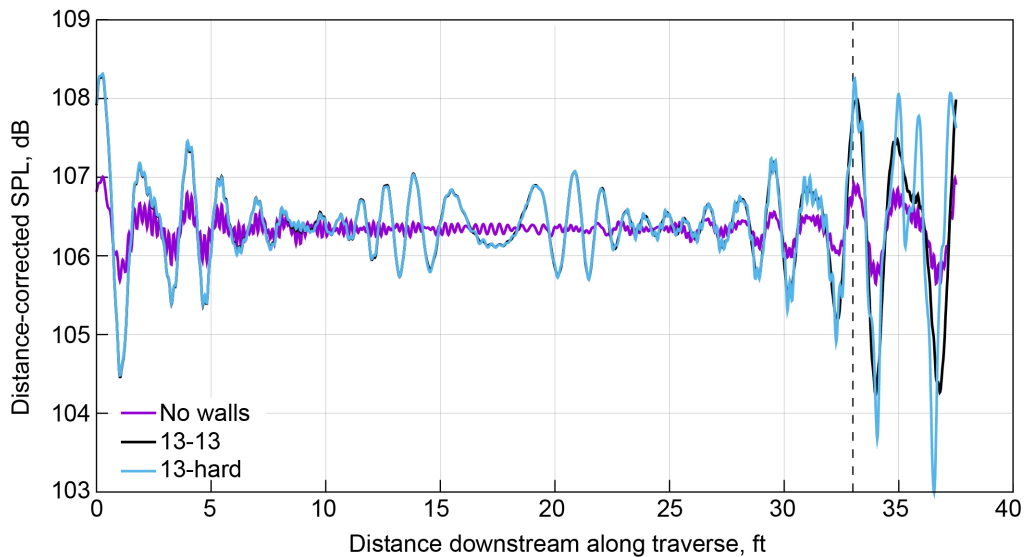


Figure 103.—Impact of diffuser acoustic treatment on test section 2.26-m (89-in.) sideline 30-cm (1-ft) lossless sound pressure level (SPL) at 3,500 Hz. Test section end at 33 ft.

7.8 Traverse Corners

The sideline traverse in the 1986 design, shown in Figure 87, sits on top of the acoustic treatment. For the redesign, it was proposed that the mechanics of the traverse be placed outside the test section, specifically in the outside corners above the wall treatment, and to the side of the ceiling and floor treatment. These regions are not occupied by treatment, and access only requires a change to the upper and lower sidewall boxes to allow for passage of a support structure through a slot. Several designs were evaluated for the penetration, to assess how to acoustically shield the hard reflective actuation mechanism and the wall penetration.

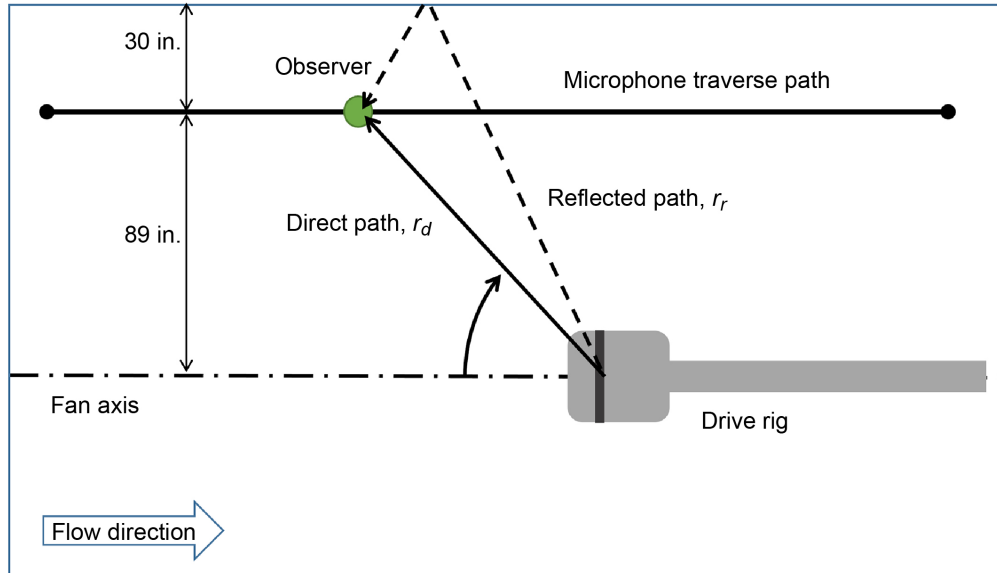


Figure 104.—Single-reflection representation of contamination of microphone measurements due to reflections.

The concept of using a corner slot was selected for the traverse mechanism, but the final design was not ready when the tunnel upgrade began. Details of the traverse, and analyses to guide design decisions, will be in a future report.

8.0 Analytical Study

A number of analytical methods were also used to evaluate 9×15 LSWT renovation concepts and specifically to estimate the error due to nonideal acoustic treatment. The first step was a simple model to account for the error introduced into a measurement microphone by a single contaminating reflection, as shown in Figure 104.

An estimate of the error for this single-reflection situation, the sound measured by a microphone, p_{mic} , is

$$p_{mic} = p_d \pm p_r \quad (3)$$

where p_d is the direct sound that we wish to measure and p_r is reflected sound that contaminates the measurement. The \pm accounts for either constructive or destructive interference, as the relative phase of the two signals is unknown. Assuming the sound source is omnidirectional, and thus, radiated at equal amplitude in all directions, we can calculate the amplitude of the reflected component as a ratio of path lengths, where r_r is the reflected path and r_d is the direct path. This accounts for spherical spreading as the amplitude decays inversely with distance,

$$\frac{p_r}{p_d} = \frac{r_d}{r_r} \quad (4)$$

or

$$p_r = p_d \frac{r_d}{r_r} \quad (5)$$

which does not yet take into account the reduction in amplitude of the reflection due to the acoustic treatment. The definition of absorption coefficient C_a is

$$C_a = 1 - \frac{p_o^2}{p_i^2} \quad (6)$$

where p_i is the sound incident on the sample and p_o is the sound outbound from the sample, not to be confused with p_r , which includes the effect of spherical spreading. Rearranging Equation (6) gives

$$\frac{p_o}{p_i} = \sqrt{1 - C_a} \quad (7)$$

To account for the acoustic treatment, the reflected sound amplitude of Equation (5) is multiplied by Equation (7) to give

$$p_r = p_d \frac{r_d}{r_r} \sqrt{1 - C_a} \quad (8)$$

Plugging Equation (8) into Equation (3) gives

$$p_{mic} = p_d \pm p_d \frac{r_d}{r_r} \sqrt{1 - C_a} \quad (9)$$

or

$$\frac{p_{mic}}{p_d} = 1 \pm \frac{r_d}{r_r} \sqrt{1 - C_a} \quad (10)$$

In decibels, the error is thus,

$$\text{dB error} = 20 \log_{10} \left(\frac{p_{mic}}{p_d} \right) = 20 \log_{10} \left(1 \pm \frac{r_d}{r_r} \sqrt{1 - C_a} \right) \quad (11)$$

A quick inspection of this equation shows the expected behavior. In the limit of a reflected path very much longer than the direct path ($r_d \ll r_r$), the error approaches zero. Also, if the acoustic treatment is perfect and the absorption coefficient is 1, error is also zero. The two path lengths are calculated from knowledge of the source and observer locations and the geometry of the wind tunnel. The method can also be extended to account for multiple reflections, from say the floor, walls, and ceiling. Again, the relative phases of the reflections are unknown, so using \pm to assume perfect constructive or destructive interference is assumed to give bounds for the error.

8.1 Maximum Theoretical Tone Error: One-Dimensional

As a first example, consider a 1D situation with an observer at 90° to the tunnel axis, so the incident and reflected path are along the same line. At the usual sideline traverse distance of 226 cm (89 in.) from the model and 76 cm (30 in.) from the wall, the ratio of path lengths is essentially 0.6. The decibel error is given in Figure 105 as a function of absorption coefficient. It can be seen that for error to be less than ± 1 dB, the absorption coefficient should be very high, above 0.96.

Another perspective is seen by varying the distance on a straight line along the 90° directivity path. This gives a theoretical measurement distance radius to achieve a certain error. Results are shown in Figure 106. This confirms the same result of ± 1 dB at 226 cm (89 in.) for $C_a = 0.97$.

8.2 Maximum Theoretical Tone Error: Two-Dimensional

Considering the 2D single-reflection scenario pictured in Figure 104, it can be seen that the 90° case has the lowest error, as the ratio of direct to reflected path lengths gets smaller upstream and downstream. For a microphone moving along the traverse path at a 226-cm (89-in.) sideline from the model axis, the error is shown in Figure 107. The 90° perpendicular case is given at a distance of zero. This is offset from the center of the plot because the typical fan model location is downstream of the center of the test section.

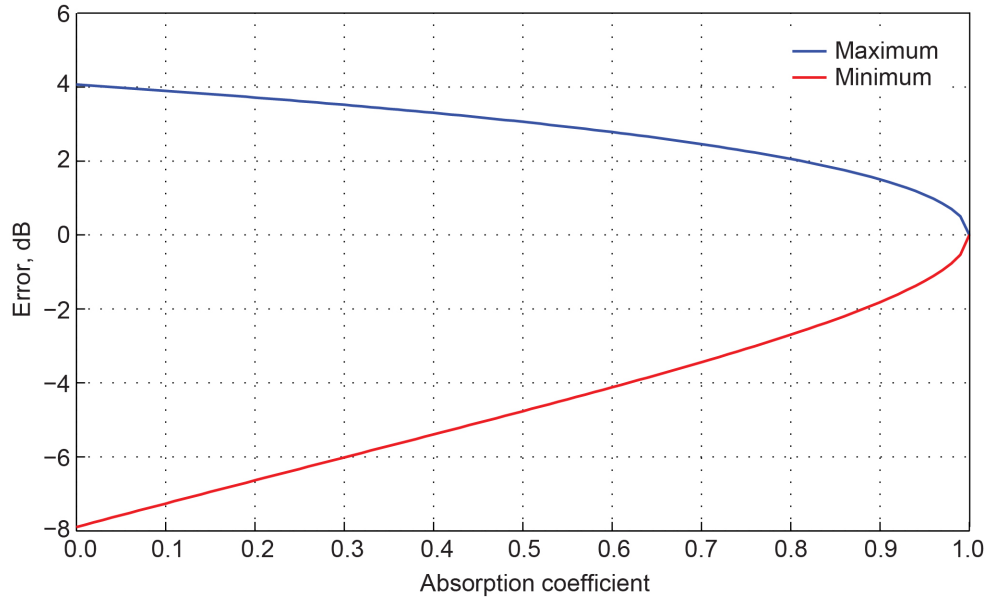


Figure 105.—One-dimensional theoretical worst-case error due to imperfect absorption coefficient C_a . Observer at 226 cm (89 in.) from source and 76 cm (30 in.) from reflection-causing wall. Perfectly absorptive wall with absorption coefficient of one gives zero error, as seen at right edge of plot.

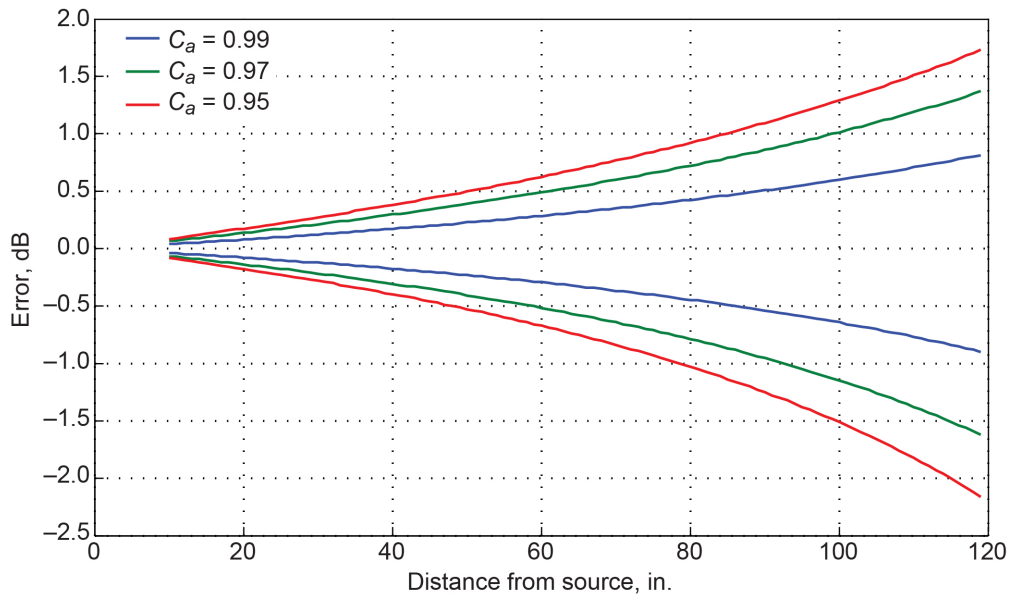


Figure 106.—One-dimensional theoretical worst-case error due to three values of absorption coefficient C_a . Distance varies from source. Smallest error is found for observer close to source and is seen at left of graph.

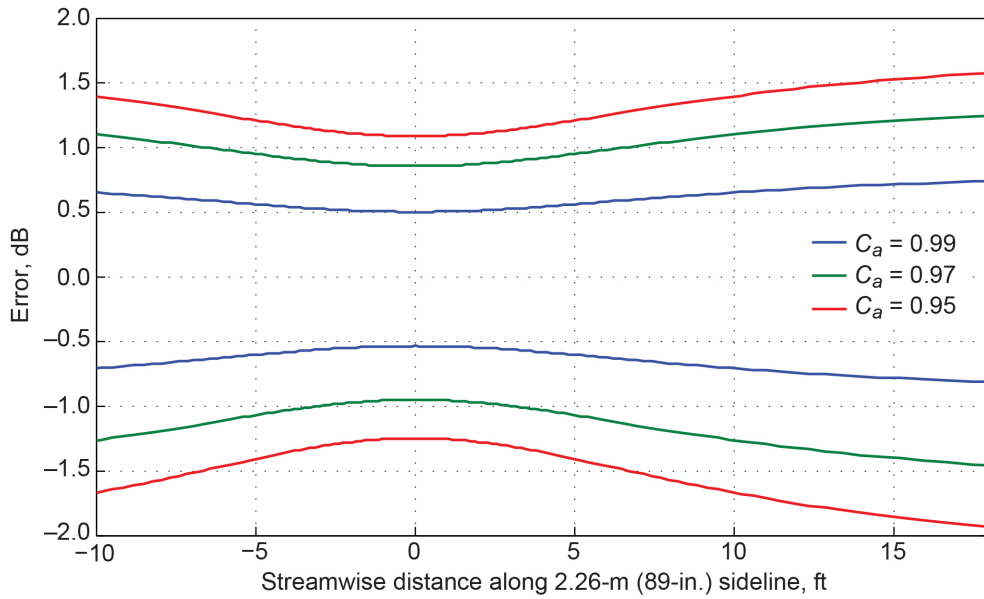


Figure 107.—Two-dimensional theoretical worst-case error due to imperfect absorption coefficient C_a , dependence on tunnel location used as shown in Figure 104.

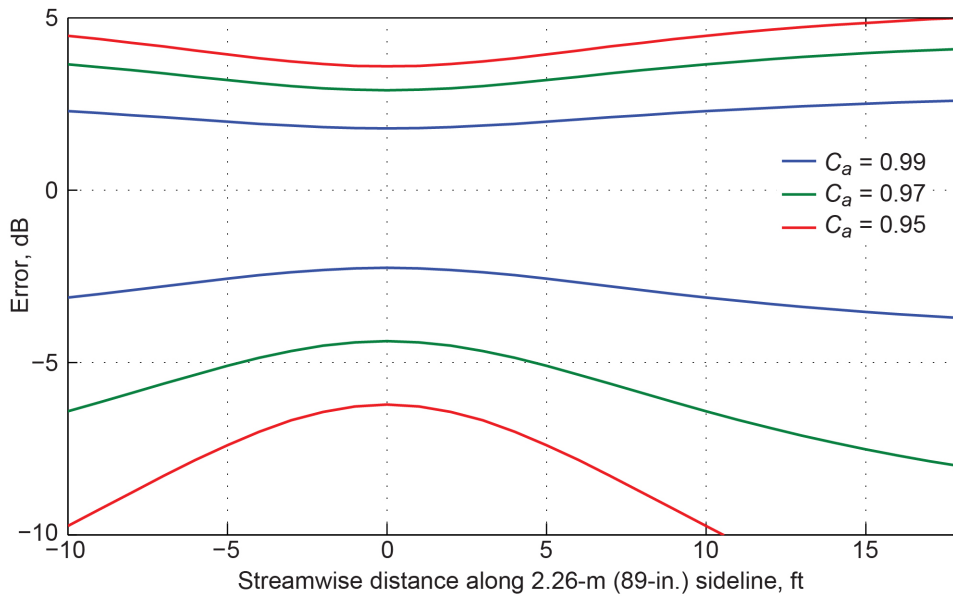


Figure 108.—Three-dimensional theoretical worst-case error due to imperfect absorption coefficient C_a .

8.3 Maximum Theoretical Tone Error: Three-Dimensional

A further assessment can be given by considering reflections from all four tunnel surfaces. Naturally, it is unlikely that all four reflections will occur in phase simultaneously, but this represents a true worst-case scenario. The resulting error for four reflections is quite extreme, with errors of -8 to 4 dB with $C_a = 0.97$. The resulting error is shown in Figure 108.

9.0 Conclusion

A multiyear effort to study technologies for improving the background noise of the 9- by 15-Foot Low-Speed Wind Tunnel was presented. The major noise reduction benefit came from replacing the exposed perforated panels of the test section with micronic wire cloth diffusion bonded to perforate. This material is essentially similar to the flow surface installed in the NASA Ames Research Center 40- by 80-Foot Wind Tunnel during a retrofit in the mid-1990s. The self-noise reduction was gained in exchange for reduced absorption for frequencies below 4 kHz, at least in the component testing presented in this report. A companion report to this report will document the installed performance of the acoustic treatment and quantify the improvement to the facility.

References

1. Yuska, Joseph A.; Diedrich, James H.; and Clough, Nestor: Lewis 9- by 15-Foot V/STOL Wind Tunnel. NASA/TM X-2305, 1971. <https://ntrs.nasa.gov>
2. Rentz, Peter E.: Hardwall Acoustical Characteristics and Measurement Capabilities of the NASA Lewis 9 x 15 Foot Low Speed Wind Tunnel. NASA CR-135025, 1976. <https://ntrs.nasa.gov>
3. Rentz, Peter E.: Softwall Acoustical Characteristics and Measurement Capabilities of the NASA Lewis 9 x 15 Foot Low Speed Wind Tunnel. NASA CR-135026, 1976. <https://ntrs.nasa.gov>
4. Dahl, Milo D.; and Woodward, Richard P.: Comparison Between Design and Installed Acoustic Characteristics of NASA Lewis 9- by 15-Foot Low-Speed Wind Tunnel Acoustic Treatment. NASA TP-2996, 1990. <https://ntrs.nasa.gov>
5. Dahl, Milo D.; and Woodward, Richard P.: Acoustical Evaluation of the NASA Lewis 9- by 15-Foot Low Speed Wind Tunnel. NASA TP-3274, 1992. <https://ntrs.nasa.gov>
6. Woodward, Richard P., et al.: Background Noise Levels Measured in the NASA Glenn 9- by 15-Foot Low-Speed Wind Tunnel. NASA TM-106817 (AIAA 95-0720), 1995. <https://ntrs.nasa.gov>
7. Stephens, David B.: The Acoustic Environment of the NASA Glenn 9- by 15-Foot Low-Speed Wind Tunnel. AIAA 2015-2684, 2015.
8. Soderman, Paul T., et al.: Design and Development of a Deep Acoustic Lining for the 40- by 80-Foot Wind Tunnel Test Section. NASA/TP-2002-211850, 2002. <https://ntrs.nasa.gov>
9. Soderman, Paul T., et al.: Acoustic Quality of the 40- by 80-Foot Wind Tunnel Test Section After Installation of a Deep Acoustic Lining. NASA/TP-2002-211851, 2002. <https://ntrs.nasa.gov>
10. Duell, Edward, et al.: Recent Advances in Large-Scale Aeroacoustic Wind Tunnels. AIAA 2002-2503, 2002.
11. Duell, Edward, et al.: Boundary Layer Noise in Aeroacoustic Wind Tunnels. AIAA 2004-1028, 2004.
12. Hersh, Alan S.: Experimental Investigation of Surface Roughness Generated Flow Noise. AIAA 87-0786, 1983.
13. Howe, M.S.: Surface Pressures and Sound Produced by Turbulent Flow Over Smooth and Rough Walls. *J. Acoust. Soc. Am.*, vol. 90, no. 2, 1991, p. 1041.
14. Liu, Yu; and Dowling, Ann P.: Assessment of the Contribution of Surface Roughness to Airframe Noise. *AIAA J.*, vol. 45, no. 4, 2007, pp. 855-869.
15. Grissom, Dustin L., et al.: Rough-Wall Boundary Layer Noise: An Experimental Investigation. AIAA 2007-3418, 2011.
16. Alexander, W. Nathan; Devenport, William; and Glegg, Steward A.L.: Aerodynamic Noise From Sparse Surface Roughness. AIAA 2011-2740, 2011.
17. Awasthi, Manuj, et al.: Sound Radiation From Rounded Steps and Gaps. AIAA 2013-2048, 2013.

18. Alexander, William N.; and Devenport, William J.: Noise From Boundary Layer Flow Over Fabric Covered Perforate Panels. AIAA 2014–2908, 2014.
19. Alexander, William N.; and Devenport, William J.: Noise Produced by Fabric and Wire Mesh Covered Panels in Low-Speed Anechoic Wind Tunnels. AIAA 2015–3261, 2015.
20. MATLAB. Software Package, Version 9.1.0.441655 (R2016b), The MathWorks, Inc., Natick, MA, 2016.
21. Seifert, Avi; and Pack, LaTunia G.: Active Flow Separation Control on Wall-Mounted Hump at High Reynolds Numbers. AIAA J., vol. 40, no. 7, 2002, pp. 1363–1372.
22. Cooper, Beth A.: Design and Construction of a Convertible Hemi/Anechoic Acoustical Laboratory for Testing Space Flight Hardware at the NASA Glenn Research Center. J. Acoust. Soc. Am., vol. 108, no. 5, 2000, p. 2473.
23. Eaton, John W., et al.: GNU Octave—A High-Level Interactive Language for Numerical Computations. Edition 4 for Version 4.2.0, 2016.
24. Welch, P.: The Use of Fast Fourier Transform for the Estimation of Power Spectra: A Method Based on Time Averaging Over Short, Modified Periodograms. IEEE Trans. Audio Electroacoust., vol. 15, no. 2, 1967, pp. 70–73.
25. Dahl, Milo D.; and Rice, Edward J.: Measured Acoustic Properties of Variable and Low Density Bulk Absorbers. NASA TM–87065, 1976. <https://ntrs.nasa.gov>
26. Ver, Istvan L.; and Beranek, Leo L.: Noise and Vibration Control. McGraw-Hill, New York, NY, 1971.
27. Bies, David H.; Hansen, Colin H.; and Campbell, Richard H.: Engineering Noise Control. J. Acoust. Soc. Am., vol. 100, no. 3, 1996.
28. Allard, Jean; and Atalla, Noureddine: Propagation of Sound in Porous Media: Modelling Sound Absorbing Materials. Second ed., John Wiley & Sons, Chichester, 2009.
29. Phong, Vincent; and Papamoschou, Dimitri: Acoustic Transmission Loss of Perforated Plates. AIAA 2012–2071, 2012.
30. Rice, E.J.: A Model for the Acoustic Impedance of Linear Suppressor Materials Bonded on Perforated Plate. AIAA 81–1999, 1981.
31. Yu, Jin; Ruiz, Marta; and Kwan, Hwa Wan: Validation of Goodrich Perforate Liner Impedance Model Using NASA Langley Test Data. AIAA 2008–2930, 2008.
32. Gerhold, Carl H.; Cabell, Randolph H.; and Brown, Martha: Development of an Experimental Rig for Investigation of Higher Order Modes in Ducts. AIAA 2006–2637, 2006.
33. Gerhold, Carl H., et al.: Report on Recent Upgrades to the Curved Duct Test Rig at NASA Langley Research Center. AIAA 2011–2896, 2011.
34. Gerhold, Carl, et al.: Configuration Effects on Acoustic Performance of a Duct Liner. AIAA 2008–2977, 2008.
35. COMSOL Multiphysics. Software Package, Stockholm, Sweden, 2021.
36. Rice, Edward J.: A Theoretical Study of the Acoustic Impedance of Orifices in the Presence of a Steady Grazing Flow. NASA TM X–71903, 1976. <https://ntrs.nasa.gov>
37. Malmary, Cecile, et al.: Acoustic Impedance Measurement With Grazing Flow. AIAA 2001–2193, 2001.
38. Schmitt, Jeff G.; and Stahnke, Brian: 9- by 15-Foot Low-Speed Wind Tunnel Acoustic Free Field Evaluation. NASA/CR—2017-219509, 2017. <https://ntrs.nasa.gov>

